Morphology Informed Approaches to Soft Robotic Resilience

M. Pontin

Department of Automatic Control and Systems Engineering
University of Sheffield

This dissertation is submitted for the degree of
Doctor of Philosophy

2023

Morphology Informed Approaches to Soft Robotic Resilience

Marco Pontin

Department of Automatic Control and Systems Engineering
University of Sheffield

This dissertation is submitted for the degree of
Doctor of Philosophy

September 2023

Mater artium necessitas

Declaration

I hereby declare that, except where specific reference is made to the work of others, the contents of this dissertation are original and have not been submitted in whole or in part for consideration for any other degree or qualification in this, or any other university. This dissertation is my own work and contains nothing which is the outcome of work done in collaboration with others, except as specified in the text and Acknowledgements.

Marco Pontin
September 2023

Acknowledgements

I would like to thank Dr. Dana D. Damian for her support and guidance in my development as a PhD candidate and researcher. I would also like to acknowledge the support of my family, who put up with me during the worst, most stressful times, and of all the members of the Sheffield Biomedical Robotics Lab and of the Sheffield Microrobotics Lab, who have been at my side throughout this intense, challenging and exciting journey. To Joanna, thanks for being a friend, for always caring for me and for always trying to make the lab a better place (your cakes will remain the stuff of legends!). To Abi, thanks for the smiles, the good vibes and for pushing me to always look on the bright side. To Freddy, Quentin and Cameron, thanks for the fun, the chats and for always being there for me.
To all of you, from the bottom of my heart I say

Thank you.

Abstract

Soft robotics has become a thriving field of research, encompassing control theory, material science, robotics, and fluid dynamics. The aim is to create robots with compliant bodies and novel capabilities, such as morphologic change, allowing for better adaptability in diverse, unknown and challenging environments.

Several problems still prevent the widespread adoption of soft robots in the real world, though, from complex manufacturing, to the challenges in modelling and control. Recently, concerns have also emerged regarding their resilience and durability. At the material level, soft robots are prone to wear, degradation, and failures due to environmental factors, more so than traditional rigid robots made from metal alloys. Their low hardware redundancy and tight integration of form and function exacerbate these issues. Self-healing materials have been investigated as a solution, but challenges still stand. Furthermore, a solution that can bridge the gap between controller driven approaches and material-based ones is yet to be demonstrated.

This work addresses some of the challenges of soft robotic resilience and presents two approaches to achieve it, inspired by the concepts of morphological computation and embodied intelligence. First, a software-based framework is applied to a flexible extendable robotic implant and the compliant morphology of the robot is used to gain information and achieve fault detection and identification. The second approach, intended for pneumatic soft robots, uses novel fully soft valves to achieve distributed embodied resilience. These valves autonomously detect and isolate bursts and offer protection against overpressurisation, providing a novel, pre-emptive type of resilience, therefore reducing hardware and computational complexity. As a whole, this work represents the embryo of a new form of resilience for soft robots, a morphology-informed one based on embodied computation. It enhances the adaptability of soft-robots and addresses critical limitations of self-healing solutions, therefore representing an important stepping-stone towards more resilient soft robots.

Table of contents

List of figures

Chapter 1

Introduction

1.1 Overview and motivation for the research

In the last twenty years, soft robotics have become an ever growing field of research, spanning multiple disciplines: control theory, material science, robotics and fluid dynamics, just to name a few [1]. Proposed applications range from space exploration to industrial manipulation, to human robot interaction, to medical devices [2, 3]. The main idea is to create robots whose body, or parts of it, are compliant, either flexible or fully soft, and leverage the new capabilities that this enables, including better adaptation in unstructured and unknown environments and morphological change. Over the years, researchers in the field of morphological computation have also shown how these capabilities can be used to reduce controller complexity and computational effort [4]. As a result, one soft robotic manipulator can grasp delicate objects of many different sizes and shapes, with minimal control-loop effort and hardware: the compliant fingers naturally curl and adapt to each new shape they are interacting with. This extreme level of adaptation has prompted research in the usage of soft robots for extreme and difficult to reach environments such as search and rescue missions, space exploration and implantable medical technologies [5, 6, 3, 7, 8]. All of these applications, as diverse as they are, have one thing in common: limited knowledge about the operating environment. Adaptation therefore becomes an essential resource for success. In addition to the sheer novelty provided by their compliance, soft robots have been investigated by material scientists as a platform for testing novel functional materials such as hydrogels and polymers, in order to merge sensing and actuation into the fabric of the robot body [9, 10].

Together with these new capabilities that soft robots have introduced, a number of challenges also emerged. Manufacturing usually still involves manual steps performed by expert researchers. Novel additive manufacturing techniques are being explored in order to

automate the process and improve overall repeatability, but material selection is still quite limited and price becomes a factor when dealing with 3D-printers capable of multi-ink high-precision printing. Control has also posed a number of challenges. If on the one hand, compliance makes human-robot interaction inherently safe and robot-environment interaction easier to manage, on the other hand, the high number of degrees of freedom (dof) of these robots (which can become almost infinite in continuum robots) means that very complex control strategies have to be devised [2, 11, 12]. Sensor number and placement also becomes an issue, with researchers usually finding trade-offs between the amount of sensors/computational complexity and need for information. One solution that has been proposed in the case of high-dof robots is camera tracking. This, though, is not a viable alternative in most of the applications previously cited as cameras would have to be placed in a fixed reference frame, far enough from the robot to be able to capture it in its entirety, resulting in less compact, partially rigid systems. Other approaches include those that use fluidic controllers, moving away from traditional software-based control, with the goal of producing more biologically inspired soft robots.

More recently, resilience has being highlighted as one of the critical aspects that need solving, before large scale adoption of soft robots can happen [13, 14]. This is for one main reason: durability. When compared to traditional rigid robots made out of metal alloys, soft robots are far more prone to failures due to wear, interaction with sharp edges and general degradation due to environmental factors. These faults can be gradual, or sudden (a burst in a pneumatic soft robot), but usually translate in a complete or near complete loss of functionality of the robot. This is due to the tight integration of form and function in soft robots, that carries with it low hardware redundancy. In the case of pneumatic soft robots, for example, a small leakage can therefore have catastrophic consequences. Fault-tolerant approaches, that do not rely on sheer hardware redundancy have been known for decades, but usually require a detailed model of the system and enough sensory information, both of which can be unattainable in the case of soft robots due to the high number of dof and complex hyperelastic material behaviour. Recently, special materials have been discovered, that show self-healing capabilities: the matrix of the material, if damaged, can, in time, reform the severed chemical bonds, returning to its pristine form [13, 15, 16]. In the case of soft robotics, both polymers and hydrogels have been found, displaying this property, with some of the latter even being biodegradable [17]. As promising as this discovery is, challenges still stand. In the best scenario, the healing process still requires time, the edges of the cut have to be kept together for the process to be successful, which might become impossible if material was removed during the damage. In the case of fluidically actuated soft robots, which represent the majority of cases, this translates into the need to keep the

robot powered down while the healing occurs, as the fluid being pumped into the body of the robot would leak out through the cut, preventing the edges from going back together.

Finding a solution to the problem of soft robotic resilience translates into easier path to their widespread adoption, with the long-term goal of making robots that, inspired by biology, can carry out tasks, even when damaged, heal their bodies and, in the end, degrade and provide resources for other organisms/robots to use.

1.2 Objectives and contributions of the research

Before delving into the contributions of the research contained in this work, it is beneficial to provide a definition of the term resilience.
The word has a long history. First used in the early 1600s, it generally refers to the capability of both animate and inanimate objects and system to withstand stress and adversities. In the case of robotic systems, one can define resilience as the ability of the system to recover from faults and maintain the prescribed functionality, even if to a lesser degree than the original, undamaged system. Thanks to its generality, the word encompasses a multitude of strategies that have successfully been used to impart fault-coping capabilities to robots. As no mention is made to the recovery mechanism or whether or not the prescribed functionality is still achieved through the same behaviour and hardware, very different approaches such as hardware redundancy, software fault-tolerance and material self-healing, can all be grouped under the same umbrella of techniques for robotic resilience.

The research in this work tries to address the challenges, previously highlighted, regarding soft robotic resilience. In doing so, it presents two ways of achieving resilience in soft robots. First, a software-based approach is studied and applied to a hybrid rigid-soft robotic implant. The device can mechanostimulate tissue for regeneration purposes and elongate, or "grow", with the tissue. The second approach translates the ethos of work done in software into an embodied version, through the use of fully soft valves embedded in the body of pneumatic soft robots. As a whole, the work tries to understand what are the limitation of these types of resilience, their trade-offs and boundaries, both between themselves and compared to self-healing approaches.

The contributions of the thesis can therefore be split into two groups. With respect to the work on the robotic implant presented in Chapter 3, the fault detection and identification framework that has been developed does not require a precise model of the system and can therefore adapt to many different architectures. Although only tested with a limited number of sensors, the approach, based on Canonical Correlation Analysis, should be able to scale to larger number of sensors with little additional computational load. Probably, the

most interesting aspect is the ability of the framework to exploit the flexible morphology of the robot to perform self-tests and acquire additional knowledge on the state of the system for identification purposes. This is done to overcome disambiguation issues due to lack of redundancy in sensor information. The second main contribution of this chapter is the development of a robotic soft tissue simulator to test the resilience of robotic implants. The platform uses impedance control to simulate both the viscoelastic behaviour of soft tissue, as well as long-term tissue growth. In doing so, it provides a physiologically relevant environment for preliminary testing of robotic implants, both rigid and soft, for tissue mechanostimulation. As such, the simulator can be used for in-depth long-term testing of devices, before in-vivo implantation, reducing the need for in-animal testing and shortening the path to clinical trials.

Moving to the embodied soft valve approach, Chapters 4 and 5 focus on a novel way of achieving local, distributed resilience in pneumatic soft robots. The valves, starting with the first version presented in Chapter 4, can passively and autonomously detect and isolate faults in pneumatic soft actuators, in less than 30 ms. No controller intervention is needed, therefore reducing the need for sensors, additional external hardware, such as valves and tubing, and lowering modelling and computational complexity. In addition, as the action is in situ, only the faulty part of the system is isolated, meaning that the rest of the soft robot can still be actuated. This aspect provides a link to self-healing approaches, as this selective deflation can provide the minimum prerequisites for the healing to occur, while keeping the remaining system functional. On top of this achievement, the soft valve presented in Chapter 5 can also provide protection against overpressurisation, therefore shifting the perspective from "reactive" to "pre-emptive" resilience. This is possible as the asymmetric internal structure of the valve triggers two distinct behaviours when inlet and outlet are swapped. This represents a contribution in itself as soft pneumatic components present in the literature are usually not reversible, or, when they are, the behaviour is unchanged. In the final sections of Chapter 5, two of the newly developed soft valves are paired together to create a two-stage soft valve which represents a fully self-contained unit to endow soft actuators with resilience against burst. The new soft component, consisting of a main stage and a delay stage, can generate its own control signal, by self-tuning its operation to the soft actuator it is attached to. Although at present the valve has only been tested with supply pressures of up to 30 kPa, this might represent a real drop-in solution for soft roboticists, independent of the soft actuators being used. No external control signal is necessary, meaning that the valve is transparent to any software or fluidic controller managing the actuators. For the valve to operate correctly, the delay stage valve autonomously swaps between its two logic behaviours, making this a first of its kind in soft robotics.

1.3 Structure of the thesis

Chapter 2 presents the broader literature review on the fields of robotic resilience, self-healing materials, embodied intelligence, morphological computation and soft-robotics. Throughout the chapter, high-level connections and research gaps with respect to the topic of soft robotic resilience are highlighted.

Chapter 3 presents the research conducted on the Flexible Robotic Implant and the robotic soft tissue simulator. The chapter consists of two publications, each with a more granular literature review, prefaced by an introduction and a summary of the work. The first publication focuses on the development of the Robotic Tissue Simulator platform capable of replicating the viscoelastic behaviour and growth process of soft tissue. The second one presents the fault detection and isolation framework created for the robotic implant and evaluates its performance by pairing the implant with the tissue simulator platform.

Chapter 4 introduces the first prototype of the soft valve for passive autonomous fault isolation in pneumatic soft robots. The chapter starts with an introduction and a summary of the work. The associated publication then follows, analysing the finite elements analysis and experimental characterisation of the valve.

Chapter 5 focuses on the second prototype of the soft valve with improved performance and additional capabilities. After the introductory part, each section deals with a specific aspect of the valve, from the conceptual development phase, to manufacturing, to the experimental results and their analysis.

Chapter 6 concludes the thesis and contains a reflection on the overall work included in the thesis, its interconnections with the state of the art in the field of soft robotics and possible future developments.

1.4 Publications

1.4.1 Conference publications

1. M. Pontin, S. Miyashita and D. D. Damian, "Development and Characterization of a Soft Valve for Automatic Fault Isolation in Inflatable Soft Robots," *2022 IEEE 5th International Conference on Soft Robotics (RoboSoft)*, Edinburgh, United Kingdom, 2022, pp. 62-67

Contributions of each author

M. Pontin: came up with the concept and the experiments, manufactured the samples, designed and assembled the experimental platforms, collected and analysed the data, prepared the figures, videos and text for the manuscript.

D. D. Damian and S. Miyashita: supervised the work, provided feedback on the methodology and helped to finalise the manuscript.

1.4.2 Journal publications

1. M. Pontin and D. D. Damian, "A Physical Soft Tissue Growth Simulator for Implantable Robotic Devices," in *IEEE Transactions on Medical Robotics and Bionics*, vol. 2, no. 4, pp. 553-556, Nov. 2020

   Contributions of each author

   M. Pontin: came up with the concept and the experiments, designed and assembled the experimental platforms, collected and analysed the data, prepared the figures, videos and text for the manuscript.

   D. D. Damian: supervised the work, provided feedback on the methodology and helped to finalise the manuscript.

2. M. Pontin and D. D. Damian, "Data-Driven and Compliance-Based Fault-Tolerance for a Flexible and Extendable Robotic Implant Coupled to a Growing Tissue," in *IEEE Robotics and Automation Letters*, vol. 8, no. 4, pp. 1943-1950, April 2023

   Contributions of each author

   M. Pontin: came up with the concept and the experiments, designed and assembled the experimental platforms, collected and analysed the data, prepared the figures, videos and text for the manuscript.

   D. D. Damian: supervised the work, provided feedback on the methodology and helped to finalise the manuscript.

Chapter 2

Literature Review

This chapter discusses the state of the art of research in robotics in a number of fields relevant to the scope of the research. To keep it organised, the discussion is divided into sections, each analysing a specific group of topics. The four sections are: hard-robots resilience, self-healing materials, embodied intelligence, robotic implants and soft robotics. The first section provides an overview of how the problem of robotic resilience has been dealt with at the software and hardware level in the context of rigid-bodied robots and aims at providing a ground reference for the capabilities of state-of-the-art resilient machines. The second section highlights a novel approach to resilience, which stems from the research on material engineering. The key benefit of the approaches falling in this category is the potential of achieving resilience in a highly distributed way, without the need for a control system. The research on embodied intelligence, the focus of the third section, tries to understand how computational capabilities can be assigned to the physical body of a robot, to simplify the control logic. As such, it provides a framework for analysing how traditional software-based fault detection and identification techniques could be extended to soft robots through embodiment. The fourth and last section presents a collection of works from the fields of robotic implants and soft robotics to provide an overview of the state of the art and open challenges in these fields.

2.1 Hard-robots resilience

The idea of machines that are intelligent enough to overcome problems, adapt and keep working even in the presence of faults, has probably always been with engineers, ever since the first robot was created. Computers gave the first opportunity to experiment with this concept and, in the 1950s and 1960s, engineers developed the first machines capable of detecting their own errors and correcting them [18]. A big leap forward was provided by

space exploration missions, as satellites and space vehicles represent classic applications where fault-tolerance is key in guaranteeing the longevity and reliability of the systems [19, 20].

In 1998, Blanke et al. [21] tried to give a synoptic view of fault-tolerant processes. Although only limited to software, the discussion leads to an interesting distinction between fail-safe systems and fault-tolerant ones. In particular, the former are able to withstand any single point fault without showing decreases in functionality. They usually do this by exploiting a high level of redundancy in sensing, actuation and processing and are therefore very expensive. In contrast, fault-tolerant systems use redundancy in information to detect and identify faults and accept a reduction in functionality after a fault, provided that they can still reach the predefined goal. Thanks to the ever-increasing computational power, new approaches have been developed that mix software and hardware reconfiguration, making the landscape more complex and leading to the problem being called "resilience".

In a review article of 2017, Zhang et al. [22] try to give an holistic view of the situation as it stands using a system modelling technique called FCBPSS decomposition, or Function-Context-Behaviour-Principle-State-Structure decomposition. They arrive to the conclusion that the same problem can be approached and solved using three main strategies. One uses a change in behaviour of the remaining system to overcome the faults, the second one exploits reconfiguration of the remaining system, while the third one uses changes in shapes of the components (e.g. lengthening of a leg). If the first strategy is focused on finding a new, adapted control law, the second one tries to move one step towards hardware by mixing a new control scheme with a new hardware architecture. The last one, instead, exploits the shape-change capabilities of some robots, soft robots among these, to find a solution. Although the classification they propose is interesting and includes a lot of cases, material level self-healing still eludes the proposed standard classification. In addition, it is foreseeable that, in the future, resilient robots will mix all of these strategies together, to maximise their potential.

As previously discussed, software has been the first area of research in the field of resilience. With the advancements in control theory and increasing popularity of machine learning approaches, researchers have tried to mimic the natural behaviour of animals [23–26]. When a fault occurs, the robot performs some tests to understand its new configuration, compared to the fully functioning one, and then explores the space of possible remaining behaviours to adopt a new one. Some works have even started implementing evolution in the search algorithms, to get to better solutions in shorter time scales [27, 28]. These works also show the possibility of approaching the problem with simplified or even without mathematical models of the system. This lack of previous knowledge, although tempting

given its generality, can sometimes lead to longer periods of inactivity between the fault and the eventual recovery, as the controller is trying to synthesise a new behaviour. That's why in [25] a map of possible solutions was generated beforehand, in order to reduce the search space and speed up the solution process. Nevertheless, this kind of approach still requires a great amount of time being spent in simulations before the robot is deployed.
A critical limitation emerging in the literature is the fact that the dimensionality of the search space increases with the number of degrees of freedom, quickly leading to complex and even intractable problems. Even when this is not the case, the existence of one or more local minima in the search space can lead to a sub-optimal recovery. Finally, these techniques tend not to address the faults, but rather to find ways around them, by looking for alternative behaviours that still allow to satisfy, at least partially, the goal of the system.

A slightly different approach, that could resolve some of the limitations of the "behaviour change" strategy, is the one based on modularity and reconfiguration. Research on modular self-reconfiguring robots dates back to the 1980s, with the works by Fukuda, Nakagawa and Murata [29, 30]. Examples of platforms are the CEBOT, the M-TRAN, M-TRAN II and M-TRAN III robots, the Odin robot, the soldercubes and many more [31–37]. The robots are composed of interchangeable homogeneous and heterogeneous modules, arranged in chains or lattices, that can attach and detach from each other to create various shapes. The goal is to achieve a form of programmable matter, so that the robot can change its morphology based on the task. These capabilities could be used to increase the resilience of the system, the idea being that, if a fault occurs, the broken component can be swapped out for a functioning one. This development of the technology though has been hindered by computational complexity: it has been shown that the optimal reconfiguration problem is an NP-complete problem [38], leading to long periods of time before a solution can be found, if any exists.

In summary, the literature on hard-robots resilience seems to reaffirm the dichotomy of brain versus body and approaches have either focused on software level behaviour change or hardware level redundancy and reconfiguration. Although reconfiguration can lead to the necessity of partial behaviour change, there is still a lot of ground to cover before these approaches can be brought together. Still, as mentioned, solutions such as material level self-healing are ignored.

2.2 Self-healing materials

Directly connected to the previous section, self-healing is a research topic that acquired momentum in the last decade. Inspired by nature, researchers try to find materials that are capable of restoring the molecular structure after this has been disrupted by an external dis-

turbance. More generally, the distinction is made between self-healing and self-regeneration [15, 39], the latter being a capability only found in some biological systems where the entire living organism is regenerated starting from a portion of it. Although examples of self-healing exist in all types of materials, from bio-materials and hydrogels [40, 17] to ceramics and concrete, the discussion here will mainly focus on polymers, as these represent the most popular choice for soft robots [39, 41].

The healing process itself can be described and analysed in different ways [15, 41]: a mobile phase that gets activated when the damage occurs and mixes with a non-mobile one; a two-step process based on a sealing phase and an healing one. In addition, self-healing polymers use many different chemical principles, from strong covalent bonds to weaker Diels-Alder bonds, hydrogen bonds and π-π-interactions and can be classified in a number of different families. Researchers distinguish between intrinsic and extrinsic self-healing, and autonomic and non-autonomic self-healing [39, 41–43]. In the case of extrinsic self-healing, the material does not have healing capabilities in itself, and techniques such as micro-capsule or micro-vascular based self-healing are used [44–47]. Conversely, intrinsic self-healing materials exploit reversible chemical bonds during the healing process [48, 43, 13].
The distinction between autonomic and non-autonomic healing looks at the trigger of the healing process. In autonomic self-healing, the damage itself acts as initiator and, as soon as the material structure is compromised, the healing process begins. Examples can be found in [48, 44, 45, 49–51]. Non-autonomic self-healing on the other hand requires a modest external trigger, for example in the form of temperature [13, 43].

Although the healing process can happen in many different ways, the literature seems to agree on how to evaluate the process itself. The two main features are the number of healing cycles and the healing efficiency. In both cases, the higher the better. Some mechanisms, like the micro-capsule based one [44, 45], are only usable once, in the sense that if the crack occurs again in the same spot, no healing is possible. Others, like the microvascular based one presented in [46], can reach seven or eight healing cycles. There are then some that show potentially infinite healing capabilities as those presented in [47, 43, 13, 48].

The second important parameter to be considered is the healing efficiency. It is defined as:

$$\eta = \frac{P_{healed}}{P_{virgin}} ,$$

where P_{virgin} represents the load at which the original specimen fractures and P_{healed} is the load at which the healed one breaks. In the case of a perfect healing process, the efficiency should therefore tend to one. In reality, despite there being agreement on the theoretical definition, the way the healing efficiency is computed differs among researchers. Some for example notch or dent the samples to be sure it always cracks in the same spot [46, 47], while

others do not [48, 13], the choice being justified by the fact that if the sample cracks in a different spot, perfect healing was achieved during the previous healing cycle.

One key limitation of most processes presented so far remains the time to healing. This can vary if the process is influenced by external factors such as temperature, but it usually last from a several seconds to a full day [43, 13, 48, 46, 47]. In all cases, the recovery is a continuous process in the sense that mechanical properties are gradually restored. It is therefore possible to stop the healing cycle sooner, at the cost of a decreased mechanical performance.

As new materials capable of self-healing are introduced, researchers have started looking at ways to use them in rapid prototyping scenarios, where the most common manufacturing techniques, in the case of soft-robotics, are moulding and stereolithography. Roels et al. [52] recently showed the possibility of 3D-printing a Diels-Alder polymer capable of self-healing. The printing process required modifications with respect to classic extrusion-based 3D-printing, as these polymers do not melt, even above their glass transition temperature. Unfortunately, the authors do not give clear details on the resolution achievable with this revised technology. They also tested their process by manufacturing a soft gripper and showing that the healing capabilities of the original material are completely recovered by the printed component 24 hours after printing.

As these materials get more popular, they also find their way to the field of soft-robotics. Their use in more classic examples can be found in [43, 13] where soft pneumatic actuators and grippers are developed, starting from sheets of self-healing polymer. Recently, there have also been studies focusing on self-healing of functionality rather than mechanical integrity, in particular in the field of stretchable electronics [16, 53]. In [49], Li et al. developed the inkjet based printing of galinstan, a Ga-In-Sn liquid metal. Using the newly developed printing process, the authors embedded an electric circuit into a PDMS substrate and showed that, after being severed, the circuit can still function without any visible loss in conductivity, once the two halves are brought back in contact. A slightly different approach is that in [50, 54] where EGaIn, an eutectic gallium-indium based liquid metal, is used. In this case, droplets of the metal are dispersed in the elastomeric matrix during fabrication. As an oxide film forms on the surface of each droplet, making them electrically insulated from one another. Electric circuits can then be created by a mechanical sintering process during which the tip of a stylus is run on top of the surface. The pressure causes adjacent droplets to coalesce, creating a continuous conductive path. This circuit can then be used to transfer current for fault detection purposes [50] or to actuate the matrix through Joule heating [54].

These examples, apart from [50] and very recent works [55], show that the focus, in terms of applications, is the local level response from the material and there is no real integration

with the high-level controller, which remains uninformed of the local fault. An example is the work by Terryn et al. [13], where the damage is inflicted using a scalpel knife and then the actuator or gripper are put in the oven for the healing cycle to occur. In the entire process, the controller is not aware of the fault being present and does not adapt to help the healing process. A similar analysis is valid for [54]. The authors show a very interesting performance of their joule actuated soft device, which is capable of functioning even after severe damage. The main limitation is that there is no detection and feedback of that and consequently the system remains unaware of how close it is to catastrophic failure.

2.3 Embodied-intelligence and morphological computation

In recent years, researchers in the field of robotics have put increasing attention on cognition and what makes cognition possible. In particular, some say cognition has always been inextricably linked to the abstract concept of computation and they support this view by affirming that the body is as important as the mind in the cognitive process [56, 57]. To prove their point, they refer to instances where it seems that natural evolution led the morphology of living beings to be somewhat optimised for a specific task. In particular, they cite how softness plays a key role in helping animals and humans in achieving balance on uneven and rough surfaces. These observations, further elaborated, have led to the creation of the idea that the mind outsources computation to the body.

This novel view has sparked debates, specifically on what computation actually means. Some authors remain critic, stating that morphological computation is just another form of physical computation [58]. In particular they argue that the concept of outsourcing is actually hiding the fact that computation is just avoided. Some others try to further distinguish systems in various classes. For example, Müller et al. [59] define "(1) morphology that facilitates control, (2) morphology that facilitates perception, and the rare cases of (3) morphological computation proper". This distinction serves to focus the problem by trying to eliminate the clear cases of physics driven behaviour and physical computation. An example they propose is the passive walker, a contraption that can mimic human walking without any active control taking place.

Despite the debate, the field has produced some interesting results and has linked itself to the field of soft robotics. Being their body made of soft, stretchable materials, soft robots represent the best ground for testing the founding hypotheses of morphological computation. In [60], the authors exploit the selective stiffness of soft-rigid hybrid fingers to obtain a robotic hand that can exhibit adaptive performance. Hauser et al. [61] try to give a theoretical framework to morphological computation applied to compliant robots. In particular, they

create an analogy between the soft body and the artificial neural networks programmed in computers. The material is modelled as a system of masses interconnected by nonlinear springs. Exactly as happens in their software counterparts, some points on the surface represent the inputs to the neural networks, while others are chosen as outputs. The inputs are mechanically stimulated and the readout from the system is represented by the displacement of the output points. This analogy has been successfully implemented in [62, 63], where a soft body tentacle actuator was controlled using only the shape of the robot itself as input. This example, known as reservoir computing, pushes the analogy a step further by mixing artificial neural networks and morphology-based computation [64]. The full computational network consists of an input and output layers implemented in software and the hidden layers represented by the soft body. Only the weights of the output layer can be tuned, making the learning process much faster.

The literature on embodied intelligence shines a light on the fact that the body can be more than just an agglomerate of different materials and indeed can be used to help the controller in carrying out complex tasks. Despite some interesting results having been achieved in this respect, it seems that the application to soft robots is still limited. In particular, it is believed that morphological computation can be one important tool in pursuing the goal of resilience. In fact, by combining purposeful mechanical design, sensing and interaction with the environment, one should be able to achieve local level computation and use it to drive localised resilient responses as well as feed the results back at system-level to gain behaviour adaptation.

2.4 Soft robotics and robotic implants

The landscape of surgical devices is rapidly changing as more and more robotic tools are developed and employed. Many solutions have been proposed for actuation and motion transfer, as well as techniques to miniaturise the end effectors [65, 66]. Despite this increasing popularity of robotics in surgeries, its use in long term treatments is still very limited. This is linked to the necessity to meet very strict safety and reliability standards as well as intelligent control algorithms capable of facing complex and uncertain conditions and of taking the necessary decisions without threatening the surrounding tissues and organs. Despite these difficulties, the envisaged benefits of robotic implants are nearly countless. In terms of the treatment itself, one can list customisation, continuous and more precise control and closed loop control [67]. By carefully selecting exteroceptive sensors, doctors can monitor in real time the status of the tissue the implant is operating on and consequently adapt the treatment.

In addition, if compared to traditional surgical robots, some benefits are reduced hardware cost and bulkiness [67].

In recent years, with the advent of soft robotics, things have started to change, with the introduction of devices that can help in treating heart conditions, long-gap oesophageal atresia, short bowel syndrome, neurological disorders and others [7, 68, 69, 67, 8, 70–73]. In all these applications, compliance plays a key role in achieving the necessary safety in implant-tissue interaction, with minimised tissue inflammation and foreign body response, and that is also why soft robotics is now heavily used in the field of biomedical engineering.

Soft robots were first developed in industrial settings to provide better grippers that could interact with soft or fragile objects or adapt to various shapes. A vast number of polymeric materials have been used during the years and new ones are constantly being introduced and studied, some also showing self-healing capabilities [74, 2, 75, 54, 13]. Alongside these, less standard materials have been developed such as biogels and hydrogels that are biocompatible and biodegradable [17, 40]. More recently, researchers have started merging mechanical compliance with advanced functionalities such as conductivity, leading to the development of stretchable electronic circuits [49, 50, 54, 72, 71]. Another important area of research has been that of soft sensors. The aim is to provide robots with closed loop control and localised sensing, while still maintaining their compliance. Examples of sensors range from strain sensors to pressure sensors, to humidity and temperature sensors [76–78, 17, 54].

In terms of actuation, the approaches have been diverse in nature, based on the type of material used. The most common choice amongst researchers is pneumatics, but other means of actuation include hydraulics, electricity, and temperature or Joule-heating based actuation. Often, the goal is that of mimicking actuators present in biological systems. Artificial muscles have been extensively investigated and vary widely in technology: McKibben muscles, also known as artificial pneumatic muscles, are among the oldest; shape memory elastomer based muscles exploit temperature changes or electrical stimuli to obtain contraction of the matrix; a similar approach is used in tensile and torsional yarn actuators [79–83, 43, 75]. Gong et al. [84] even achieved a soft rotary actuator based on peristaltic motion. This diversity in approaches has led to the development of soft robots capable of outstanding shape-change abilities (e.g. strains over 100%, shape matching). In [85–88] the authors developed a completely soft robot that can grow from the tip, like the roots of a plant would do, and reshape in different coiling configuration as well as retract and change growing path. Yim and Sitti [89] developed an example of programmable self-assembling soft matter able to switch between a pre-programmed three dimensional shape and a string of tiny interconnected cubes. Morin et al. [90] even experimented with camouflage by developing soft devices capable of changing colour, apparent shape, pattern and luminescence by exploiting microfluidic

networks embedded in the elastomeric body. The literature on soft grippers provide a vast number of examples of the capabilities of soft robots in terms of compliance to the outside environment and deformation capabilities: upon actuation, these grippers deform and adapt to the shape of the objects they need to grasp [91–93]. Other examples of shape matching include the work by Jin et al. where kirigami patterns are used to control the deformation and final shape of pneumatic soft actuators upon inflation [94]. In contrast, sheer softness and deformability of materials are usually exploited in wearable devices such as the sensorised patches developed in [17, 95, 96].

With the discovery of new materials and the ever-increasing complexity of designs, there has been a growing need for novel rapid prototyping techniques to be used in the fabrication of soft robots. Alongside more traditional methods such as moulding, additive manufacturing, stereolithography in particular, is the most used technology. Nowadays, researchers have access to multimaterial 3D-printers, capable of layering soft and bio-inspired materials and self-healing polymers [97, 52]; this results in faster and more precise fabrication as well as increased complexity of achievable geometries.

Despite the advances in design, materials and fabrication, soft robotics is still a newer research area and key challenges remain to be solved. In particular, if on the one hand compliance is one if not the key advantage of soft robots when compared to traditional hard ones, on the other hand it leads to very complex problems in terms of modelling and control [98, 99, 2]. The lack of rigid components has highlighted the profound difficulties of traditional methods when dealing with highly non-linear systems with infinite or nearly infinite degrees of freedom [2, 99, 100]. A common approach in the field is to exploit the recent results in machine learning and artificial intelligence to learn direct and inverse kinematics by trial and error [100–102, 79]. Despite such methods having been successfully applied, it is difficult to use them to extract the same amount of information that a traditional model would provide. Another key challenge to solve is that of accurate sensing. Having only a very limited number of sensors when compared to the degrees of freedom leads to overlapping conditions, where the same joint sensory output corresponds to different states of the robot [100]. In addition, most of the design phase is still linked to previous experience and a clear and comprehensive design framework is still lacking [99]. Modularity could help in this respect, even though most of the examples analysed so far heavily depend on the application and the reuse of the same geometries for different purposes is challenging.

Despite all of these challenges, soft robots have been capable of interesting performances such as shape change and growth, sometimes leading to novel solutions to known problems, a clear example being the universal gripper [103]. In recent years they even showed the possibility of integrating with micro-fluidics, leading to completely soft robots, without

on-board electronics, substituted by microfluidic controllers [104, 105].
One key challenge that remains to be solved in a comprehensive and pervasive way is that of resilience. If it is true that compliance makes robot-environment interactions safe, this is only true for the environment, as soft robots can easily fail when coming in contact with sharp objects, for example. Although some researchers have started looking at material self-healing as a possible solution [43, 13, 50, 106], we believe the approach still lacks generality and potential in the diversification of responses to faults. Moreover, in most cases it still depends on the intervention of human operators for the healing process to occur [43, 13], which is in open contrast with the goal of fully autonomous and self-sufficient machines.

Chapter 3

Software-based resilience for a Flexible Extendable Robotic Implant

This chapter presents the development of a sensor fault detection and identification framework for an extendable flexible robotic implant and that of a robotic tissue simulator developed to validate such framework. This work is part of two journal publications. In the following section, an overview of the work is introduced, followed by a more in-depth analysis of the contributions and the methodology used for the study. The two papers then follow, as submitted to the *IEEE Transactions on Medical Robotics and Bionics* and to the *IEEE Robotics and Automation Letters*.

3.1 Summary of the publications

The Flexible Extendable Robotic Implant, or FERI, was developed to treat specific medical conditions, such as long-gap oesophageal atresia and short bowel syndrome, through mechanostimulation. Upon implantation and over a period of several weeks, the robot is meant to gently pull on the soft tissue it is connected to, stimulating cell proliferation and overall tissue growth. After the tissue has lengthened the desired amount, the implant is removed through a second surgery.

The lengthening of tissue over time means that the implant must be capable of extending, or "growing" with the tissue, in order to maintain the effectiveness of the treatment. In addition, previous studies have found that fully rigid implants can cause tissue scarring and fibrosis and it is generally accepted that these conditions can be reduced by matching the stiffness of the implant to that of the surrounding tissue.
As visible in Fig. 3.1A, the FERI achieves this with its flexible rack, which grants bending

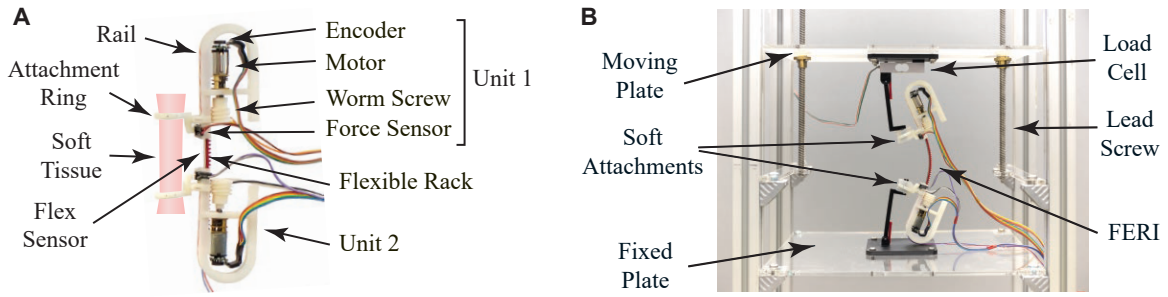

Fig. 3.1 **Details of the FERI and the robotic tissue simulator** (**A**) The Flexible Extendable Robotic Implant (FERI) and its main components. Two mirrored unites are connected together through a flexible rack. Special attachment rings allow the robotic implant to be sutured to tubular soft tissue. (**B**) The FERI connected to the robotic tissue simulator. A load cell measures the force being exerted by the robotic implant and feeds it back to the controller of the tissue simulator which in turn controls the motion of the moving plate.

capabilities as well as some torsional flexibility. The device consists of two mirrored units, each composed of a U-shaped rail, an attachment ring, a DC-motor with magnetic encoder and a worm screw. A force sensor is placed between the attachment ring and the rail, to feed back the force that the device is exerting on the tissue. The coupling between the worm screw and the rack gives the FERI the capability of extending up to a maximum of 80 mm. In addition, a flex sensor is attached to the back of the flexible rack and allows the bending angle of the rack to be measured. Upon implantation, the robot is connected to the soft tissue by suturing the attachment rings to it. It then proceeds to extend, tensioning the tissue, until the target reaction force is reached. This process is called mechanostimulation and is meant to stimulate tissue growth through faster cell proliferation. One of the key advantages of the FERI compared to previous non-robotic treatments, is the possibility of having precise real-time measurements of the force in situ, as well as the capability of tuning the treatment based on the readings coming from the sensors. As the tissue grows, the robot extends to maintain the correct pulling force on it, encouraging further cell multiplication.

One of the key requirements for such medium/long-term robotic implants to be adopted is resilience: for any hardware fault that makes the device unresponsive or, worse, dangerous, surgery is needed to replace the faulty device with a new one. This in turn translates into higher risk and discomfort for the patients. As presented in the literature review section of this manuscript, an array of software-based techniques have been investigated in the past, as a way of endowing robots with resilience. Although varied, these can be generally categorised into model-driven and data-driven. As the name suggests, the first ones require a more or less accurate model of the robotic device, that is then used to detect and identify possible

faults in sensors and actuators. Approaches that do not require a model fall in the second group. In this case, a large amount of data is collected from the robot during a training stage, while no fault is present. This data is then compared with sensory output when the robot is deployed and, if a large enough discrepancy is found, a fault is detected and then identified through different algorithms. In the case of this study, a data-driven approach was selected due to the lack of information about the behaviour of biological soft tissues, which constitute a surrounding environment for the implants, their changing viscoelasticity and growth. The dynamic interaction between tissue and robot is made even more difficult by the compliant nature of the body of the FERI. Experimental validation would require in-vivo implantation in animals, which cannot be considered a viable solution in the initial phases due to cost and animal welfare.

Any fault-detection and identification framework has to be able to take into account the effect of the growth of the soft tissue, which produces a gradual lengthening of the FERI itself. In order to be able to perform extensive characterisation of the implant performance, a robotic tissue simulator was developed first. Fig. 3.1B shows some of its key components. The robotic implant is placed between a fixed plate and a moving one. A load cell can sense the force that the robot is exerting and it feeds it back to the simulator controller, which in turn uses an impedance control algorithm to move the moving plate according to the desired viscoelastic model and parameters. These can be easily changed, in real time, to simulate changes in the behaviour of the soft tissue, such as increased stiffness due to fibrosis. In addition to replicating the viscoelastic behaviour of soft tissue, the simulator can, in principle, be used to replicate the growth of the tissue, by gradually moving the two plates further apart. Due to the limited amount of information available in the literature, in this study, a linear relationship between applied force and growth rate was used. The growth rate factor was chosen solely based on the requirements of achieving the full FERI extension over a period of 24 hours.

With the tissue simulator ready, a fault detection and isolation framework for the FERI was finally developed and tested. The framework only deals with sensor faults and can only cope with single point failures, meaning that only one sensor can become faulty at any given instant. The method is a data-driven one, based on Canonical Correlation Analysis (CCA) between the sensor readings, and can take into account tissue growth over time. In this approach, the readings from one or more sensors are used to predict the readings of a target sensor. If the residual between the prediction and the true value coming from the sensor surpasses a set threshold, a possible fault is detected. The identification step poses some additional challenges due to the limited number of sensors that are present. In the case of the force sensors, the identification is straightforward, as each sensor reading can be predicted in

two ways: using the other force sensor readings and using a combination of encoders and flex sensors readings. For the encoders and flex sensor, it is not possible to directly disambiguate which of the two is faulty by just applying the residual generation and comparison steps. Both predictions of the flex reading made using the force sensors and encoders feedback generate residuals over the threshold, but there is no way of knowing if this is due to an abnormal value of the encoders, or of the flex sensor. To overcome this problem, which originates from a lack of redundancy of sensory information about the length and the bending angle of the robot, an active identification strategy was devised. In this process, the robot actively gains information about its own state through a partial retraction and re-elongation. These transient forces all signals to vary in a controlled way: all signals should decrease in value during the retraction and increase again during the re-elongation. Throughout the process, two correlation coefficients are computed: the one between the flex sensor and one of the force sensors and the one between the encoders and the same force sensor. At the end of the active identification process, If the sensor is working, its correlation coefficient with the force sensor is close to 1.0, while it becomes low, or even negative, when the sensor is faulty. Thanks to this added information, the disambiguation between flex sensor and encoders faults can be achieved without the need for additional sensors.

The contributions of this chapter can be subdivided between the two platforms. First, looking at the robotic tissue simulator, the device demonstrates a flexible way of simulating viscoelastic properties of soft tissue and tissue growth. In doing so, it represents a first of its kind attempt at developing a physical simulator for tissue regeneration robotic implants. In the case of the FERI, the main contribution is a data-driven approach at making a resilient robotic implant, through the development of a fault detection and identification framework that can exploit the flexible morphology of the robot to couple sensor signals and actively gain knowledge on the state of the system in case of a fault. In addition, the framework doesn't require steady-state conditions to be achieved. Finally, the two platforms together demonstrate an attempt to fully test a resilient robotic implant in a physiologically relevant environment, as a future viable alternative to in-vivo experiments in animals.

3.2 Publications

Page left intentionally blank

A physical soft tissue growth simulator for implantable robotic devices

Marco Pontin and Dana D. Damian

***Abstract*—In the development of surgical technologies, one of the challenges in their initial validation has been the creation of accurate bench-top tissue phantoms. Tissue phantoms made of elastomeric material have fixed mechanical properties and are not able to increase in size, so they cannot mimic growth process or change in mechanical properties of their real counterparts. In this work we present a novel real-time soft tissue simulator aimed at testing the in vivo dynamic behavior of robotic implants. The simulator is capable of reproducing mechanical properties of the biological tissue, e.g. viscoelasticity, as well as its metabolism, being able to grow up to 260 mm. A control strategy based on impedance control enables the simulation of changing mechanical properties in real-time, in order to recreate conditions such as fibrosis or tissue scarring. We finally show the platform in use with a soft implant. The electric actuation in conjunction with the 500 Hz control loop frequency guarantees fast and accurate response. We believe our platform has the potential to reduce the need for in vivo preclinical studies and shorten the path to clinical experimentation.**

***Index Terms*—Internal robots, Physical soft tissue simulator, Robotic implant, Tissue growth simulator**

I. Introduction

In the development of surgical technologies, one of the challenges in their initial validation has been the creation of accurate bench-top tissue phantoms [1], [2]. In vivo testing in animals still plays a key role in understanding the interaction between implants and the tissue they are operating on. Although these tests will remain an important step towards human implantation, reducing the need for these types of validation experiments should be a priority for researchers. A possible solution could be the development of bench-top soft tissue simulators that mimic the behavior of various soft tissues, making it possible to fully test the dynamic performance of the implants before in vivo experimentation. In the case of regenerative robotic implants (RI) that grow soft tissues as a result of mechanical stimulation [3]–[5], the tissue phantom should not only simulate the mechanical properties, but also simulate the metabolism of the tissue, e.g., its growth. This is of the utmost importance to fully test the safety and operation performance of such robots before in vivo implantation.

Soft tissue has been modeled using a number of approaches, ranging from simple linear elastic models to more complex and accurate viscoelastic ones [6]–[8]. In [9] the authors model the multi-layer esophageal soft tissue using Mooney-Rivlin, Ogden, and Neo Hookean models and then compare the three in terms of accuracy. Nekouzadeh et al. [10] propose an adaptive quasi-linear viscoelastic (QLV) model to simplify experimental tuning of the parameters and then test it by predicting the behavior of pure reconstituted collagen. In [11] the authors use a modified Voigt model to better describe the behavior of soft tissue at high frequencies.

Usual applications for these models are medical training, haptics, or for the automation and control of novel surgical tools [12], [13]. Computer based simulation is another possible use case, where the model is used in robotic surgical devices to provide feedback during surgical training. In [14], a model for esophageal tissue based on QLV is proposed and the parameters are tuned using samples of porcine esophagi. Ortiz and Lagos [15] develop a modified Kelvin model of viscoelasticity to be used in real-time surgical simulations. The same goal is pursued in [16], where the authors prefer an approach based on neural networks: both isotropic and anisotropic materials can be modelled and the resulting architecture is implemented in a physical haptic feedback device. Similarly targeting real-time simulation of soft tissues, Bao et al. [2] propose

M. Pontin is with the Sheffield Biomedical Robotics Lab, Automatic Control and Systems Engineering Department, University of Sheffield, Sheffield, UK (e-mail: mpontin1@sheffield.ac.uk).

D. D. Damian is with the Sheffield Biomedical Robotics Lab, Automatic Control and Systems Engineering Department, University of Sheffield, Sheffield, UK (e-mail: d.damian@sheffield.ac.uk).

This work was supported by the EPSRC under Grant EP/S021035/1, and EPSRC ERC DTP Scholarship.

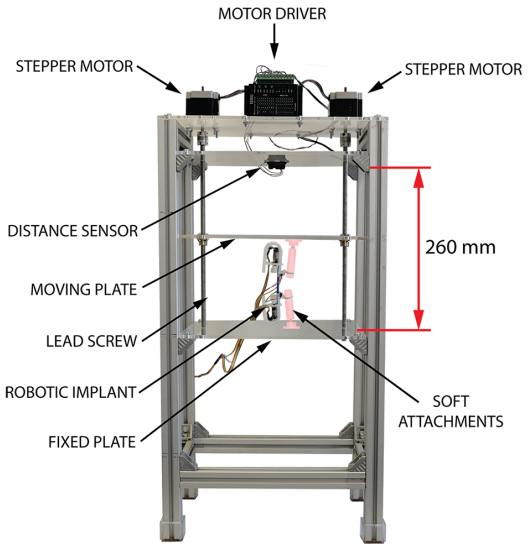

Fig. 1. The soft tissue simulator platform. The platform is used to validate robotic implants for tubular tissue growth.

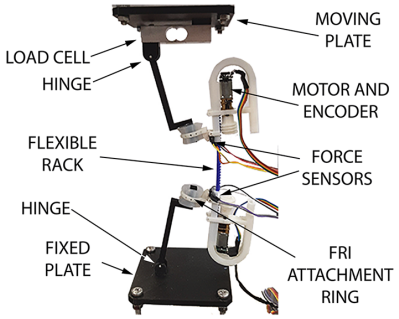

Fig. 2. Detail of the Flexible Robotic Implant (FRI) connected to the tissue simulator.

an hybrid model based on a multilayer structure of spheres interconnected using a three-parameter viscoelastic model. The resulting architecture is then tested against a porcine liver specimen. While these works offer useful insights for modelling biological soft tissues, they mainly entail simulation and do not address tissue growth.

The aim of this work is to develop the prototype of a robotic platform, shown in Fig.1, that simulates both the mechanical properties of the tissue, as well as its growth.

In previous works from our lab, we developed robotic implants that grow tubular organs, such as the esophagus or the intestine, by applying mechanostimulation [3], [5], [17], [18]. Both implants, when interacting with the organs, need to adapt the treatment based on the changing status of the tissue, which could show inflammation, scarring or fibrosis. The development process of the physical soft tissue simulator was therefore guided by two main requirements: flexibility in the types of tissue models that can be implemented and the ability to change model parameters in real-time. Such capabilities will be highly relevant in testing the robotic implants' dynamic operation as expected in vivo. An approach resembling that of impedance control was therefore used to achieve these requirements and provide fully tunable performance. Another important design goal was to have a large enough growth simulation potential so that the platform could be used to test applications such as long-gap esophageal atresia, where the tissue is expected to grow up to 100 mm during the treatment.

II. Materials And Methods

A. Physical Simulator

The platform simulates the viscoelastic properties of soft tissue, as well as its growth. It consists of a moving plate and a fixed one (Fig.1). The distance between these two plates represents the platform's capacity for growth simulation and, as displayed in Fig.1, this can reach 260 mm. A robotic device, able to extend itself (e.g. the FRI of Fig.2), is to be connected between the two plates and trigger the lengthening/shortening of the tissue phantom by applying forces. Two NEMA-23 stepper motors (57STH56, Phidgets), controlled by drivers (TB6600, TopDirect), move the top plate via a lead screw mechanism; meanwhile the force that the robotic implant is exerting is measured by a force sensor placed between the robot attachment and the same plate. The displacement is directly computed counting the motor's steps.

B. Controller

Controllers implemented in software dictate the behavior of the moving platform based on the interaction with the robotic implant. The viscoelastic controller designed for this application is shown in Fig.3a and was digitally implemented on an Arduino Nano microcontroller. In the block diagram, the transfer function $G_{tissue}(z) = \frac{\Delta x}{F}$ represents the

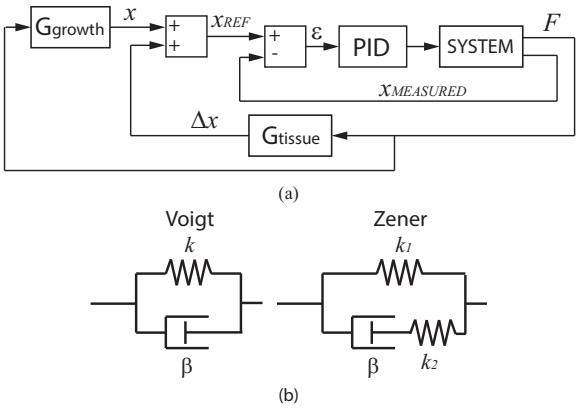

Fig. 3. (a) Block diagram of the system. x and Δx are the displacements due to growth and viscoelasticity, x_{REF} is the target displacement of the moving plate, ϵ the error between target and measured displacement $x_{MEASURED}$ and F is the measured force. (b) Mechanical equivalents of the Voigt and the Zener models.

model of the soft tissue and is used with the measured force to compute the appropriate displacement solely due to viscoelasticity. The force is also used in conjunction with the function $G_{growth}(z) = \frac{x}{F}$ to calculate the growth rate of the tissue. These two contributions, the one caused by the viscoelastic response of the tissue and that due to the growth, are then added together to generate the reference signal for the moving plate. A PID compensator finally serves as the position controller for the system.
To test the flexibility of the platform, G_{tissue} was first considered to be that of the Voigt model (Eq.1), whose mechanical equivalent is a spring and a dashpot in parallel as in Fig.3b; a second model, the Zener one (Eq.2) and Fig.3b, was then implemented. Meanwhile, G_{growth} was a simple linear function of the force applied by the robotic device.

$$F = kx + \beta\dot{x} \tag{1}$$

$$F + \frac{\beta}{k_2}\dot{F} = k_1 x + \frac{\beta\,(k_1 + k_2)}{k_2}\dot{x} \tag{2}$$

These two models are widely used in literature as benchmarks for describing viscoelasticity and have been also adopted to model the behavior of soft tissues [6]–[8], [11], [15]. Although being simple compared to other alternatives, we believe these two models strike a good balance between accuracy, ease of implementation, speed of computation and overall simplicity in parameter tuning, only requiring the knowledge of up to three coefficients to describe the viscoelastic behavior of the tissue. In particular, the ability to perform the simulation in real-time is key for this application. Both the PID controller loop and the tissue model that serves as input to the controller are updated at a frequency of 500 Hz. This frequency suffices for the envisaged application, as high frequency phenomena, over tens of Hertz are unlikely to occur.

C. Flexible Robotic Implant (FRI)

Before analysing the results, we briefly present the FRI, as this was used to explore the potential of the platform to mimic tissue properties while interacting with a real implant. The FRI uses a worm gear-rack mechanism to extend/retract with changing tissue length. The rack is flexible for mechanical compliance and force sensors transduce the tension applied to the tissue. During normal operation, a force controller ensures that the desired target mechanostimulation is maintained [3], [5]. As detailed in Fig.2, the FRI is coupled to the plates of the simulator using custom designed 3D printed components. The connection is achieved by sliding the Ecoflex 00-30 cylinders inside the implant's attachment rings. Hinges at the top and the bottom provide the necessary degrees of freedom during operation.

III. Results

In order to test the performance of the platform, preliminary experiments were conducted, generating the force signal directly in the software. Fig.4 shows the results of a ramp increase in the force input, from 0 to 2 N, with the growth disabled. The value of 2 N is consistent with what is realistically applied to the esophageal tissue during the Foker technique in the treatment of long-gap esophageal atresia [4]. One can observe the nonlinear behavior of the tissue due to G_{tissue}, mostly in the beginning and end of the transient phase. Both the Voigt and the Zener models were used: in the first case, the stiffness k was equal to 200 N/m, while the damping factor β was 20 Ns/m; in the second k_1 was 200 N/m, k_2 was 100 N/m and β was 20 Ns/m. These values were selected to make visualisation of the viscoelatic behavior easier. The test also shows that the PID controller is capable of following the desired reference signal with no overshoots. Fig.5 shows the results of a test where the growth was

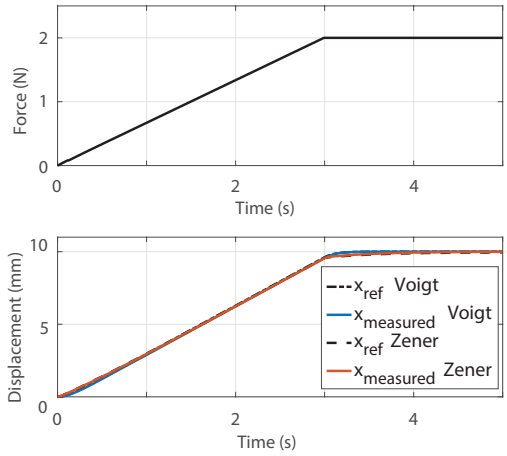

Fig. 4. Comparison between Voigt and Zener models with growth disabled and a ramp increase in the force input. (Top) Force input. (Bottom) Output target and measured displacements, using both the Voigt and the Zener models.

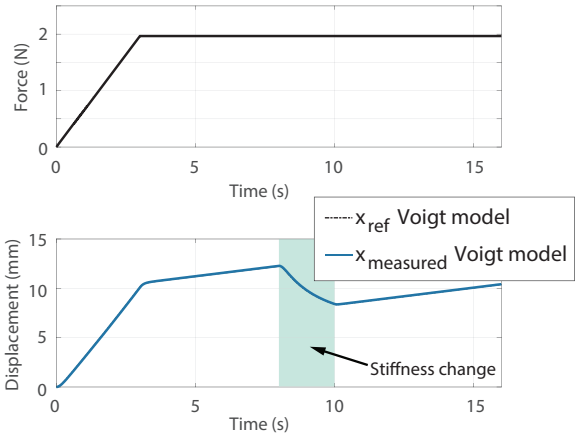

Fig. 5. Results of an experiment with tissue growth enabled and stiffness change at $t = 8$ s from 200 N/m to 300 N/m in 2 s. (Top) Force signal. (Bottom) Target and measured displacement of the moving platform of the tissue simulator.

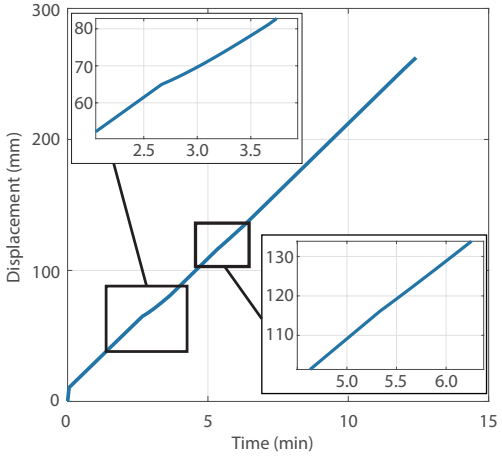

Fig. 6. Results with growth enabled throughout the experiment and two stiffness changes at $t = 2.6$ min and $t = 5.3$ min; with each transient lasting 1 min. The stiffness was first increased from 200 N/m to 400 N/m and finally to 600 N/m. The experiment shows the growth simulation potential of the platform, which can reach 260 mm.

enabled and equal to 0.35 mm/s and the simulated stiffness changed in a ramp from 200 N/m to 300 N/m in 2 s, from $t = 8$ s to $t = 10$ s. The viscoelastic model used for this test was the Voigt one. A similar experiment was then performed, but in this case the growth was enabled within the entire range, from 0 to 260 mm (Fig.6). Also, two tissue stiffness changes were simulated, one at $t = 2.6$ min and the second at $t = 5.3$ min, with each transient lasting 1 min. The stiffness varied from 200 N/m to 400 N/m and finally to 600 N/m. The Voigt model was used to simulate viscoelasticity. The ability to change the model in real-time means one can also simulate different conditions of the tissue, like scarring and fibrosis. This could be important in testing customized reaction strategies by the robotic implant, designed to prevent excessive strain on the tissue.

A second part of the experiments was devoted to a more realistic case study, with a robotic implant interacting with the simulator. The robotic device we used is the FRI. Fig.7 shows some preliminary results. The target force of the FRI, visible in the top chart of the figure, has a sudden drop from 0.45 N to 0.15 N. Consequently, the FRI starts retracting and the signals corresponding to the output of the force sensors and the force sensed by the load cell of the tissue simulator drop to the new value as well. The bottom chart shows the retraction of the platform, as a result of the decreased tension on the tissue phantom, according to a Voigt model with $k = 200$ N/m and $\beta = 80$ Ns/m. The results demonstrate good agreement between the various signals. Moreover, we can conclude that the dynamic performance of the platform is in line with that required for the application.

Discussion And Conclusion

In this work we presented a physical soft tissue growth simulator. The envisaged application is in

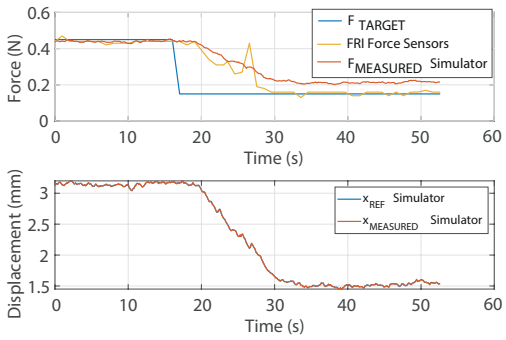

Fig. 7. Experiment with the Flexible Robotic Implant connected to the platform. (Top) The target force is decreased from 0.45 N to 0.15 N; (Bottom) as a consequence, the moving plate of the tissue simulator also retracts following the desired viscoelastic behavior. For this test the Voigt model was used with $k = 200$ N/m and $\beta = 80$ Ns/m.

conjunction with robotic implants in order to test their capabilities in a dynamic physical environment that can simulate dynamic changes in metabolism, e.g., tissue growth, and physiology, e.g. tissue fibrosis, relaxation. The approach is flexible, enabling different viscoelastic models to be simulated, as shown in the results section of the paper. The architecture makes it also possible to introduce real-time changes in the parameters, in order to simulate variations in the characteristics of the tissue itself such as increased stiffness. Although the biological tissue growth rates are lower, the values in this study were used to visualize the simulator's operation; the same holds true for the parameters k and β.

The physical platform could find broader applications in tissue engineering, control engineering and computer science as it enables the real-time simulation of viscoelastic tissue behaviors. Future developments include the use of the simulator in conjunction with the FRI to further study its fault-tolerant control strategy [3] and with soft implants [17], [18] to characterize their dynamic behavior.

References

[1] C. Choi, H. Han, B. An, and J. Kim, "Development of a surgical simulator for laparoscopic esophageal procedures," in *2006 International Conference of the IEEE Engineering in Medicine and Biology Society*, pp. 819–822, 2006.

[2] Y. Bao, D. Wu, Z. Yan, and Z. Du, "A new hybrid viscoelastic soft tissue model based on meshless method for haptic surgical simulation," *The open biomedical engineering journal*, vol. 7, pp. 116–124, 2013.

[3] L. Balasubramanian, T. Wray, and D. D. Damian, "Fault tolerant control in shape-changing in vivo robots," in *IEEE International Conference on Robotics and Automation (ICRA)*, pp. 5502–5508, 2020.

[4] D. D. Damian, K. Price, S. Arabagi, I. Berra, Z. Machaidze, S. Manjila, *et al.*, "In vivo tissue regeneration with robotic implants," *Science Robotics*, vol. 3, no. 14, 2018.

[5] M. Atwya, C. Kavak, E. Alisse, Y. Liu, and D. D. Damian, "Flexible and expandable robot for tissue therapies – modeling and design," *IEEE Trans on Biomedical Engineering*, 2020.

[6] N. Famaey and J. V. Sloten, "Soft tissue modelling for applications in virtual surgery and surgical robotics," *Computer methods in biomechanics and biomedical engineering*, vol. 11, no. 4, pp. 351–366, 2008.

[7] H. Delingette, "Toward realistic soft-tissue modeling in medical simulation," *Proceedings of the IEEE*, vol. 86, no. 3, pp. 512–523, 1998.

[8] R. K. Korhonen and S. Saarakkala, "Biomechanics and modeling of skeletal soft tissues," in *Theoretical biomechanics*, pp. 113–132, InTech Rijeka, Croatia, 2011.

[9] P. HajHosseini and M. Takalloozadeh, "An isotropic hyperelastic model of esophagus tissue layers along with three-dimensional simulation of esophageal peristaltic behavior," *Journal of Bioengineering Research*, vol. 1, no. 2, pp. 12–27, 2019.

[10] A. Nekouzadeh, K. M. Pryse, E. L. Elson, and G. M. Genin, "A simplified approach to quasi-linear viscoelastic modeling," *Journal of biomechanics*, vol. 40, no. 14, pp. 3070—-3078, 2007.

[11] X. Yang and C. C. Church, "A simple viscoelastic model for soft tissues in the frequency range 6-20 mhz," *IEEE transactions on ultrasonics, ferroelectrics, and frequency control*, vol. 53, no. 8, pp. 1404—-1411, 2006.

[12] D. D. Damian, A. H. Arieta, and A. M. Okamura, "Design and evaluation of a multi-modal haptic skin stimulation apparatus," in *2011 Annual International Conference of the IEEE Engineering in Medicine and Biology Society*, pp. 3455–3458, IEEE, 2011.

[13] S. Misra, K. Ramesh, and A. M. Okamura, "Modeling of tool-tissue interactions for computer-based surgical simulation: a literature review," *Presence: Teleoperators and Virtual Environments*, vol. 17, no. 5, pp. 463–491, 2008.

[14] W. Yang, T. Fung, K. Chian, and C. Chong, "Viscoelasticity of esophageal tissue and application of a QLV model," *ASME. J Biomech Eng*, vol. 128, no. 6, pp. 909—-916, 2006.

[15] J. E. Ortiz and R. Lagos, "A viscoelastic model to simulate soft tissue materials," *Journal of Physics: Conference Series*, vol. 633, no. 1, p. 012099, 2015.

[16] J. Zhang, Y. Zhong, and C. Gu, "Neural network modelling of soft tissue deformation for surgical simulation," *Artificial intelligence in medicine*, vol. 97, pp. 61–70, 2019.

[17] E. R. Perez-Guagnelli, S. Nejus, J. Yu, S. Miyashita, Y. Liu, and D. D. Damian, "Axially and radially expandable modular helical soft actuator for robotic implantables," in *2018 IEEE International Conference on Robotics and Automation (ICRA)*, pp. 4297–4304, 2018.

[18] E. Perez-Guagnelli, J. Jones, A. H. Tokel, N. Herzig, B. Jones, S. Miyashita, and D. D. Damian, "Characterization, simulation and control of a soft helical pneumatic implantable robot for tissue regeneration," *IEEE Transactions on Medical Robotics and Bionics*, vol. 2, no. 1, pp. 94–103, 2020.

Page left intentionally blank

IEEE ROBOTICS AND AUTOMATION LETTERS. PREPRINT VERSION. ACCEPTED JANUARY, 2023 1

Data-Driven and Compliance-Based Fault-Tolerance for a Flexible and Extendable Robotic Implant Coupled to a Growing Tissue

Marco Pontin[1] and Dana D. Damian[1,2]

***Abstract*—Robotic implants for real-time and long-term monitoring and therapies are being researched and could open new frontiers in the medical field. For these devices to see widespread adoption, though, key challenges still need to be overcome, including reliability. Over the years, many computational techniques have been developed to impart fault-tolerance to robots and industrial plants. However, the application of these approaches to robotic implants is still challenging, due to the lack of information about the complex behavior of soft tissue (e.g. growth, viscoelasticity) and robot-tissue interaction. In this paper, a novel fault detection framework for a flexible extendable robotic implant is presented. Based on Canonical Correlation Analysis, the approach exploits the flexibility of the robot to extrapolate information for fault identification purposes. The experiments are conducted with a soft tissue simulator, which can emulate the viscoelastic properties of tissue as well as its growth, providing a realistic testing platform. The experiments prove the reliability of the flexible extendable robotic implant and its robustness to system-level external disturbances. Long-term tests are also presented, where the implant extends 80 mm, to its full length, counteracting simulated hardware faults over a 24-hour period, and provide a promising basis for future in-vivo trials.**

***Index Terms*—Medical Robots and Systems, Failure Detection and Recovery, Compliant Joints and Mechanisms**

Manuscript received: September, 29, 2022; Revised November, 26, 2022; Accepted January, 20, 2023. This paper was recommended for publication by Jessica Burgner-Kahrs upon evaluation of the Associate Editor and Reviewers' comments. This work was supported by the EPSRC under Grant EP/X017486/1, and EPSRC ERC DTP Scholarship. Data available on the ORDA, doi 10.15131/shef.data.21163399.

[1]M. Pontin and D. D. Damian are with the Automatic Control and Systems Engineering Department, University of Sheffield, Sheffield, UK (e-mail: mpontin1@sheffield.ac.uk, d.damian@sheffield.ac.uk).

[2]D. D. Damian is with the Insigneo Institute for in silico Medicine, University of Sheffield, Sheffield, UK.

Digital Object Identifier (DOI): see top of this page.

I. INTRODUCTION

Over the last decade, robotic devices have become increasingly present in the medical field [1]. From teleoperated surgical robots to novel endoscopes, these systems are augmenting the capabilities of surgeons and enabling minimally invasive surgical procedures to benefit patients. The next frontier of medical technologies is represented by fully autonomous robots, that can navigate inside the human body, to the desired location, and perform a variety of tasks, potentially reducing surgical trauma and improving therapies beyond the surgical theater. Ingestible robots, guided by magnetic fields, are being researched to replace traditional surgical tools, endoscopes and drug delivery devices [2], [3], [4], [5]. Among these, origami micro-robots exploit folding and unfolding to adapt their capabilities through changes in body morphology, using smart materials and composites [6], [7], [8], [9], [10]. Implantable devices are being developed to carry out longer procedures over periods of weeks or months. Roche et al. presented a pneumatic soft heart sleeve to provide ventricular assistance [11], while our group previously researched an implantable robot that grows tissue to treat long-gap esophageal atresia and similar rare conditions [12]. Towards the same goal, in [13] and [14], pneumatic soft robots were developed.

Key obstacles to the widespread adoption of these robots still stand. Among these, concerns about their reliability need to be addressed, especially for implantable devices used for long-term therapies. Robots need to be resilient, so that their capabilities are not fully impaired by simple faults in one sensor or actuator. In terms of materials, new self-healing polymers have recently been discovered and used to develop resilient soft robots [15], [16], [17], [18]. On the software side, a significant amount of work

has already been done on fault detection and isolation techniques for industrial plants and robots, to develop fault-tolerant control strategies. Next to traditional model-based approaches, data driven ones have been investigated, that do not require precise models of the systems [19], [20], [21], [22]. More recently, with the advent of artificial intelligence, researchers have also experimented with machine-learning techniques for further improvement [23], [24].

In soft and flexible robotic implants for tissue growth, the adoption of such techniques is challenged by the lack of information about the behavior of biological soft tissues, which constitute a surrounding environment for the implants. Studying the dynamic interaction between tissue and robot is made even more difficult by the fact that these devices have bodies capable of morphology changes (e.g. extension, bending). In addition, experimental validation requires in-vivo implantation in animals, especially for tissue growth and regeneration robots, but this cannot be considered a viable solution in the long term due to cost and animal welfare.

This paper focuses on a Flexible and Extendable Robotic Implant (FERI) developed for multi-week tissue growth therapies by mechanostimulation (tissue tensioning), within the gastrointestinal tract [25], [26], [27]. The main contribution is the development of a fault detection and identification framework for the FERI, robust to system-level external disturbances and unaffected by the physical elongation of the robot and simultaneous growth of the tissue over time. The technique exploits the flexible nature of the FERI, which couples all sensors' signals together, and displays how softness and flexibility can be harnessed to extract information for fault detection purposes. A further contribution is the use of a robotic soft tissue simulator (STS) platform [28] to fully test the proposed framework. This serves both as a way to provide a comprehensive controlled environment to carry out experiments on the FERI, as well as a viable alternative to in-vivo testing to reduce animal use.

II. FAULT DETECTION FRAMEWORK

The goal of this work is to develop a general fault detection and isolation technique for the FERI, one that can cope with its flexion and extension capability, and corresponding tissue growth, and be expanded in the future if more sensors are added to the system. In addition, the data-driven approach of the CCA technique used in this study makes transferring the method to other implantable robotic devices simpler.

A. The Flexible Extendable Robotic Implant in details

The FERI, shown in Fig. 1(a), consists of two identical and mirrored units connected by a flexible PolyLactic Acid (PLA) rack, onto which a flex sensor (Spectra Symbol FS-L-095-103-ST) is attached. Each unit is composed of a 3D-printed Acrylonitrile-Butadiene-Styrene (ABS) rail, a DC motor (Pololu Micro Metal Gearmotor 298:1 HPCB 12V dual-shaft) with magnetic encoder (Pololu 12CPR Magnetic Encoder Kit), a 3D-printed ABS worm gear connected to the motor, an ABS attachment ring, also 3D-printed, that is used to connect the robot to the soft tissue, and a force sensor (Honeywell FSS1500NSR) to measure the tension applied to the tissue. The FERI soft encapsulation, consisting of a biocompatible sleeve, is ignored in this study.
When the robot is active and attached to a tissue, the worm gear transfers its motion to the rail through the rack, causing the implant to extend or retract, therefore increasing or relaxing the tension applied to the tissue, which has been shown to lead to tissue growth [12]. The overall elongation potential for the robot is 80 mm. A closed loop control is used to keep the target force equal to an optimal value and reject external disturbances while tensioning the tissue. Fig. 1(b) shows the FERI connected to the plates of the robotic STS, described in section III-A.

B. Sensor output models

A fault detection and identification framework for the FERI was developed and presented in [26]. This was based on comparing the Pearson correlation coefficients between readings from pairs of sensors and could reliably detect sensor faults when tested with a silicone tissue phantom. The phantom was capable of replicating viscoelastic properties, but could not achieve growth like a live tissue. When tissue growth is taken into account, however, this method could lead to false positives. As the esophageal tissue grows, the FERI extends with it

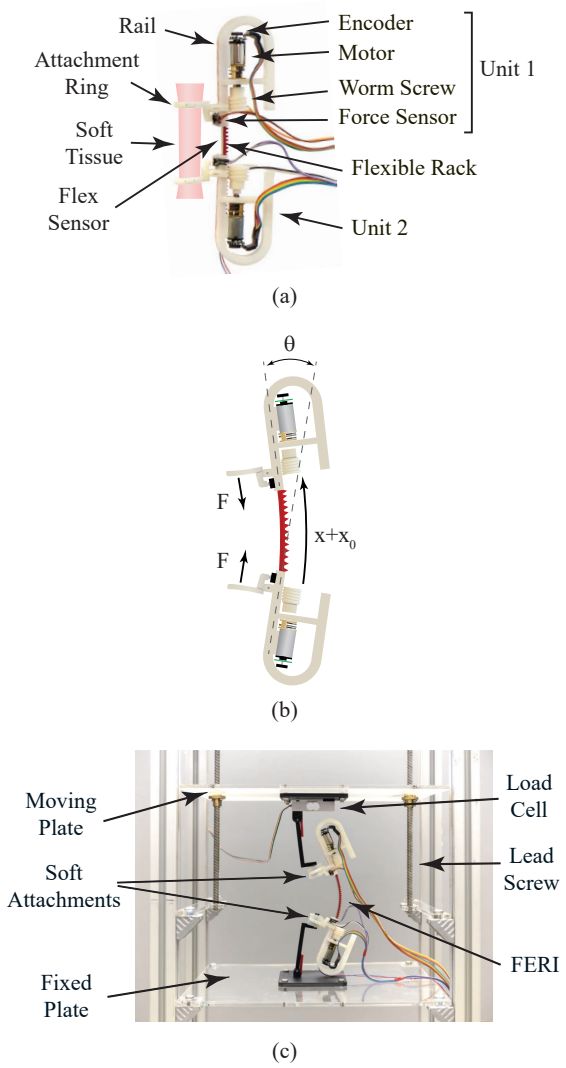

Fig. 1. The Flexible Extendable Robotic Implant. (a) Detailed view of the robot and all its components. (b) Degrees of freedom of the FERI system and forces acting on it. (c) Detailed view of the FERI connected to the plates of the robotic STS. The soft attachments are important to simulate the in-vivo coupling and degrees of freedom. In the photo the FERI is bending from the force it applies to the two plates.

and the length of the rack subject to bending stresses increases. As a result, even when the force being applied to the esophageal stub is constant, the rack deformation increases. The consequent increase in the flex sensor output leads to a drop in the correlation coefficient between this and the force sensors. Computing the correlation coefficient over a fixed time frame T, using a sliding window approach, is not a solution either. The correlation coefficient relies on the data having definite trends, but the FERI operates in steady state for most of the time. A more general detection and identification strategy is therefore needed, one which takes into account the growth process.

The fault detection algorithm presented here is derived from a Canonical Correlation Analysis (CCA) based method [29], [30], [31]. We assumed all sensors' output can be described by

$$y_i = k_i u_i + \epsilon_i \quad ,$$

where y_i is the output from sensor i, u_i is the corresponding physical input and ϵ_i is the measurement noise. We also made the following standard assumption on the noise:

$$\epsilon_i \sim \mathcal{N}(0,\, s_i^2) \quad ,$$

which is to say that the noise is normally distributed with zero mean and constant variance s_i^2.
Let us first consider the two force sensors. Being connected to the same flexible rack, these should measure the same force, minus a constant offset due to gravity and manufacturing tolerances. One can therefore write a simple linear relationship between the two:

$$\hat{F}_1 = aF_2 + b \quad . \tag{1}$$

$\hat{F}_1$ represents the predicted value of sensor F_1 using the data collected from sensor F_2. The coefficients a and b are to be computed through a least square approach, using experimental data. At this stage, the variance σ^2 between the data and the model is also calculated. A similar approach can be used for the relation between the encoders and the flex sensor. Analysing the FERI, one can think of the flex sensor output θ as a function of the length of the robot and the force applied to the tissue. Therefore:

$$\hat{\theta}_i = f\,(x, F_i) \quad i = 1, 2 \quad ,$$

where only a generic encoder term x is considered, representing the sum of the two encoder outputs, hence the total elongation of the rack. $\hat{\theta}_1$ is the predicted flex sensor output based on the readings from F_1, while $\hat{\theta}_2$ is based on the readings from F_2. Here, the function f assumes the form:

$$f\,(x, F_i) = c_1 x + c_2 F_i + c_3 \quad , \tag{2}$$

to represent a linear relationship between force and length and bending angle of the rack. The coefficients and the variance between model and data

are computed as previously described. The detailed experimental procedure for the data acquisition and the results of the calibration procedure are described in section III.

C. Fault detection and identification process

While in operation, the FERI is performing force control, to achieve the desired tensioning of the soft tissue. In parallel, at each time step, the sensors are sampled and residuals are computed by comparing the current sensors' outputs with their predicted values:

$$e_{F_1,F_2} = F_1 - (aF_2 + b) \tag{3}$$

$$e_{x,F_1,\theta} = \theta - (c_1 x + c_2 F_1 + c_3) \tag{4a}$$

$$e_{x,F_2,\theta} = \theta - (c_1 x + c_2 F_2 + c_3) \quad . \tag{4b}$$

The fault detection relies on a T^2-test on these residuals. For each e_i, the algorithm computes the statistic

$$J_i = \frac{e_i^2}{\sigma_i^2} \ ,$$

where σ_i^2 is the variance computed at the training stage as detailed before. A fault is detected if $J_i > J_i^{th}$, where J_i^{th} is an appropriate threshold value, which can be determined in a number of ways [29], [30], [31]. In this study, the Fisher–Snedecor distribution $\mathcal{F}$ was used [29]:

$$J_i^{th} = \frac{p\,(N^2-1)}{N\,(N-p)} \mathcal{F}\,(p, N-p, \alpha) \quad . \tag{5}$$

Where p is the number of variables used for the prediction, N is the number of data points used for the training and $\alpha \in [0, 1]$ is the significance level. This last parameter plays an important role in the fault detection process. A high value of α increases the threshold value, meaning the algorithm is less prone to detecting false positives. At the same time, a higher residual e_i is needed to trigger the detection, which in turn delays the recognition of real faults in the sensors. When a fault is detected, the FERI proceeds to the isolation step. In the case of the two force sensors, the process is straightforward. When $J_{F_1,F_2} > J_{F_1,F_2}^{th}$ the FERI checks $J_{x,F_1,\theta}$ and $J_{x,F_2,\theta}$. If the first is greater than the threshold $J_{x,F,\theta}^{th}$, then F_1 is deemed faulty, else if $J_{x,F_2,\theta}$ surpasses the threshold, then F_2 is considered faulty.

In the case of the flex sensor and the encoders, it is not possible to disambiguate solely based on the information coming from the T^2-test. This is because a value of $J_{x,F_i,\theta}$ above threshold could be caused either by an abnormal value of the encoder or flex sensor. No additional insights come from J_{F_1,F_2}, which remains below its threshold value. To overcome this problem, an active identification strategy is used, that involves a partial retraction of the FERI. Exploiting the fact that the possible fault does not influence the force sensors, the FERI retracts until a predetermined ΔF is achieved. It then elongates back to reach the target force again. During this transient, the output from one of the force sensors, the flex sensor and the encoder are used to compute and update two correlation coefficients: $\rho_{F,\theta}$ between the force sensor and the flex sensor and $\rho_{F,x}$ between the encoder and the same force sensor. At the end of the test, the two correlation coefficients are compared. As the sensors' signals are highly correlated, both correlation coefficients should be close to one. In the case of a fault, one naturally drops, therefore identifying the faulty sensor. The entire control strategy is shown in Fig. 2, while all the fault detection and identification conditions are summarized in Table I. As visible in the figure, the fault detection is performed at each time-step, every 10 ms in reality, which in turn corresponds to the maximum delay between a fault first appearing and it being picked up by the algorithm.

TABLE I
SUMMARY OF FAULT DETECTION AND IDENTIFICATION CONDITIONS

Sensor	Condition
F_1	$J_{F_1,F_2} > J_{F_1,F_2}^{th}$, $J_{x,F_1,\theta} > J_{x,F,\theta}^{th}$
F_2	$J_{F_1,F_2} > J_{F_1,F_2}^{th}$, $J_{x,F_2,\theta} > J_{x,F,\theta}^{th}$
θ	$J_{x,F_1,\theta} > J_{x,F,\theta}^{th}$, $J_{x,F_2,\theta} > J_{x,F,\theta}^{th}$, $\rho_{F,\theta} < \rho_{F,x}$
x	$J_{x,F_1,\theta} > J_{x,F,\theta}^{th}$, $J_{x,F_2,\theta} > J_{x,F,\theta}^{th}$, $\rho_{F,x} < \rho_{F,\theta}$

III. EXPERIMENTS AND RESULTS

The experimental setup, visible in Fig. 1(b), consists of the FERI and the STS that our group developed and presented in [28]. This platform enables the simulation of the viscoelastic properties of soft tissues and also simulates their growth process, making it ideal to test the new fault detection framework of the FERI.

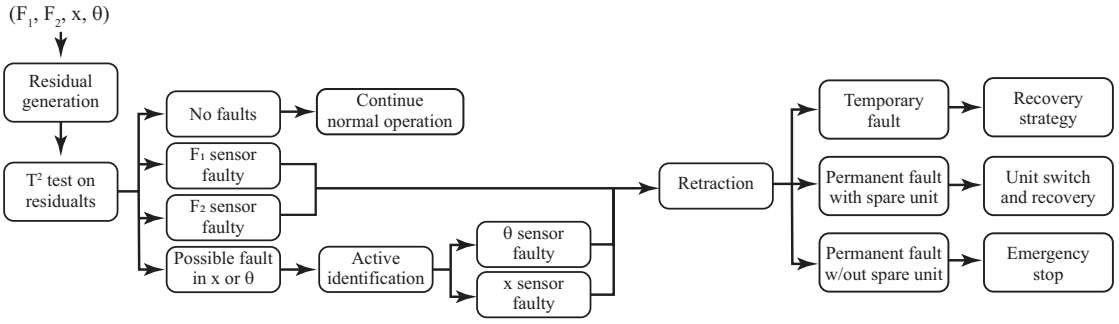

Fig. 2. Flowchart of the overall fault-tolerance framework of the FERI system. At each time step, if no faults are detected, the FERI continues working as normal. If a fault is detected in one of the force sensors, the retraction reflex is immediately triggered to prevent damage to the soft tissue. When a possible fault in the flex sensor, signal θ, or encoder, x, is detected, the active identification strategy is executed to disambiguate between the two. Once a complete identification is obtained, the FERI retracts. The subsequent recovery strategy is attempted twice. If it fails both times, the fault is deemed permanent and a unit switch occurs. If both units are faulty, the FERI retracts and executes an emergency stop.

A. The soft tissue simulator

As visible in Fig. 1(b), the STS consists of a fixed plate and a moving one. A load cell is placed between the implant being tested and the moving plate, in order to measure the force that the implant is applying. With this information, the STS controller uses a viscoelastic model (the Voigt model in this study) to compute the equivalent displacement that a soft tissue subject to the same force would display and moves the plate accordingly. In addition, a very slow movement, linearly dependant on the force, is imparted to the moving plate to simulate long-term tissue growth. The STS has a full range of motion of 260 mm, while its non-backdrivable nature makes it possible to simulate a variety of stiffness values, from very soft, to fully rigid. As visible in the figure, the robotic implant is connected to the plates of the STS using two Ecoflex™ 00-30 attachments, designed to simulate in-vivo attachment to a soft tissue while still preserving all the relevant degrees of freedom.

B. Off-line training of the fault-tolerance framework

In order to calibrate the coefficients of equations (1) and (2), the FERI was placed in the STS and the plates were set at a fixed initial distance $L_0 = 15$ mm. No viscoelastic behavior was simulated at this stage. The FERI was then programmed to go from 0 N to 2 N and back to 0 N in a linear fashion. Meanwhile, the signals from encoders, force sensors and the flex sensor were recorded. The plates of the STS were moved further apart in 5 mm increments before the cycle was repeated. The maximum value of L_0 that still allowed the FERI to reach 2 N was $L_0 = 50$ mm. The off-line training of the fault detection algorithm started with the force sensors, F_1 and F_2. The result of the calibration procedure, shown in Fig. 3(a), led to a value of $a = 1.15$ and $b = -0.03$ ($R^2 = 0.89$, $RMSE = 0.23$), while the resulting standard deviation was $\sigma^2 = 0.05$. In the case of the joint calibration of the flex sensor with the encoders and force sensors, the fitting procedure resulted in $c_1 = 0.21$, $c_2 = 7.65$, $c_3 = -2.79$, $\sigma^2 = 6.17$ when using F_1 ($R^2 = 0.89$, $RMSE = 2.49$) and $c_1 = 0.29$, $c_2 = 8.19$, $c_3 = -5.85$, $\sigma^2 = 7.30$ using F_2 ($R^2 = 0.87$, $RMSE = 2.70$). Fig. 3(b) and (c) show the results of this data fitting process. As visible in the figures, although no viscoelastic behavior was simulated, the FERI could still elongate exploiting the flexibility of its rack.

Having computed all the necessary parameters, the thresholds for the fault detection algorithm, set according to (5) with $N = 1860$ and $\alpha = 0.95$, are $J^{th}_{F_1,F_2} = 3.84$ and $J^{th}_{x,F,\theta} = 6.00$. As a consequence, a prediction residual e_{F_1,F_2} of 0.19 N would be needed to achieve $J_{F_1,F_2} > J^{th}_{F_1,F_2}$, while errors $e_{x,F_1,\theta} = 37.0°$ and $e_{x,F_2,\theta} = 43.7°$ are needed for $J_{x,F_1,\theta}$ and $J_{x,F_2,\theta}$ to surpass their threshold. Table II summarizes the values and meaning of the main parameters.

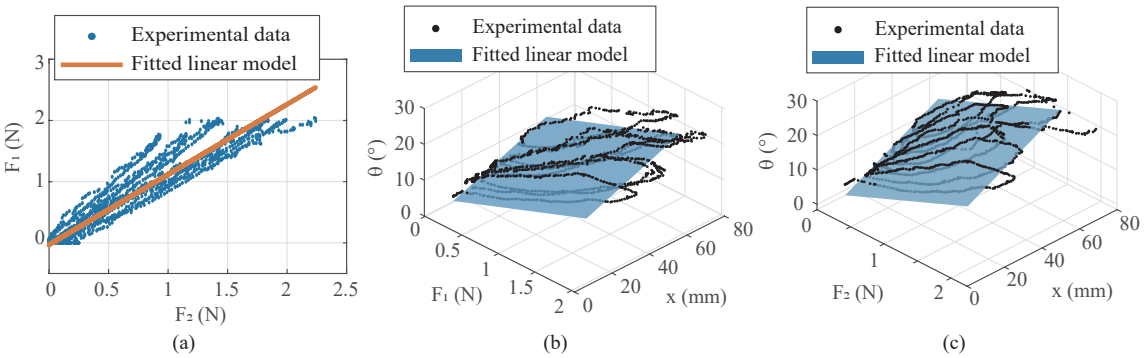

Fig. 3. Off-line training results. (a) Linear fitting between force sensors F_1 and F_2 data. (b) Linear fitting of the flex sensor data θ using the information from F_1 and the encoders x. (c) Linear fitting of the flex sensor data θ using the information from F_2 and the encoders x.

TABLE II
SUMMARY OF FAULT DETECTION AND IDENTIFICATION PARAMETERS

	Parameter	Value	Meaning
$\hat{F}_1$	a	1.15	Coefficients used for the prediction of F_1 readings
	b	-0.03	
	σ^2	0.05	
$\hat{\theta}_1$	c_1	0.21	Coefficients used for the prediction of θ readings using F_1 and x
	c_2	7.65	
	c_3	-2.79	
	σ^2	6.17	
$\hat{\theta}_2$	c_1	0.29	Coefficients used for the prediction of θ readings using F_2 and x
	c_2	8.19	
	c_3	-5.85	
	σ^2	7.30	
	α	0.95	Significance level of the T^2-test on the residuals
	N	1860	Number of data-points used for the training
	$J^{th}_{F_1,F_2}$	3.84	Threshold value for the T^2-test on $\hat{F}_1$
	$J^{th}_{x,F,\theta}$	6.00	Threshold value for the T^2-test on $\hat{\theta}_1$ and $\hat{\theta}_2$

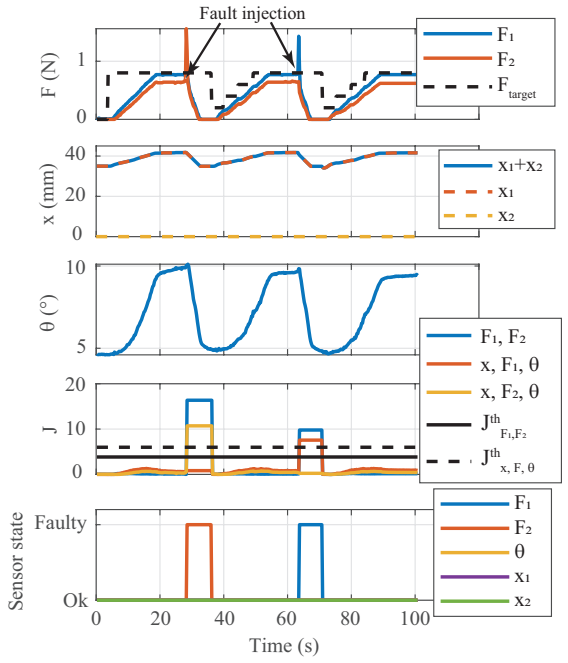

Fig. 4. F_1 and F_2 sensors fault examples. During this test, two abnormal reading faults were injected into the FERI system: one in F_2 at $t = 27.5$ s and the second in F_1 at $t = 63.25$ s. Each fault was recognised and correctly classified (third and bottom charts). After the identification, the FERI fully retracts for safety purposes and then gradually elongates back, continuously checking if the fault is still present. If the robot can reach the target force without detecting the fault for a second time, the recovery is considered successful and normal operation is reestablished.

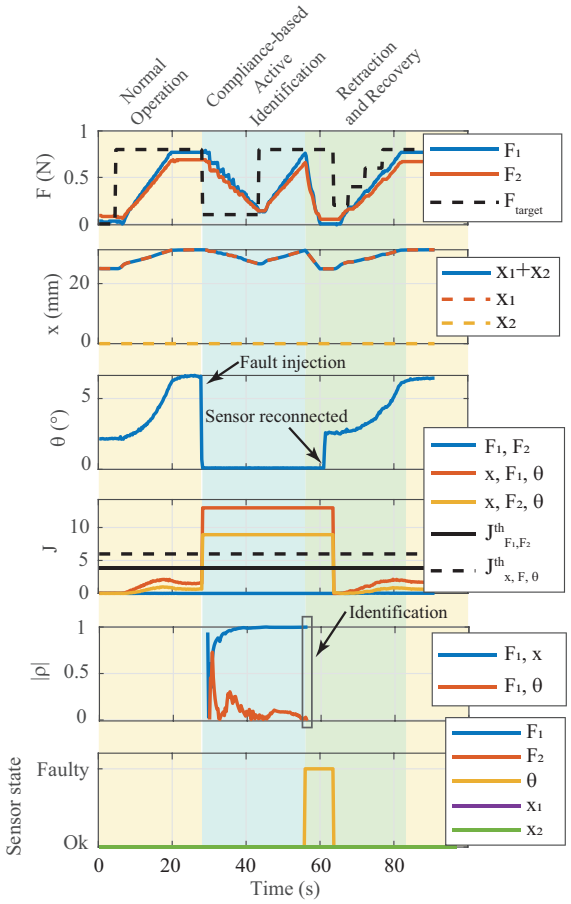

Fig. 5. Active fault identification strategy. A fault in the flex sensor was injected into the system by disconnecting the sensor from the controller board. The sensor reading dropped causing $J_{x,F_1,\theta}$ and $J_{x,F_2,\theta}$ to surpass the threshold. J_{F_1,F_2} remained below its threshold, triggering the active identification step ($t = 27.8$ s). The target force was decreased and increased again, causing a retraction followed by an elongation of the FERI. At the end of the transient ($t = 56.0$ s), the correlation coefficient analysis resulted in $|\rho_{F_1,x}| = 0.98$ while $|\rho_{F_1,\theta}| = 0.04$, The flex sensor was therefore correctly identified by the FERI as the faulty sensor.

C. Short-term fault-tolerance experiments

The STS controller was set up to replicate the viscoelastic properties of esophageal tissue using a Voigt model with $k = 100$ N/m and $\beta = 20$ Ns/m [28]. The growth of the soft tissue was modelled in the code as a linear function of the force measured by the load cell of the STS: $\frac{dl}{dt} = \gamma F$, with $\gamma = 1.5$ μmN^{-1}s^{-1}. Short experiments were first run to test the performance of the proposed fault-tolerance framework. Fig. 4 shows an experiment where faults were injected in both F_2 ($t = 27.5$ s) and F_1 ($t = 63.25$ s). This was achieved by pressing on the force sensors, producing an abnormal spike in the readings. Each fault caused one pair of J-statistics to surpass the relevant thresholds (fourth chart in Fig. 4), therefore triggering the detection process. In both cases, the FERI was capable of correctly identifying the faulty sensor by using the residual testing procedure described in section II-C, as visible in the bottom chart of Fig. 4. After the identification, the FERI fully retracts for safety purposes and then gradually elongates back, continuously checking if the fault is still present. If the robot can reach the target force without detecting the fault for a second time, the recovery is considered successful and normal operation is reestablished. Fig. 5 is an example of a flex sensor fault that was achieved by fully disconnecting the sensor from the controller board (third chart from the top in Fig. 5). The sensor signal suddenly dropped to zero, causing $J_{x,F_1,\theta}$ and $J_{x,F_2,\theta}$ to surpass the threshold value, $t = 27.8$ s in the fourth chart. This triggers the active identification strategy to disambiguate which sensor is faulty between the flex sensor and the encoder of the FERI unit in use at the moment of the fault. As mentioned before, this procedure exploits the flexible morphology of the FERI and the high interplay between its sensory information. The target force signal is used to cause the FERI to retract and then elongate. This "V" shaped transient is chosen to enhance the correlation coefficient based identification process. If the faulty sensor had a constant downward drift for example, a simple retraction of the FERI would still lead to a high value of the correlation coefficient ρ, making a positive identification more difficult. Inverting the slope of the force sensor reading during the identification step, by retracting and then elongating the FERI, makes it possible to overcome such scenarios. In the experiment, the active identification phase lasted 25 s, during which the correlation coefficients $\rho_{F_1,x}$, between F_1 and the encoders, and $\rho_{F_1,\theta}$, between F_1 and the flex sensor, were constantly updated (fifth chart in Fig. 5). When the transient was over ($t = 56.0$ s), the correlation coefficients had an absolute value of 0.98 and 0.04 respectively, clearly identifying the flex sensor as the faulty one.

D. Long-term fault-tolerance experiments

Long-term experiments were then conducted, to evaluate the performance and robustness of the

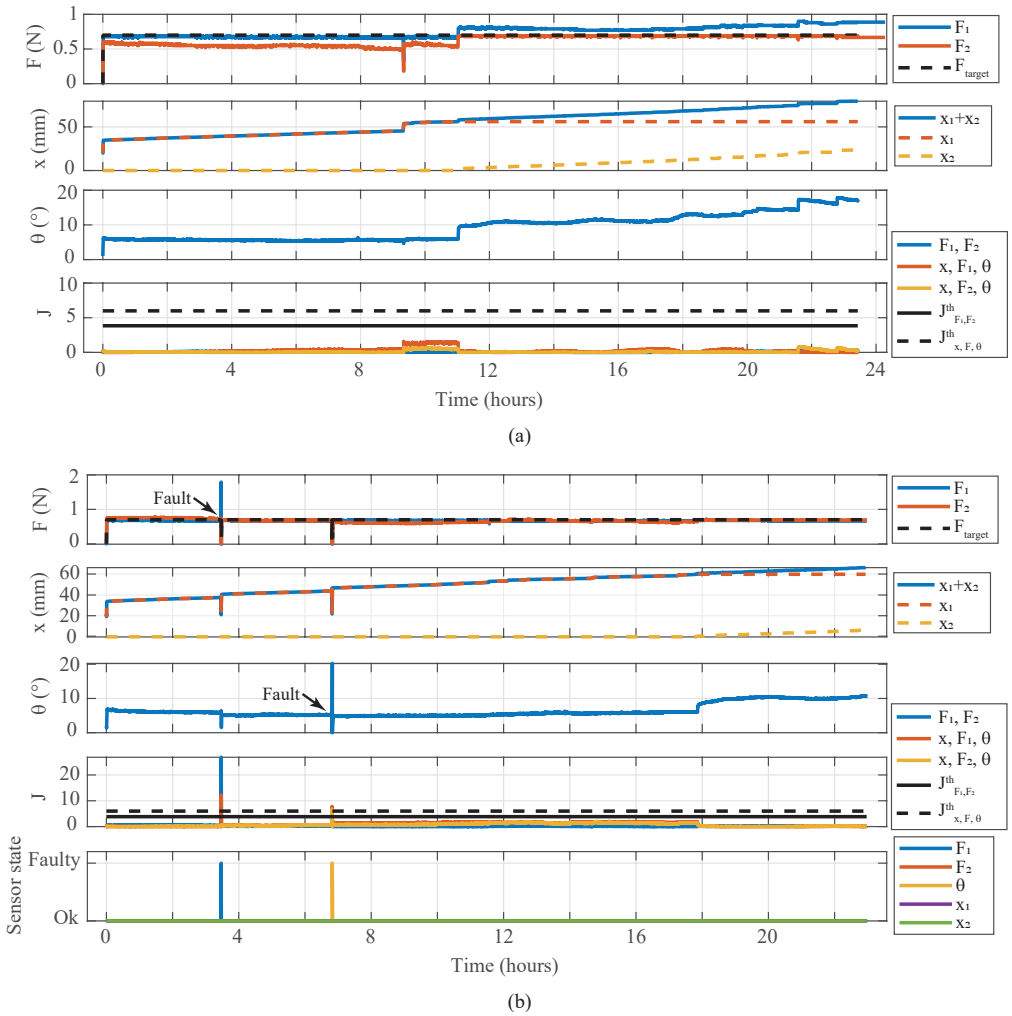

Fig. 6. Long-term experiments. (a) The FERI was left to work in the STS platform for about 24 hours. No faults were injected in the FERI hardware and tissue growth simulation was enabled in the tissue simulator. Over the 24 hours, the FERI was therefore capable of reaching its full elongation potential with a total length of 80 mm. The second chart from the top also shows how, once one side of the rack has fully come out of the rail of the first unit, the FERI automatically switches to the mirror unit to continue the elongation. Around the 9 hours and 20 minutes mark, a glitch in the behavior of the STS resulted in a sudden movement of the moving plate, causing the FERI to react quickly. As the information coming from all sensors during the event remained coherent, the residuals remained well below the threshold values (fourth chart from the top), proving good robustness of the fault detection framework against external disturbances acting on the FERI system as a whole. (b) This second experiment lasted 23 hours. Temporary faults were injected in the force sensor F_1 ($t = 3h28m$) and the flex sensor ($t = 6h4m8$). Both of them were correctly identified by the FERI (bottom chart). The recovery after each fault was successful, so the robot went back to normal operation and kept elongating till the end of the experiment.

system over longer periods of time, as well as over the entire elongation range. Fig. 6 presents the results of two of such experiments. The first one, Fig. 6(a), lasted about 24 hours and the FERI elongated from an initial length of 10 mm, to its limit of 80 mm. This experiment was used as a reference for the behavior, so no faults were injected in the FERI hardware. In spite of this, a glitch in the STS code led to a sudden movement of the moving plate, which in turn caused the FERI to react ($t = 9h20m$ hours in the figure). This external disturbance was picked up by all sensors and their outputs remained coherent with each other, as demonstrated by the low residuals during the event (bottom chart in Fig. 6(a)). This demonstrates good robustness of the fault-tolerance framework against external disturbances acting on the FERI system as a whole. In contrast, Fig. 6(b) shows a second experiment, where two faults were injected in the FERI hardware, one in the force sensor F_1 at $t = 3h28m$ (top chart in the figure) and one in the flex sensor at $t = 6h48m$ (third chart). Both faults were promptly detected and correctly identified, as visible in the bottom chart of the figure. As the faults were only temporary, after the recovery step, the FERI continued functioning and elongating for the remainder of the experiment, almost reaching full elongation. The experiment was terminated by the STS, whose moving plate reached its end-stop.

DISCUSSION AND CONCLUSION

In this paper, we presented a novel CCA-based fault detection and identification framework for a flexible extendable robotic implant. The approach uses the information coming from a number of in-situ sensors and exploits the flexibility of the robot for fault identification. The new framework is advancing the previous one [26], based on the Pearson correlation coefficient. This previous method had the advantage of not requiring any training data, only relying on the assumption that sensor signals in the FERI system are highly correlated. This simplifying assumption, though, is broken due to the coupling between the robot and a growing tissue, which leads to a loss of correlation between the sensor readings and consequent false positives as the FERI gradually elongates. The new framework is fully tested in multiple experiments, with the help of a robotic soft tissue simulator platform. Finally, the FERI behavior and capabilities are assessed in long-term experiments, lasting around 24 hours. These last experiments are a first step in a further performance evaluation of the FERI over weeks-long trials, to simulate in-vivo long-term implantation.
The CCA-based framework exploits the strong relation between the sensors on board the FERI, enabled by the flexible nature of the robot itself. The softness was imparted to the robot to reduce scarring and damage to the surrounding soft tissue upon implantation, but also proves to be a key factor in the new fault detection process. If the rack was rigid, the flex sensor would not measure any meaningful deformation, therefore removing any link between the force readings and the encoder measurements. To cope with the limited number and types of sensors available on board, both of which further decrease when a fault occurs, an active identification step was devised. This is used to acquire additional information, in the form of correlation coefficients between sensor readings, when disambiguating which sensor is the faulty one.

Once tuned using training data, the fault detection framework proved to be a fast and reliable way to isolate possible faults in the sensors. The experiments also showed how the proposed framework is robust to system level external disturbances on the FERI, as, during these, the sensor signals vary unexpectedly, but the coherence between them is maintained. Localized disturbances, that only affect the readings of one sensor, have not been considered in developing the fault detection process. Using a significance level α of 0.95, prediction errors of 0.19 N, $37.0°$ and $43.7°$ are needed to trigger the fault detection thresholds. These were considered a good starting point for this study. Reducing them further could be done in the future in two ways: by reducing α, which also means increasing the probability of false positives in the detection process, or by reducing the standard deviation σ of the residuals at the training stage. The first solution does not pose a threat to the soft tissue, but could compromise the long-term effectiveness of the FERI. The second alternative necessitates better models, for more precise predictions. This, though, is rendered difficult by the nature of the 3D-printed flexible rack, which shows pronounced hysteretic behavior, as well as by the uncertainty of the in-vivo implantation and interaction between the robot and the surrounding tissue. The use of simpler linear

models to generate the predictions was preferred, knowing that this would lead to higher standard deviations, to compensate, at least in part, for these uncertainties. In-vivo experiments might provide insights and training data, which could lead to better models and lower standard deviations as a result.
One current shortcoming of the proposed method is the fact that it can only predict single point faults, meaning that only one fault can be present at any given moment and if two sensors become faulty, the algorithm does not have enough information to reach a conclusion. In the future, this could be overcome by adding more sensors which would lead to overall redundancy in information. Additionally, the STS platform can be further adapted to create a more physiologically relevant environment for the FERI overall. In conclusion, this study shows how soft body morphology can be harnessed to gain additional information on a system and represents a first step in developing more resilient soft implantable growing robots, which is key for their adoption in the real world.

REFERENCES

[1] P. E. Dupont, B. J. Nelson, M. Goldfarb, B. Hannaford, A. Menciassi, M. K. O'Malley, N. Simaan, P. Valdastri, and G.-Z. Yang, "A decade retrospective of medical robotics research from 2010 to 2020," *Science Robotics*, vol. 6, no. 60, p. eabi8017, 2021.

[2] B. J. Nelson, I. K. Kaliakatsos, and J. J. Abbott, "Microrobots for minimally invasive medicine," *Annual review of biomedical engineering*, vol. 12, pp. 55–85, 2010.

[3] K. Kong, S. Yim, S. Choi, and D. Jeon, "A robotic biopsy device for capsule endoscopy," *Journal of medical devices*, vol. 6, no. 3, pp. 1–9, 2012.

[4] S. Yim, K. Goyal, and M. Sitti, "Magnetically actuated soft capsule with the multimodal drug release function," *IEEE/ASME Transactions on Mechatronics*, vol. 18, no. 4, pp. 1413–1418, 2013.

[5] S. Yim and M. Sitti, "Design and rolling locomotion of a magnetically actuated soft capsule endoscope," *IEEE transactions on robotics*, vol. 28, no. 1, pp. 183–194, 2012.

[6] Q. M. P. Lahondes, A. Wilmot, and S. Miyashita, *Origami-Inspired Microrobots*. Berlin, Heidelberg: Springer Berlin Heidelberg, 2020, pp. 1–11.

[7] K. Kuribayashi, K. Tsuchiya, Z. You, D. Tomus, M. Umemoto, T. Ito, and M. Sasaki, "Self-deployable origami stent grafts as a biomedical application of ni-rich tini shape memory alloy foil," *Materials science & engineering. A, Structural materials : properties, microstructure and processing*, vol. 419, no. 1, pp. 131–137, 2006.

[8] Y. Ge, T. D. Lalitharatne, and T. Nanayakkara, "Origami inspired design for capsule endoscope to retrograde using intestinal peristalsis," *IEEE robotics and automation letters*, vol. 7, no. 2, pp. 5429–5435, 2022.

[9] A. du Plessis d'Argentre, S. Perry, Y. Iwata, H. Iwasaki, E. Iwase, A. Fabozzo, I. Will, D. Rus, D. Damian, and S. Miyashita, "Programmable medicine: Autonomous, ingestible, deployable hydrogel patch and plug for stomach ulcer therapy," in *IEEE International Conference on Robotics and Automation (ICRA)*. IEEE, 2018, pp. 1511–1518.

[10] H. Li, G. Go, S. Y. Ko, J.-O. Park, and S. Park, "Magnetic actuated ph-responsive hydrogel-based soft micro-robot for targeted drug delivery," *Smart materials and structures*, vol. 25, no. 2, pp. 27 001–27 009, 2016.

[11] E. T. Roche, M. A. Horvath, I. Wamala, A. Alazmani, S.-E. Song, W. Whyte, Z. Machaidze, C. J. Payne, J. C. Weaver, G. Fishbein, J. Kuebler, N. V. Vasilyev, D. J. Mooney, F. A. Pigula, and C. J. Walsh, "Soft robotic sleeve supports heart function," *Science translational medicine*, vol. 9, no. 373, 2017.

[12] D. D. Damian, K. Price, S. Arabagi, I. Berra, Z. Machaidze, S. Manjila, S. Shimada, A. Fabozzo, G. Arnal, D. V. Story, J. D. Goldsmith, A. T. Agoston, C. Kim, R. W. Jennings, P. D. Ngo, M. Manfredi, and P. E. Dupont, "In vivo tissue regeneration with robotic implants," *Science Robotics*, vol. 3, no. 14, p. eaaq0018, 2018.

[13] E. Perez-Guagnelli, J. Jones, A. H. Tokel, N. Herzig, B. Jones, S. Miyashita, and D. D. Damian, "Characterization, simulation and control of a soft helical pneumatic implantable robot for tissue regeneration," *IEEE Transactions on Medical Robotics and Bionics*, vol. 2, no. 1, pp. 94–103, 2020.

[14] N. Herzig, J. Jones, E. Perez-Guagnelli, and D. D. Damian, "Model and validation of a highly extensible and tough actuator based on a ballooning membrane," in *IEEE International Conference on Robotics and Automation (ICRA)*, 2021, pp. 11961–11967.

[15] S. Liu, K. Li, I. Hussain, O. Oderinde, F. Yao, J. Zhang, and G. Fu, "A conductive self-healing double network hydrogel with toughness and force sensitivity," *Chemistry : a European journal*, vol. 24, no. 25, pp. 6632–6638, 2018.

[16] R. F. Shepherd, A. A. Stokes, R. M. D. Nunes, and G. M. Whitesides, "Soft machines that are resistant to puncture and that self seal," *Advanced Materials*, vol. 25, no. 46, pp. 6709–6713, 2013.

[17] S. Terryn, J. Brancart, D. Lefeber, G. V. Assche, and B. Vanderborght, "Self-healing soft pneumatic robots," *Science Robotics*, vol. 2, no. 9, p. eaan4268, 2017.

[18] S. Liu, O. Oderinde, I. Hussain, F. Yao, and G. Fu, "Dual ionic cross-linked double network hydrogel with self-healing, conductive, and force sensitive properties," *Polymer*, vol. 144, pp. 111–120, 2018.

[19] S. X. Ding, *Model-based fault diagnosis techniques: design schemes, algorithms, and tools*. Springer Science & Business Media, 2008.

[20] R. Isermann, "Model based fault detection and diagnosis methods," in *Proceedings of 1995 American Control Conference - ACC'95*, vol. 3, 1995, pp. 1605–1609 vol.3.

[21] T. Zhang, W. Zhang, and M. M. Gupta, "Resilient robots: Concept, review, and future directions," *Robotics (Basel)*, vol. 6, no. 4, p. 22, 2017.

[22] M. Blanke, M. Kinnaert, J. Lunze, M. Staroswiecki, and J. Schröder, *Diagnosis and fault-tolerant control*. Springer, 2006, vol. 2.

[23] J. Bongard, V. Zykov, and H. Lipson, "Resilient machines through continuous self-modeling," *Science*, vol. 314, no. 5802, pp. 1118–1121, 2006.

[24] A. Cully, J. Clune, D. Tarapore, and J.-B. Mouret, "Robots that can adapt like animals," *Nature*, vol. 521, no. 7553, pp. 503–507, 2015.

[25] M. Atwya, C. Kavak, E. Alisse, Y. Liu, and D. D. Damian, "Flexible and expandable robot for tissue therapies – modeling and design," *IEEE Trans on Biomedical Engineering*, pp. 568–578, 2020.

[26] L. Balasubramanian, T. Wray, and D. D. Damian, "Fault tolerant

control in shape-changing in vivo robots," in *IEEE International Conference on Robotics and Automation (ICRA)*, 2020, pp. 5502–5508.

[27] C. Duffield, A. F. Smith, D. Rus, D. Damian, and S. Miyashita, "Wirelessly magnetically actuated motor for tissue regeneration robotic implant," in *IEEE International Conference on Intelligent Robots and Systems (IROS)*. IEEE, 2022, pp. 465–471.

[28] M. Pontin and D. Damian, "A physical soft tissue growth simulator for implantable robotic devices," *IEEE Transactions on Medical Robotics and Bionics*, vol. 2, no. 4, pp. 553–556, 2020.

[29] S. Yin, S. X. Ding, X. Xie, and H. Luo, "A review on basic data-driven approaches for industrial process monitoring," *IEEE transactions on industrial electronics (1982)*, vol. 61, no. 11, pp. 6418–6428, 2014.

[30] Z. Chen, S. X. Ding, K. Zhang, Z. Li, and Z. Hu, "Canonical correlation analysis-based fault detection methods with application to alumina evaporation process," *Control engineering practice*, vol. 46, pp. 51–58, 2016.

[31] Z. Chen, S. X. Ding, T. Peng, C. Yang, and W. Gui, "Fault detection for non-gaussian processes using generalized canonical correlation analysis and randomized algorithms," *IEEE transactions on industrial electronics (1982)*, vol. 65, no. 2, pp. 1559–1567, 2018.

3.3 Additional results

This section aims to display the content of the video uploaded as supplementary material to the paper published in the IEEE Robotics and Automation Letters journal [107]. The experiment consists in a full test of the fault-tolerant framework, with multiple fault detection and identification steps, including the use of the active identification strategy, and a unit switch around $t = 225\,\mathrm{s}$.

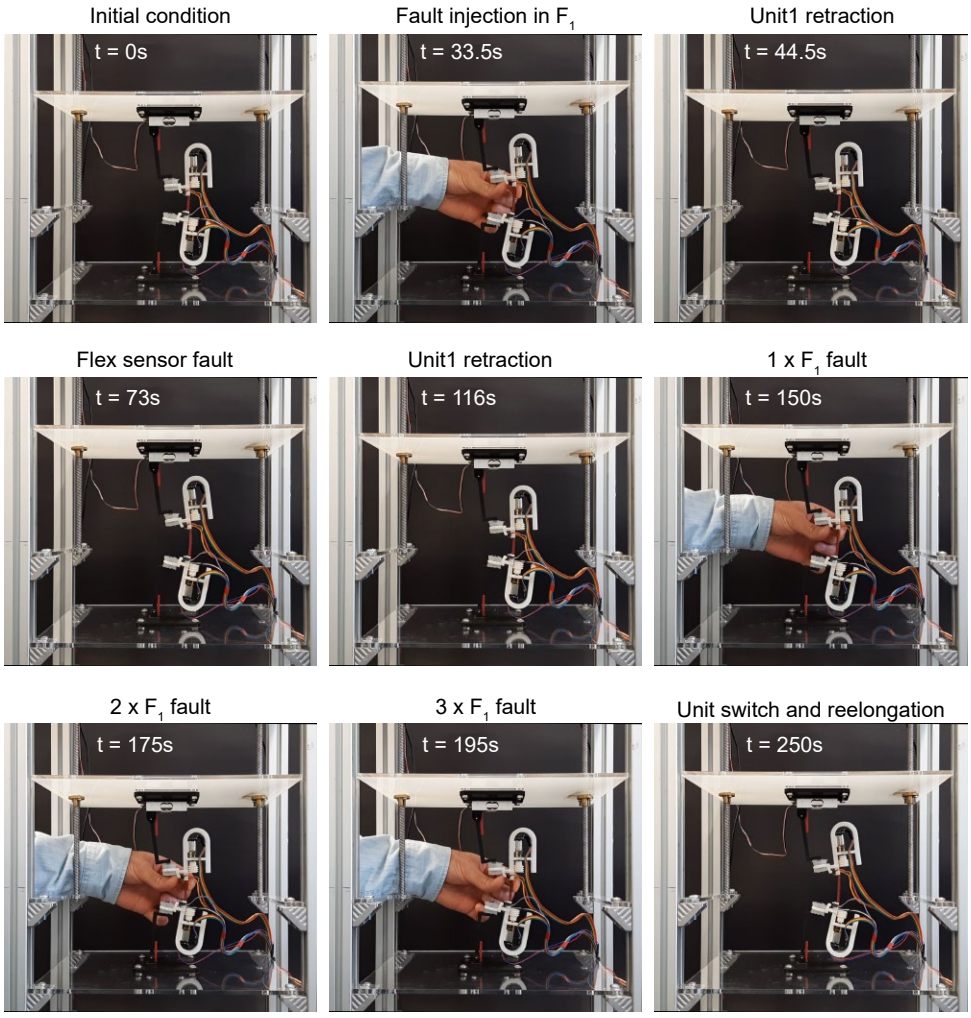

Fig. 3.2 **FERI demo video stills**. Still images pf the fault injection experiment captured from the video uploaded as supplementary material to [107]. The times refer to the charts of Fig. 3.3

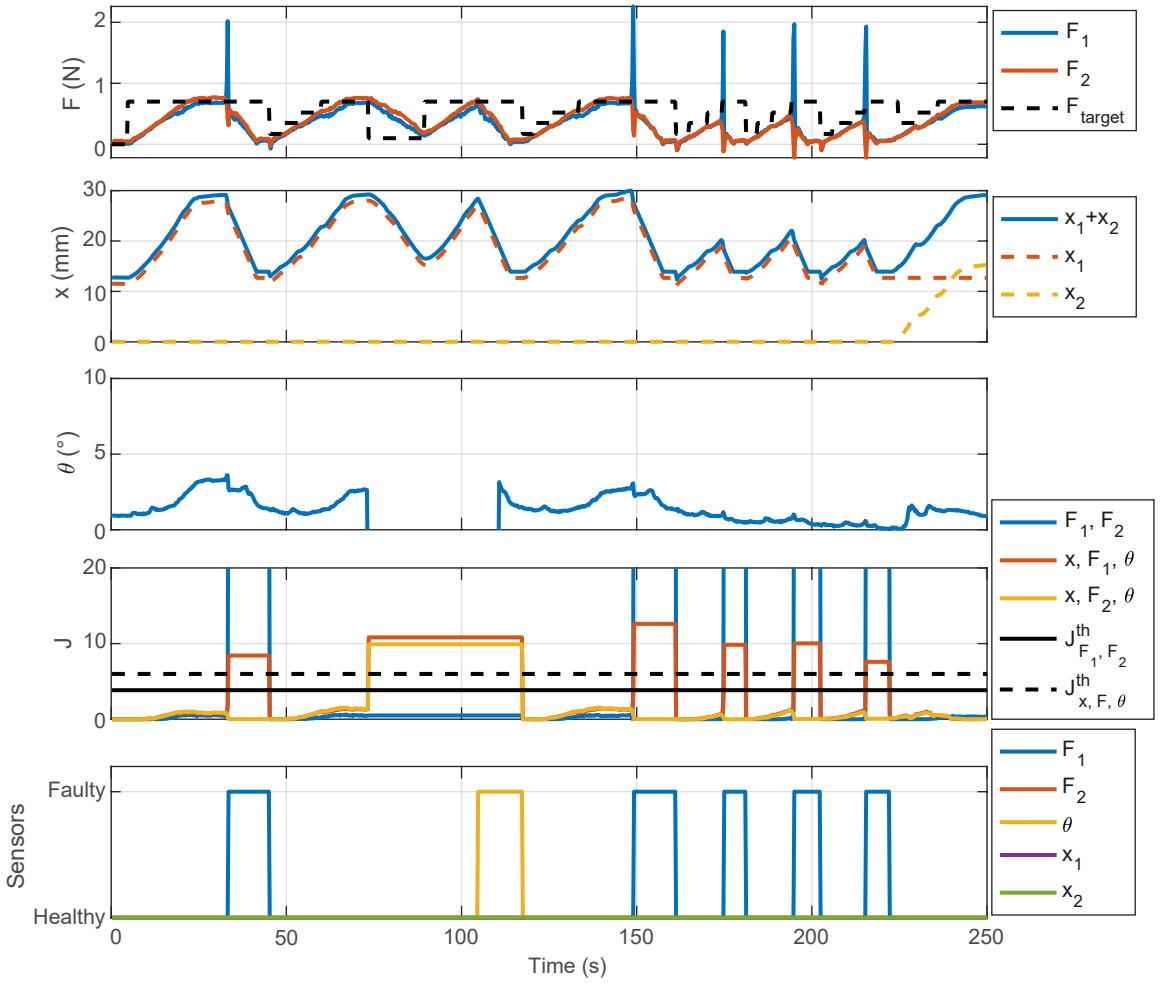

Fig. 3.3 **FERI demo video charts**. Charts of the fault injection experiment from the video uploaded as supplementary material to [107].

Chapter 4

Soft valves for autonomous fault detection and isolation in pneumatic soft robots

This chapter presents the development of a fully soft valve for passive, autonomous burst sensing and isolation in pneumatic soft actuators. This solution is meant as an embodied approach to the problem of fault detection in soft robotic systems. In the following section, an overview of the work is introduced, followed by a more in-depth analysis of the contributions and the methodology used for the study. The resulting publication, presented at the 5^{th} IEEE-RAS International Conference on Soft Robotics, follows in Section 4.2.

4.1 Summary of the publication

As discussed in the Introduction and Literature Review sections of this manuscript, soft robots present a number of revolutionary capabilities. In order for their potential to be fully harnessed, though, some challenges still stand. Among these, modelling, control and automated manufacturing have been at the forefront of the relevant literature almost from the start. One of the least discussed problems of soft robotics devices, till the advent of self-healing materials, has been resilience. In the beginning, soft robots have been described as inherently resilient due to their natural compliance and high deformability. If it is true that these traits can help in increasing resilience, many failure modes can be identified, such as interaction with sharp objects, interface de-bonding, material fatigue and, for pneumatic soft robots specifically, overpressurisation. Self-healing materials have been proposed as a promising solution to most of these problems, thanks to their capability of recreating severed chemical bonds at the molecular level. As discussed, materials have been engineered that can heal at room temperature, with almost full recovery of their structural performance. Some

problems still remain to be addressed though, such as time to healing, healing environmental requirements, and healing conditions. The healing time of most polymers present in literature can range from tens of seconds to tens of hours, with an additional distinction between partial and complete recovery of the material functionality, the second usually requiring a much longer time. In addition, as discussed in Chapter 2, some environmental conditions might be needed for a non-autonomic healing process to occur. Even when these are met, slight misalignments of the cut edges can produce sub-optimal or incomplete healing. For pneumatic soft robots in particular, that have to maintain an airtight interface with the environment, these requirements translate into long periods when the robot cannot be actuated, as air would flow out of the cut, preventing healing. Furthermore, even though inactivity creates favourable conditions for the healing process, there is no insurance that the cut edges align perfectly, leading to an airtight volume again. Finally, if the damage introduces any degree of material ablation, the whole process is almost certainly unsuccessful.

In recent years, fully soft valves, components that do not use rigid elements within their structure, have been increasingly investigated as a way of achieving control of fluidic soft robots, without the need for onboard electronics. The main advantage being that these can be more easily integrated in the body of the robot at the manufacturing stage. The work in this chapter aims at demonstrating that soft valves can become passive safety components that increase resilience without added burdens on the control or hardware required for the soft robot to operate. Each actuator is paired with a soft valve, that can automatically detect when a burst happens and isolate the faulty actuator from the rest of the system, therefore preventing the fault from propagating. The structure of the valve draws inspiration from Quake style valves used in microfluidics and consists of three distinct layers: the flow layer, the control layer and the membrane which separates the two. The flow layer connects the supply line with the actuator and presents a localised restriction underneath the control chamber. The control layer is connected to the control line and, when a big enough pressure difference is present between the control signal and the pressure in the flow layer, the membrane deforms, obstructing the flow in the flow layer.

Contrary to what happens in traditional Quake valves, the working principle of this fault isolating valve relies on the dynamic effects created by the burst itself and not on the sudden appearance of a high enough control signal. In fact, the supply and control pressure have the same level, so, in normal conditions, the valve remains open. When a burst occurs, the sudden drop in pressure at the outlet of the valve propagates back, till the restriction in the flow layer. The pressure underneath the membrane therefore drops, causing the membrane to deform and shut the valve, isolating the burst actuator. The process exploits the fact that when a fluid travelling in a duct encounters an obstacle, it experiences a sharp and localised

drop in pressure. The restriction in the flow layer is therefore key, as it temporarily decouples the supply pressure at the inlet of the valve from the ambient pressure at the outlet when the burst occurs, until the membrane has shut the flow. In fact, the absence of the restriction would permit the low pressure to travel much further back in the supply channel, potentially influencing the control pressure and making it impossible for the valve to switch.

In designing the valve, a few requirements were set, to guide the development process. The valve's structure had to be simple, in order to involve fewer manufacturing steps; the structure had to be fully soft, so that future integration in existing soft actuators is made simple; the final operation had to be passive and autonomous, requiring anything but pneumatic pressure to work, in order to make adoption in fully pneumatic robots possible. Finite element analysis was used to select an appropriate membrane thickness based on the supply/control pressure level and the material properties. In addition, the volumetric flow rate was experimentally characterised, for various geometries of the flow channel and different materials.

The main contribution of the work is the demonstration, through controlled bench-top experiments and real-world applications, that the valve can indeed detect and isolate bursts in less than 30 ms, opening the way for novel resilient soft actuators. The working principle of the fault detection and isolation can be thought of as an embodiment of the consistency-based fault detection [108] approach used for the FERI in Chapter 3. The membrane inside the soft valve constantly compares the pressure of the actuator to its known healthy state, which is supply pressure level. When the difference, or residual, between the two surpasses a threshold dictated by the membrane properties, the membrane deforms enough to obstruct the inlet of the valve, isolating the actuator, which is deemed as faulty.
As discussed in Chapter 1, one of the envisaged use cases for the soft valve, is in conjunction with self-healing materials, to selectively and automatically deflate a burst actuator in order to start the healing process, or permanently isolate it in case the healing fails.

4.2 Publications

Development and Characterization of a Soft Valve for Automatic Fault Isolation in Inflatable Soft Robots

Marco Pontin[1], Shuhei Miyashita[1] and Dana D. Damian[1]

Abstract— **Common causes of failure of inflatable soft robots are bursts due to wear, overpressurization or interactions with their surroundings. Resilience, the ability to survive such faults, is key for autonomous robotic systems, especially when human intervention is impossible or risky (e.g. robotic implants or space exploration). Although self-healing has been investigated as a possible solution, the approaches presented to date still have critical limitations. In this paper, we present a novel resilience mechanism based on soft valves. When used with soft actuators consisting of multiple inflatable segments connected in parallel, these are designed to readily isolate a burst section before the fault can propagate to the rest of the system. No additional sensing is required. The shut-off action of the valve is triggered by the pressure difference caused by the fault itself, as proved in the final application. The valve takes less than 30 ms to switch and can operate at various pressure levels: supply pressures up to 15 kPa were tested. This fault-isolating soft valve represents a new step towards soft robotic resilience, addressing soft robots vulnerabilities in difficult-to-access sites or in settings of high-risk for the system or its surroundings.**

I. INTRODUCTION

In the last decade, soft robotics has become an important and popular area of research. Soft robots have demonstrated interesting and unique capabilities: growing bodies, better ability in coping with unstructured environments, ability to survive large deformations [1], [2], [3]. Using soft materials, researchers have been able to develop actuators [4], [5], [6], sensors [4], [7], [8], and controllers [9], [10]. Their softness, though, makes them prone to failure when interacting with the surroundings or to burst if overpressurized. Repeated inflation and wear due to contact can also lead to the same result. These are all common failure modes of fluidic soft actuators and, as such, they represent a critical shortcoming for their application in robotic systems, especially in cases where autonomy and ability to overcome faults are paramount, such as robots for search and rescue, space exploration or medical robotic implants. In all of these cases, there is the necessity for the systems to autonomously detect, isolate and eventually solve potential faults, as human intervention is either impossible or very risky. Key work to overcome this problem has been carried out in the field of self-healing materials. Researchers have realized composite materials, capable of sensing and actuation, that show functional self-healing capabilities [11], [12], [13]. Focusing on inflatable soft-robots, Terryn et al. demonstrated the use of self-healing polymer-sheets to build actuators that can recover macroscopic damage [14]. A similar result was achieved by Shepard et al. using an Ecoflex™-Kevlar composite [15] and by Wallin et al. [16] through a thiol–ene click chemistry. These approaches, although promising, still show limitations. In the majority of the cases, the focus is on the chemical process itself and not on how this affects the performance of the system while healing or on the fault detection aspect. Specific materials need to be used to exploit self-healing and the self-healing process itself can require from tens of seconds to several hours to complete. Meanwhile, the actuators need to be deflated or leakage of actuation fluid occurs. Sometimes, particular environmental conditions are needed for the process to occur, such as the presence of a UV source or an increase in ambient temperature. Most importantly though, these techniques can only recover relatively small damages, such as

*This work was supported by the EPSRC under Grant EP/S021035/1, and EPSRC ERC DTP Scholarship. Data available on the ORDA doi 10.15131/shef.data.19419602.

[1]M. Pontin, S. Miyashita and D. D. Damian are with the Automatic Control and Systems Engineering Department, University of Sheffield, Sheffield, UK (e-mail: mpontin1@sheffield.ac.uk, d.damian@sheffield.ac.uk).

punctures and neat cuts, where no original material is removed. This leaves the necessity of finding ways to isolate the faulty section of the robot, either temporarily, while the fault is healing, or permanently, if the damage is unrecoverable, as not doing so could cause loss of functionality for prolonged or indefinite periods of time. Also, when multiple segments of the actuator are connected to the same supply line, one burst could lead the entire soft robot to fail. Even when a powerful supply line is present, that can cope with the outflow of actuation fluid, this translates in an overall bulkier system and in a waste of critical resources in untethered applications.

In this article, we present a novel automatic fault detection and isolation technique for inflatable soft robots, based on pressure-difference triggered soft valves. The integration of soft valves has recently been used for control purposes to create fully soft robots [10], [17], [18]. Still, little work has been devoted to fault detection and isolation. The goal of this work is to develop and characterize a pneumatic soft valve that enables sensing and isolation of bursts, with no controller intervention. The envisaged application is to create a distributed fault isolation network for inflatable soft actuators with multiple chambers connected together (Section IV). The result is a potential reduction in pneumatic supply lines as well as external sensing elements and valves to achieve similar functionality.

II. DESIGN AND FABRICATION

The soft valve consists of three main parts: the flow layer, containing the main flow channel that connects the supply line with the soft actuator, the control layer, where the control chamber is located, and the membrane, which separates the two (Fig.1(a)). Although the design of the valve originates from Quake-style valves [19], [20], the proposed valve's novelty stems from the distinct structural materials and working principle. Ecoflex™ 00-50 is used in the final application, leading to a much softer valve compared to traditional PDMS Quake valves. In addition, while Quake valves rely on a static uniform pressure difference to operate, our design exploits the dynamic creation of a pressure gradient in the flow channel caused by the burst. Key for this behaviour is the restriction in the flow layer, underneath the control chamber. The geometry produces two effects: it creates a disconnect between the inlet and the outlet, acting as a concentrated pneumatic resistance, and it reduces the distance the membrane needs to deform to shut off the flow, meaning a lower pressure difference Δp is required for the valve to switch, therefore reducing the response time of the component. The channels have square section of height H, that reduces down to a minimum height h where the raised section of the flow channel is. The control chamber, and the membrane as a result, is circular with diameter D. Finally, the membrane is characterized by its thickness t (Fig.1(b)).

Two prototypes of the valve were manufactured, one made out of PDMS silicone (Sylgard™ 182) and the second using Ecoflex™ 00-50. Molds for all the parts were fabricated using a Formlabs Form 2 SLA printer with the layer height set to $25\,\mu$m. Fig.1(a) summarizes the steps of the manufacturing process. After molding and degassing, the Ecoflex™ components were cured in an oven (SciQuip 80-HT) at $75\,°$C for 25 minutes, demolded and then irreversibly bonded using Silpoxy™ glue. The PDMS parts were cured at $125\,°$C for 30 minutes and bonded in pairs using oxygen plasma coating (Henikker Plasma HPT-200): air was used as process gas, the flow in the chamber was set to $20\,$sccm, the power to 100% and the samples were exposed for $55\,$s. Immediately after exposure to plasma, the parts were firmly pressed together for $60\,$s and then placed for 10 minutes on a hotplate set to $90\,°$C. This study will mostly focus on the Ecoflex™ 00-50 version of the valves as the material properties better reflect those typically seen in inflatable soft robots. PDMS samples are used during the experimental characterization phase as a reference: the manufacturing technique together with the higher stiffness of the material lead to more precise samples with little to no internal deformation upon pressurization.

III. FINITE ELEMENT ANALYSIS

Finite element analysis (FEA) was used to select an appropriate thickness t for the membrane. Before performing the analysis in Abaqus, uniaxial

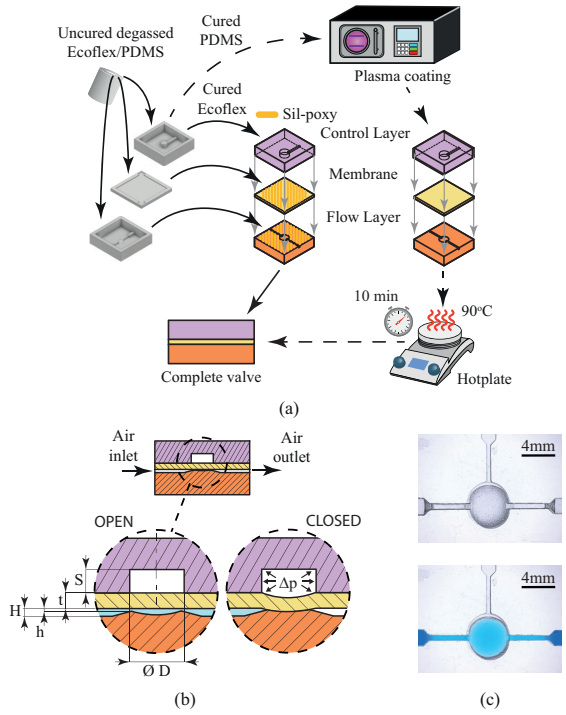

Fig. 1. Manufacturing process of the soft valve. (a) Two versions are realized using Ecoflex™ 00-50 and Sylgard™ 182. Ecoflex parts are irreversibly bonded using Sil-poxy™ glue, while oxygen plasma is used for the Sylgard™ 182 ones. (b) Sections of the open and closed soft valve with relevant dimensions. (c) Top view of a PDMS valve. The flow channel is highlighted using colored liquid.

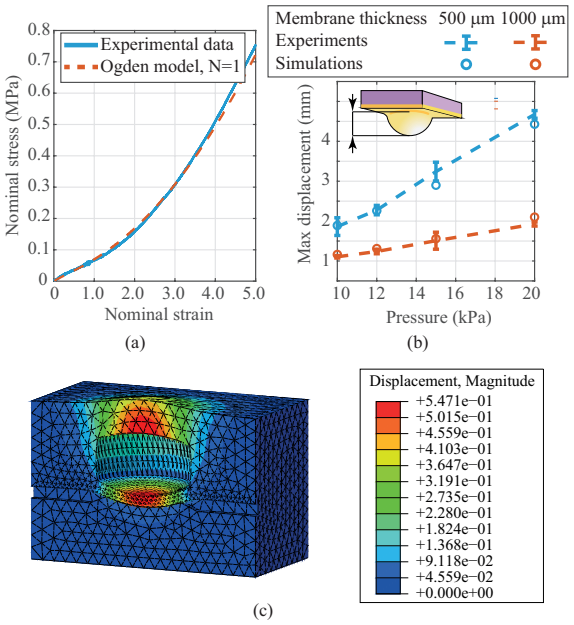

Fig. 2. FEA analysis of the valve. (a) Results of the tensile tests on Ecoflex™ 00-50 and fitting of the Ogden model. An Imada MX2 tensile testing machine was used at 50.0 mm/min. (b) Validation of Abaqus simulations using the height of the inflated membrane as metric. Two different membrane thicknesses were used and three samples per thickness were manufactured and tested at varying inflation levels. (c) Abaqus simulation of the complete Ecoflex™ 00-50 valve inflated at 7.5 kPa. Membrane thickness $t = 500\,\mu$m.

tensile tests were conducted for material characterization. Ecoflex™ 00-50 dog bone samples were molded according to the manufacturing process just presented and an Ogden model with $N = 1$ (1) was chosen to fit the model parameters to the experimental data (Fig.2(a)). Three out of ten tensile tests were used for the estimation of the material properties.

$$\sigma_{uniax} = \frac{2\mu}{\alpha}\left(\lambda^{\alpha} - \lambda^{-\frac{1}{2}\alpha}\right) \qquad (1)$$

In the equation, σ_{uniax} represents the stress and λ the strain. Fitting in Abaqus resulted in $\mu = 0.0263$ and $\alpha = 3.093$. To validate the material model, samples were built, consisting only of the control layer and the membrane, and pressurized. The experimental results were then compared to the simulations at various levels of inflation. The maximum height of the deformed membrane was used as the metric for the comparison and two membrane thicknesses were considered: $500\,\mu$m and 1 mm. Fig.2(b) shows a summary of the comparison. For the experiments, three different samples were used per each thickness and the results were then averaged. The simulated displacement proved to be in line with the experimental one, with slightly bigger discrepancies for larger deformations. The maximum error was 0.34 mm for the $500\,\mu$m at 15 kPa of internal pressure.

To guide the sizing of the membrane thickness for the valve, in line with preliminary experimental data, the assumption was made that when a burst occurs, in the flow channel, underneath the membrane, the pressure is given by the mathematical average between supply and ambient pressure. The pressure difference that causes the membrane to bend down is therefore equal to $p_{supply}/2$. One simulation of the complete valve can be seen in Fig.2(c). The flow channel is at ambient pressure,

while a uniform pressure of $7.5\,\text{kPa}$ is present in the control chamber at the top, simulating a supply pressure $p_{supply} = 15\,\text{kPa}$. The valve, with the $500\,\mu\text{m}$ thick membrane, was modelled as monolithic for simplification and internal contacts were enabled in Abaqus to simulate the interaction between the membrane itself and the bottom of the flow channel. The complex interaction between the air flow in the flow layer and the membrane was neglected and will be analyzed in future studies. According to the simulations, a $500\,\mu\text{m}$ thick membrane should be capable of deforming enough to fully obstruct the flow channel. This result was used as the baseline for the manufacturing of the soft valve.

IV. EXPERIMENTAL RESULTS

A. Characterization of the Flow Rate Through the Valves

To characterize the valves, flow rate tests were performed referring to ISO 6358. The experiments were conducted using the pneumatic circuit in Fig.3(a). The pressure inside the tank is kept constant using a PI controller, while the outflow is measured using an analogue air flow sensor. As visible in Fig.3(b) and (c), the tests are conducted on a version of the valve consisting of the flow channel and a solid top layer bearing miniature channels. These enable the insertion of syringe needles to measure the pressure right before (p_{in}) and after (p_{out}) the restriction in the flow channel. O-rings, embedded during the molding phase, provide sealing. Finally, a flow regulator is used to incrementally reduce p_{out}, from p_{supply} to ambient pressure. According to the ISO norm, the flow through a rigid valve can be expressed using (2).

$$\begin{cases} Q_N = C\sqrt{\frac{T_0}{T}}p_{in} & \text{if } \frac{p_{out}}{p_{in}} \leq b \\ Q_N = C\sqrt{\frac{T_0}{T}}p_{in}\sqrt{1-\left(\frac{\frac{p_{out}}{p_{in}}-b}{1-b}\right)^2} & \text{if } \frac{p_{out}}{p_{in}} > b \end{cases} \tag{2}$$

Pressures p are absolute and measured in bars, temperatures T are in K and Q_N, the flow rate, is expressed in Nls^{-1}. $T_0 = 293\,\text{K}$ is the reference temperature for normal conditions. The conductance C, measured in $\text{Nls}^{-1}\text{bar}^{-1}$, is directly proportional to the maximum flow rate through the valve at a given supply pressure p_{in}. Coefficient b represents the critical pressure ratio below which the flow reaches sonic speed and does not increase anymore when further decreasing the ratio p_{out}/p_{in}. It can be demonstrated that b has value 0.528 for an ideal nozzle in the absence of losses and is lower in real components, even reaching zero. In addition, in normal soft robotics applications the difference between absolute supply pressure and absolute ambient pressure is relatively small, leading to a ratio p_{out}/p_{in} close to 1. Because of these considerations, we assumed $b = 0$, leaving only the conductance to be experimentally determined.

Five different geometries of the flow channel were considered for both the Ecoflex™ and the PDMS versions of the valve: H varied in the range $[0.5,\ 1.0,\ 1.5]\,\text{mm}$, while h was equal to $100\,\mu\text{m}$, $150\,\mu\text{m}$, and $200\,\mu\text{m}$ for $H = 0.5\,\text{mm}$ and was $150\,\mu\text{m}$ for $H = 1.0\,\text{mm}$ and $H = 1.5\,\text{mm}$. All other dimensions of the flow channel were kept constant. Fig.3(d) and (e) show the results obtained with $H = 0.5\,\text{mm}$ and $h = 150\,\mu\text{m}$ for the PDMS and Ecoflex™ versions respectively. As visible, the minimum value for the ratio p_{out}/p_{in} is 0.88 for $p_{in} = 15\,\text{kPa}$, confirming our previous considerations on b. Also, contrary to the Ecoflex™ ones, flow curves for the PDMS valves overlap, reflecting what would be expected using fully rigid valves. This is also confirmed by the coefficient of variation σ/μ of the conductance C after fitting, whose average value is 0.08 for the PDMS samples and 0.30 for the Ecoflex™ ones. The difference in behavior of the valves can be ascribed to internal deformations of the softer Ecoflex™ samples when pressure is applied. These deformations lead to a wider flow channel with a resulting increase in the flow rate at any given ratio p_{out}/p_{in}. Fig.3(f) summarizes the results obtained with the various geometries: the conductance is expressed as a function of the minimum area of the flow layer. Ecoflex™ valves with an area greater than $0.1\,\text{mm}^2$ could not easily achieve p_{out} equal to ambient pressure due to their lower internal resistance. This made them unsuitable candidates for later sections of this study. Knowing the conductance makes it possible to select the appropriate geometry of the flow layer based on the application as well as

being the first step towards a complete model of the valve. For the PDMS components, a second order polynomial provides a good fitting of the experimental data points ($R^2 = 0.97$). The same cannot be done for the Ecoflex™ versions as the supply pressure level impacts the conductance. Modelling is made challenging by the non-linear behavior of the silicone material and the complex interaction between the evolving pressure gradient in the flow layer and the channel itself.

B. Shut-off Operation

When characterizing the shut-off capabilities of the valve, the pneumatic circuit of Fig.3(a) was altered as shown in Fig.4(a). A control line is now present, to switch the pressure in the control layer of the valve on and off. Also, the flow regulator is removed and an outlet valve is added downstream of the flow sensor used to measure the outflow.

Samples were created with $H = 0.5\,\text{mm}$ and $h = 150\,\mu\text{m}$, while the membrane thickness t was varied in the range $[100, 200, 300, 500]\,\mu\text{m}$. The supply pressure was increased in steps of $5\,\text{kPa}$ from $5\,\text{kPa}$ to $15\,\text{kPa}$ and four samples were tested at each pressure level. Fig.4(b) displays the testing procedure in details and shows the results obtained with a $100\,\mu\text{m}$ thick membrane. First, the desired supply pressure is stabilized inside the tank. Then, valve V1 is turned on, pressurizing the flow layer up to V2. This causes a small flow through the flow sensor, as visible in the bottom chart at the time $t = 1.00\,\text{s}$. $150\,\text{ms}$ later, V3 opens, pressurizing the control line. After $5\,\text{s}$, $V3$ is closed and V2 is opened, connecting the outlet of the soft valve to ambient pressure, thus simulating a sudden burst in a soft actuator ($t = 6.15\,\text{s}$). The air trapped between the soft valve and V2 flows out, causing a peak in the flow meter reading. If the valve works correctly, no flow should be measured in the following $3\,\text{s}$ (grayed out region in the bottom chart of Fig.4(b)). The duration of the second spike in the flow rate can be interpreted as an upper bound for the switching time of the valve and never exceeded $30\,\text{ms}$. At $t = 9.15\,\text{s}$, V1 is closed and V4 is opened, depressurizing the control line and resetting the circuit to the initial state. Immediately after opening V3, the membrane goes back to its resting position and the air trapped between V1

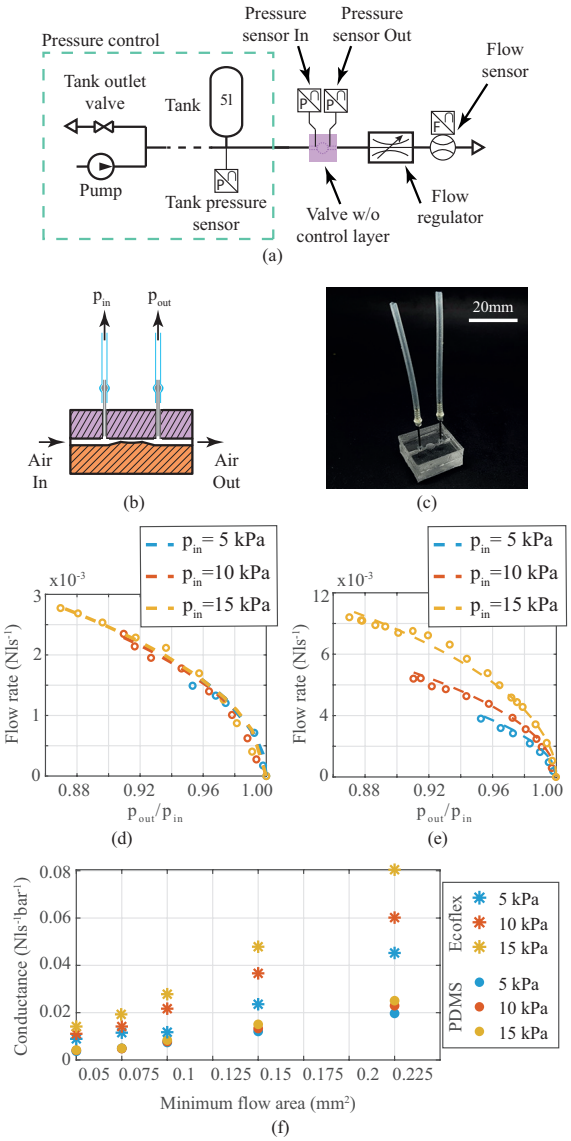

Fig. 3. Characterization of the flow rate through the soft valves. (a) Diagram of the pneumatic circuit used for the tests. (b) Section view of the component being tested. (c) Photograph of a PDMS sample: syringe needles are inserted for measuring the pressure inside the flow layer. (d) Characterization of a PDMS valve having $H = 0.5\,\text{mm}$ and $h = 150\,\mu\text{m}$. Three different supply levels were used in the range of typical soft robotics applications. Experimental data points are shown as circles, while dashed lines represent the fitting according to (2). (e) Characterization of an Ecoflex™ 00-50 valve having $H = 0.5\,\text{mm}$ and $h = 150\,\mu\text{m}$. The curves diverge due to internal deformations generated when the flow layer is pressurized. (f) Conductance of the valves as a function of the minimum area of the flow layer. Five different geometries were considered, varying both the width H and the height h of the channel. For any given geometry, the PDMS data points are closer together than the Ecoflex™ ones, highlighting the effect that the supply pressure level has on the softer material.

and the soft valve discharges, causing the third peak in the flow meter readings.

Fig.4(c) presents the results, as an average of four trials, for the four membrane thicknesses and the three supply pressure levels. As visible, contrary to the FEA simulations, the 500 μm thick membrane could not seal the flow layer and air leakage occurred during the trials for all three supply pressure levels. This is likely caused by the interaction between the air flow and the membrane, as well as the internal deformations of the flow layer caused by the pressure. In addition, the outflow increased in absolute terms with the increasing inlet pressure. The same happened for the 300 μm membrane, but this time the measured flow was lower, implying that the membrane was obstructing a larger percentage of the cross section of the flow channel. Samples with 200 μm thick membranes were capable of blocking the outflow for a supply pressure of 5 kPa, but then failed to do so for higher pressure values. The valves with 100 μm thick membranes were the only ones that could completely and reliably seal the flow layer all throughout the supply pressure range. The thinner membrane was capable of deforming enough to compensate for the internal deformations of the flow layer for all supply pressure levels. Even when not completely stopping the flow, the valves were still able to reduce it by more than 40% in the case of the 500 μm membrane and up to 80% with the 200 μm one, as summarized in the bar chart of Fig.4(d). The normalized reduction in flow rate (NRF) was chosen as the metric to compare the effectiveness of the various samples. The normalization was done using the following formula.

$$NRF = \frac{Q_{max} - Q_{out}}{Q_{max}} \tag{3}$$

Q_{out} is the outflow measured during the test and Q_{max} is the maximum flow rate achieved for the specific supply pressure level and channel geometry during the characterization experiments of Fig.3(e), where the membrane was absent. Overall, the valves proved to be effective and future work will focus on optimizing the internal geometry.

C. Application Example

To prove the effectiveness of the proposed design in real world applications, the soft-rigid actu-

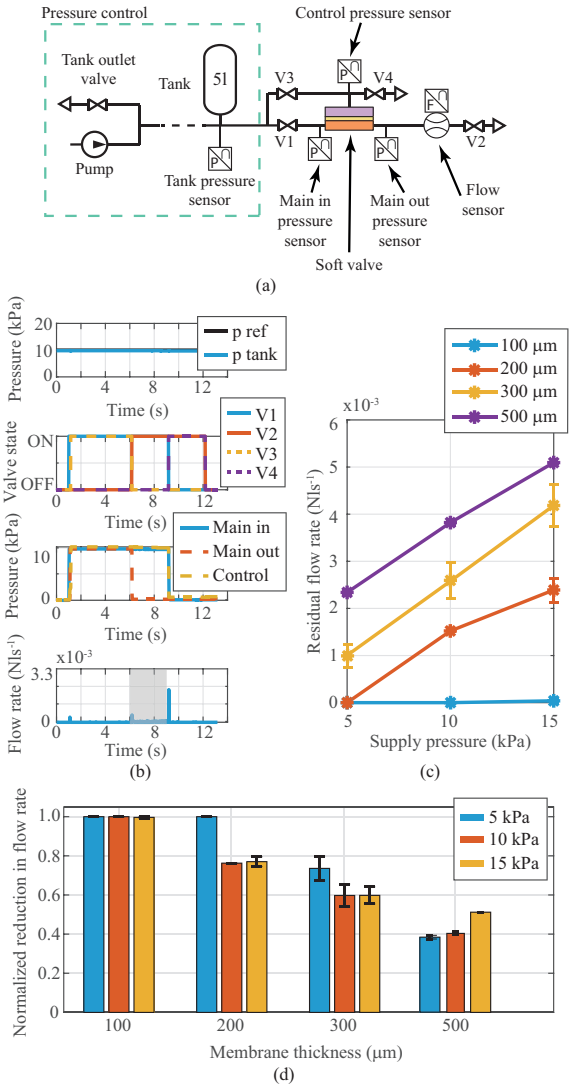

Fig. 4. Characterization of the shut-off capabilities of the soft valve. (a) Schematic of the pneumatic circuit used for the tests. (b) Experimental results obtained using a sample with $H = 0.5$ mm, $h = 150\,\mu$m and $t = 100\,\mu$m. The control layer is pressurized using an external valve (V3) 150 ms after the flow layer and is then isolated. The main outlet valve (V2) is later opened at $t = 6.15$ s to simulate a burst, but no outflow is observed (grayed out region in the bottom chart). Finally, the system is reset for the next test. The peaks in the flow rate correspond to the initial pressurization of the flow layer, to the discharge of the tubing between the soft valve and the outlet valve and to the discharge of the system during the reset phase. (c) Comparison of valves with same internal geometry and varying membrane thickness. The outflow was measured for varying levels of the supply pressure. Samples with $t = 100\,\mu$m reliably succeeded in shutting off the flow completely, while ones with thicker membranes only reduced it partially. (d) Shut-off effectiveness of the valves for varying membrane thicknesses. The normalization was done using the maximum flow rate observed for the given geometry and supply pressure level during experiments such as that in Fig.3(e). Even when not fully blocking the outflow, the valves with 200 μm, 300 μm and 500 μm thick membranes were able to reduce the outflow by 80%, 60% and 40% respectively, compared to the membrane being absent.

ator presented in [21] was used. These actuators consist of ring-shaped stackable modules, each having three independently inflatable membranes. As shown in Fig.5 and in the supplementary video, one module and three valves (V1, V2 and V3) were utilized for the demo. Each valve is connected to the common supply line and V1 is also connected to the control line. Valves V2 and V3 are passive and are only used to get similar amounts of pneumatic resistance in all three lines to the inflatable membranes (M1, M2 and M3). The decision of having only one fully connected valve was done to better highlight the behavior and effect that the valve, V1 in this case, has on the system. All three valves have $H = 0.5\,\text{mm}$, $h = 150\,\mu\text{m}$ and a $100\,\mu\text{m}$ thick membrane inside.

The actuator in its deflated state is shown in Fig.5(a), with V1 switched off. The supply line is then pressurized and the actuator inflates (Fig.5(b)). In the experiment, a supply pressure of $10\,\text{kPa}$ was used. Right after inflation, the control line of valve V1 is turned on, pressurizing the control layer and preparing the membrane to snap down in case of a fault in the inflatable membrane M1. The system is then completely isolated from the supply, by disconnecting the external rigid valves, so that the pump cannot provide any more air to the inflatable membranes. A precision knife is used to burst the actuator, but membranes M2 and M3 remain inflated (Fig.5(b) and (c)). One minute after the burst, the actuator was still inflated, with no visible change in inflation level. In Fig.5(d), the control line is finally depressurized, causing the membrane inside V1 to go back to its resting state. As a result, the air in M2 and M3 flows through V1 and out of the hole in M1, deflating the actuator (Fig.5(d)) and simulating what would occur had the valve not been present. The deflation of M2 and M3 took around $15\,\text{s}$ due to the presence of V2 and V3 that, although not being active, still provide resistance to the flow, making the overall deflation transient longer.

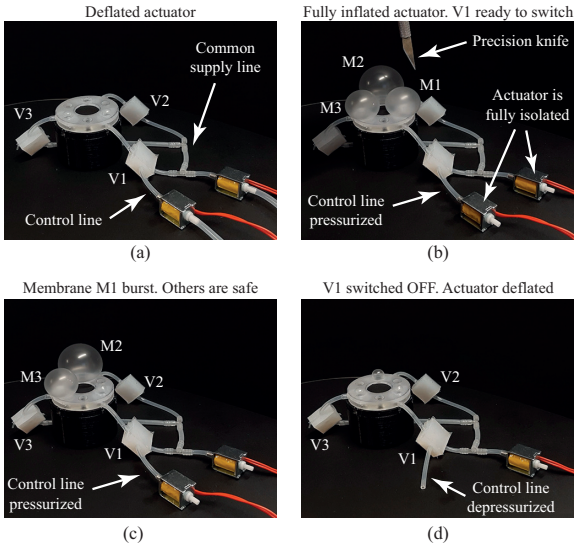

Fig. 5. Soft valves used with an inflatable actuator to demo fault isolation. (a) Soft pneumatic actuator ready for inflation. The three inlets are connected to the main supply through three soft valves. V1's control line is connected while V2 and V3 only ensure a similar level of resistance on all supply lines. (b) After inflation, the supply and control line valves are shut off and disconnected, isolating the actuator from the pump. The nonuniform inflation is due to manufacturing inaccuracies in the actuator. Membrane M1 is then burst using a precision knife. (c) The soft valve isolates the faulty membrane from the remaining ones, preventing their deflation. (d) The control line is discharged. In $15\,\text{s}$ the actuator fully deflated, with air flowing from the intact membranes out through the cut in the faulty one, further proving the effect of the soft valve.

DISCUSSION AND CONCLUSION

In this paper, we presented a soft valve designed to readily isolate a burst section of a soft inflatable actuator before the fault can propagate to the rest of the system. No additional sensing is required, as the shut-off action of the valve is triggered by the fault itself. Combined with self healing techniques, it could either isolate a faulty segment while healing occurs or act as a fail safe alternative in case of unrecoverable damage. Untethered applications, where actuation fluid is limited, could also benefit from its use.

Some of the limitations that have emerged entail manufacturing and modelling. When using Ecoflex™ 00-50, achieving a thin uniform layer of Sil-poxy™ without affecting the small features of the valve proved to be challenging. Further investigation in bonding techniques may be needed to scale down the design. In comparison, PDMS proved to be a more accurate and time efficient alternative. Its higher stiffness, though, limits its application in inflatable soft robots. With respect to modelling, discrepancies between FEA and exper-

imental results were observed and are likely to be linked to internal deformations upon pressurization and to the interaction between the air flow and the membrane. A thin membrane, $100\,\mu$m thick, granted the most reliable performance: the shut-off reaction was fast (less than 30 ms) and provided perfect sealing both during the preliminary tests as well as during the final application. In addition to the modelling aspects, future work will involve integrating the soft valve into the actuator, leading to a monolithic solution with less tubing and external rigid valves.

ACKNOWLEDGMENT

The authors acknowledge Quentin Lahondes for helping with the use of the oxygen plasma machine.

REFERENCES

[1] E. W. Hawkes, L. H. Blumenschein, J. D. Greer, and A. M. Okamura, "A soft robot that navigates its environment through growth," *Science Robotics*, vol. 2, no. 8, p. eaan3028, 2017.

[2] R. F. Shepherd *et al.*, "Multigait soft robot," *Proceedings of the National Academy of Sciences*, vol. 108, no. 51, pp. 20400–20403, 2011.

[3] M. T. Tolley *et al.*, "A resilient, untethered soft robot," *Soft Robotics*, vol. 1, no. 3, pp. 213–223, 2014.

[4] M. Baumgartner *et al.*, "Resilient yet entirely degradable gelatin-based biogels for soft robots and electronics," *Nature Materials*, vol. 19, pp. 1102–1109, Oct 2020.

[5] E. Perez-Guagnelli *et al.*, "Characterization, simulation and control of a soft helical pneumatic implantable robot for tissue regeneration," *IEEE Transactions on Medical Robotics and Bionics*, vol. 2, no. 1, pp. 94–103, 2020.

[6] B. Gorissen, D. Reynaerts, S. Konishi, K. Yoshida, J.-W. Kim, and M. De Volder, "Elastic inflatable actuators for soft robotic applications," *Advanced Materials*, vol. 29, no. 43, p. 1604977, 2017.

[7] H. Wang, M. Totaro, and L. Beccai, "Toward perceptive soft robots: Progress and challenges," *Advanced Science*, vol. 5, no. 9, p. 1800541, 2018.

[8] T. Kim, S. Lee, T. Hong, G. Shin, T. Kim, and Y.-L. Park, "Heterogeneous sensing in a multifunctional soft sensor for human-robot interfaces," *Science Robotics*, vol. 5, no. 49, p. eabc6878, 2020.

[9] M. Wehner *et al.*, "An integrated design and fabrication strategy for entirely soft, autonomous robots," *Nature*, vol. 536, pp. 451–455, Aug 2016.

[10] S. T. Mahon, A. Buchoux, M. E. Sayed, L. Teng, and A. A. Stokes, "Soft robots for extreme environments: Removing electronic control," *CoRR*, vol. abs/1903.10779, 2019.

[11] M. J. Ford *et al.*, "A multifunctional shape-morphing elastomer with liquid metal inclusions," *Proceedings of the National Academy of Sciences*, vol. 116, no. 43, pp. 21438–21444, 2019.

[12] S. Liu, O. Oderinde, I. Hussain, F. Yao, and G. Fu, "Dual ionic cross-linked double network hydrogel with self-healing, conductive, and force sensitive properties," *Polymer*, vol. 144, pp. 111–120, 2018.

[13] G. Cai, J. Wang, K. Qian, J. Chen, S. Li, and P. S. Lee, "Extremely stretchable strain sensors based on conductive self-healing dynamic cross-links hydrogels for human-motion detection," *Advanced Science*, vol. 4, no. 2, p. 1600190, 2017.

[14] S. Terryn, J. Brancart, D. Lefeber, G. V. Assche, and B. Vanderborght, "Self-healing soft pneumatic robots," *Science Robotics*, vol. 2, no. 9, p. eaan4268, 2017.

[15] R. F. Shepherd, A. A. Stokes, R. M. D. Nunes, and G. M. Whitesides, "Soft machines that are resistant to puncture and that self seal," *Advanced Materials*, vol. 25, no. 46, pp. 6709–6713, 2013.

[16] T. J. Wallin *et al.*, "Click chemistry stereolithography for soft robots that self-heal," *J. Mater. Chem. B*, vol. 5, pp. 6249–6255, 2017.

[17] P. Rothemund *et al.*, "A soft, bistable valve for autonomous control of soft actuators," *Science Robotics*, vol. 3, no. 16, p. eaar7986, 2018.

[18] D. Drotman, S. Jadhav, D. Sharp, C. Chan, and M. T. Tolley, "Electronics-free pneumatic circuits for controlling soft-legged robots," *Science Robotics*, vol. 6, no. 51, p. eaay2627, 2021.

[19] M. A. Unger, H.-P. Chou, T. Thorsen, A. Scherer, and S. R. Quake, "Monolithic microfabricated valves and pumps by multilayer soft lithography," *Science*, vol. 288, no. 5463, pp. 113–116, 2000.

[20] Y.-S. Lee, N. Bhattacharjee, and A. Folch, "3d-printed quake-style microvalves and micropumps," *Lab Chip*, vol. 18, no. 8, pp. 1207–1214, 2018.

[21] N. Herzig, J. Jones, E. Perez-Guagnelli, and D. D. Damian, "Model and validation of a highly extensible and tough actuator based on a ballooning membrane," in *2021 IEEE International Conference on Robotics and Automation (ICRA)*, pp. 11961–11967, 2021.

4.3 Limitations of the design

During the development of the first prototype of the soft valve, some challenges emerged. These can be classified in manufacturing related and functionality-based ones. In terms of manufacturing, the complex geometry of the flow channel made it difficult to properly glue the valve together. The most common defects were: glue obstructing the channel, glue residue on parts of the membrane that were supposed to remain unaffected, leaks due to uneven gluing of the surfaces. Functionality-wise, the reliability of the valve was low, with only the valves with a $100\,\mu$m reliably isolating the bursts. This is likely due to how the sealing of the flow channel happens with that design. For the sealing to be perfect, the entire side of the membrane has to form an uninterrupted contact with the hemispheric region of the flow channel. This is made more complex by the deformation of the soft valve when pressurised. In addition, the symmetric geometry makes achieving more complex behaviours, such as the one presented in the following sections, impossible. A first attempt was made to render the internal structure asymmetric, by widening the outlet section of the flow channel. This modification had the goal of reducing the outlet resistance of the valve, as well as to give an additional potential behaviour when the valve is connected in reverse. The design was quickly abandoned, though, as the manufacturing difficulties remained unaltered, leading to a 10% manufacturing success rate.

Chapter 5

Multi-modal soft valve for embodied programming of local resilient responses

This chapter analyses the development and characterisation of a novel multi-modal soft valve designed to achieve burst detection and isolation and overpressurisation protection, while overcoming limitations of the previous design. In addition, by combining two identical soft valves, an endogenously controlled valve is manufactured capable of self-tuning its operation to the actuator it is paired to, avoiding the need for external control lines.

5.1 Preface

Starting from the requirements and limitations highlighted at the end of Chapter 4, a new soft valve was developed. Compared to the previous design, the main structure remained

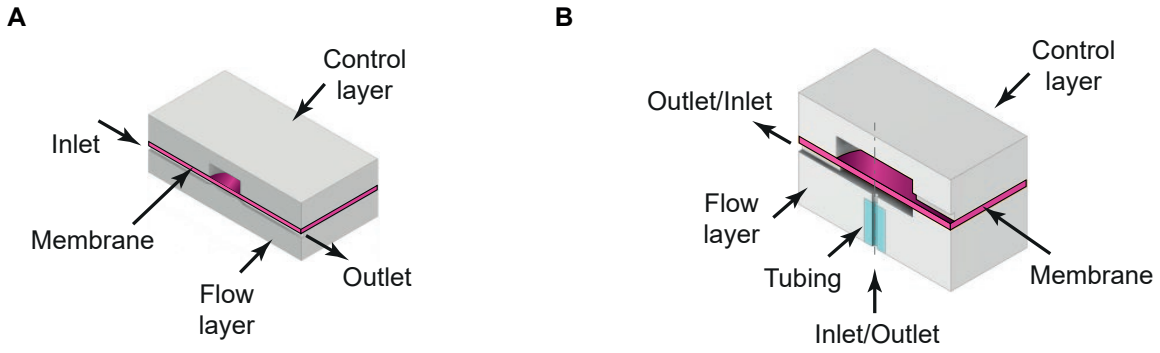

Fig. 5.1 **Comparison of the soft valve designs.** (**A**) Internal structure of the original soft valve design and main components. (**B**) Section view of the new soft valve design and its main elements.

mostly unaltered, as displayed in Fig. 5.1: one flow layer and one control layer separated by a soft membrane. For consistency, the external dimensions of the valve were also kept constant between the two versions. The main changes consist in having an inlet channel which runs orthogonal to the membrane and then bends 90° to reach the outlet (Fig. 5.1). The addition of tubing, embedded at the inlet section of the valve, prevents the channel from deforming when pressurised, leading to the possibility of carefully controlling the pneumatic resistance of the valve at the design stage. Having the inlet channel running orthogonal to the membrane, makes it possible to increase the size of the control chamber, making better use of the surface area of the valve, also reducing the length of the outlet channel and its pneumatic resistance.

Thanks to its internal geometry, the new design achieves separation of function. In the original soft valve, the pneumatic resistance of the valve was dictated by the overall internal geometry of the flow channel and of the central restriction in particular. The restriction also had to be designed so that the interaction with the membrane would provide the shut off capability. Therefore, a change in the geometry of the restriction to achieve better sealing for example led to a resulting change in pneumatic resistance, affecting the switching performance of the valve. This is not the case with the new design. The diameter and length of the inlet channel are used to carefully tune the overall input impedance of the valve, provided the outlet resistance is kept low in comparison.
Looking at functionality, having the inlet channel orthogonal to the membrane greatly improves the sealing capability of the valve: the part of the membrane which deforms the most is the one that is shutting the flow, contrary to what was happening in the previous design. This, together with the increased diameter of the control chamber makes it possible to increase the height of the flow layer chamber, use thicker membranes and achieve perfect sealing even with lower control pressure levels, due to the decreased rigidity of the membrane. From a manufacturing standpoint, the new structure provides two major improvements: the inlet channel is now fully formed after the moulding stage, which completely removes the risk of leakages, and the gluing is made easier by the simplified perimeter of the flow layer. In addition, the glue stops further away from the critical areas of the valve, namely where sealing action occurs, which is in the centre of the membrane. These aspects combined led to an increase in the manufacturing success rate from 10% to 100% (more than 45 soft valves of the new type were manufactured).

In addition to solving critical manufacturing challenges with the previous design, the new version of the soft valve was designed with the ultimate goal of achieving endogenous control: the capability of the valve of generating its own control signal autonomously. To accomplish this, two identical valves have to be combined, each exhibiting two distinct behaviours,

depending on how it is connected to the rest of the system. In particular, two of the three ports on the body of the valve can alternatively be used as the inlet. The asymmetric internal structure of the valve makes it then possible to obtain a forward operation mode (FOM) and a reverse operation mode (ROM). In FOM, the valve behaves as a PNP-transistor or a resettable fuse, replicating the burst detection and isolation capability shown in Chapter 4. In ROM, the behaviour is that of a Zener diode and can be used to protect soft actuators against overpressurisation. The two behaviours combined enable the endogenous control capability of the two-stage soft valve, which represents the culmination of the work of this chapter. In addition to achieving autonomous burst detection and isolation, this last design uses pressure feedback from the soft actuator it is paired with to time the generation of its control signal. As a result, the valve demonstrates self-tuning operation, which makes it possible to pair it with a variety of actuators without changes in valve design, as demonstrated in Section 5.4.1. All channels are internally routed and only two ports, inlet and outlet, remain open to the outside, making this last design a truly self-contained unit for burst detection and isolation in soft actuators.

The content of this chapter has been structured for submission to the journal "Science Robotics". The *Introduction* is followed by a *Results* section, where an in depth analysis of the experimental results is conducted. The subsequent *Discussion* summarises the results and highlights the impact of the work from a higher level perspective. The *Materials and Methods* section goes over the manufacturing and details about experimental procedures and protocols. The chapter is concluded by the *Supplementary Materials* which present additional interesting results that were deemed non critical in highlighting the capabilities of the soft valve.

5.2 Introduction

Inspired by living creatures and leveraging the compliance of their bodies, soft robots achieve integration between body, sensing and actuation and show promising potential for applications such as human robot interaction, medical robots, and marine and space robotics [7, 75, 6, 3, 109]. This property, paired with fluidic actuation, grants faster fabrication, better blending of form and function and a near infinite number of degrees of freedom. In most cases, actuators consist of enclosed volumes separated in one or more chambers. To tame the large deformation potential and the many degrees of freedom, roboticists use various means to selectively stiffen portions of the actuator's body so that, upon pressurisation, the intended deformation can be achieved. Control units, consisting of software, pressure sources, valves and pressure sensors, complete the robots, adding thought to bare matter.

Despite their promising potential, fluidic soft robots are more prone to failure compared to traditional robots made of durable, rigid materials. Bursts from cuts or overpressurisation represent a common and critical mode of failure [13, 55], which leads to unresponsive robots, therefore reducing their reliability and potential for adoption [110, 13]. When compared to the living creatures which serve as inspiration, soft robots appear like unevolved counterparts, unable to cope with the simplest of setbacks. Vulnerabilities in machines have been a well known problem since the dawn of robotics, with recognised unfavourable economic consequences and risks to humans. The classical fault-tolerant framework [22], built around rigid machines, relies on complex control algorithms to achieve behaviour adaptation after a critical fault, to salvage as much of the capabilities of the system as possible [23, 25]. In the same framework, reconfigurable and self-assembling systems have also been researched, to grant robots spare parts in case of breakages [111, 112]. These approaches, however, assume discrete, addressable points of failure, such as a sensor, actuator or link, making it difficult to scale the approach to high degrees-of-freedom machines or to the entire body of a robot. Additionally, the entire framework is based on a centralised architecture, where the controller takes decisions based on the feedback from various sensors. This often requires precise models, or extensive training, usually becoming computationally demanding. On the other end of the spectrum, self-healing materials, which take advantage of chemically-enabled repairs (e.g. reversible Diels-Alder bonds and H-bonds) are highly distributed, and do not require a model or computation, making them good candidates for soft robotic resilience [13, 14, 54, 40, 17, 39, 55]. Limitations still exist, though. Healing typically is time consuming and, most often, external stimuli or human intervention are needed for the process to be successful. In addition, fluidic actuators have to be deflated, for the healing to occur and, if material is removed during the fault, chances of recovery are drastically diminished. The effects of environmental contaminants on the healing process success and efficiency are also still to be investigated thoroughly.

Resilience in living creatures, on the other hand, shows a level of nuance that robots are still lacking. In humans, for example, a wounded finger triggers a tightly coordinated cascade of reactions on different time scales [113, 114, 15]. First, blood-borne platelets clump together to stop blood loss. An inflammatory response is then triggered and lymphocytes and macrophages converge to the site to protect against infections. In the medium term, growth factors are released to trigger collagen production, used as scaffolding by the reproducing dermis cells to form new tissue. While this is taking place, passively and unconsciously, the conscious self guides the human to a change in behaviour, meant to aid the recovery of the injured finger.

If software-based fault-tolerance in rigid robots can be equated to this high-level conscious

response and self-healing materials achieve the later stages of the healing process, the immediate and unconscious set of reactions which form haemostasis and enable tissue regeneration have yet to find an analogous in the world of soft robotics resilience. Bio-inspired approaches could instantly isolate faults, such that the damage does not propagate further, and maintain the system in operation until full recovery is achieved through material-level healing. Alternatively, faults could be prevented altogether, by endowing robots with stress relief mechanisms for critical, life-threatening situations. Inspired by the passive, autonomous nature of these solutions, in this chapter a fully soft valve is presented, capable of multi-modal behaviour to achieve passive distributed resilience in pneumatic soft robots.

Soft pumps and valves have been developed in the past to achieve electronics-free control and actuation of soft robots [115–118]. The development of valves in particular, inspired by the well known parallel between fluidic and electric systems modelling, have usually targeted the replication of functionalities obtained with CMOS technologies [119, 120]. Other designs have exploited more complex behaviours, such as bistability and buckling, to create oscillators for robot control and locomotion purposes [121–124]. When comparing these results to silicon technologies, limitations still remain. While some of these, such as speed of computation, are inherent to the medium, others, like manufacturing autonomy and average component size, have shown promising developments. Microfluidics research has demonstrated the possibility of replicating complex digital logic circuits [125–127] while achieving compact designs with 36 gates/cm^2 [128]. In addition, recent advancements in 3D-printing techniques and materials have permitted the creation of monolithic soft robots that merge control logic and actuators in one unit [129, 130, 104], decreasing production costs and time. Furthermore, the combination of state of the art inkjet printing and research on monopropellant fluids [131] has led to soft robots that include fluidic controllers and onboard pressure generation [104]. Despite these advancements in replicating complex behaviours through ingenious fluidic circuits, these approaches assume the soft robot is equipped with pressure sensors and valves for every functional fluidic chamber, has a centralized control and a quick response time. All of these increase both the hardware and computational burdens. The use of soft valves for soft robotic resilience is a recent development. In [132], our group designed and characterized a valve capable of achieving automatic burst detection and isolation, while in [133] Bosio et al. proposed a soft fuse valve for the same goal. In this paper, a novel multi-modal soft valve is presented, capable of achieving distinct resilient behaviours without changes in design or structure. In addition, the multi-modality of the valve can be used to create an endogenously controlled two-stage soft valve, through self-tuned operation. This two-stage valve can generate its own control signal, not only avoiding the need for an externally actuated line, but also making it possible to use the same valve

with soft actuators irrespective of their size and without previous knowledge about their behaviour. In summary, the innovations in this work respond to shortcomings in existing soft robotic resilience, by demonstrating embodied fluidic circuits which can achieve pre-emptive fault detection or isolation, and represent a glimpse into an embodied unified platform for bio-inspired fluidics-based soft robotic resilience.

5.3 Results

5.3.1 Soft Valve Design and Structure

The pneumatic soft valve, visible in Fig. 5.2A, consists of three functional layers. A membrane separates the control layer, where the control chamber resides, from the flow layer, which connects the main inlet and outlet ports. The integrated tubing in the valve acts as a constraint, preventing the associated section of the channel from expanding when pressurised, and serves as a localized resistance for the airflow. The single-material design and compact structure enable simple integration in existing soft robots. The geometry and position of the internal channels have been chosen to grant multi-modality, that is, different operation modes depending on how the valve is connected to a soft actuator, with a single supply pressure. In particular, we distinguish between a Forward Operation Mode (FOM) and a Reverse Operation Mode (ROM).

In FOM, the narrow vertical channel serves as the inlet (Fig. 5.2B). With the membrane in its resting position, the airflow is unimpeded and the valve is open. When a sufficiently high pressure difference is reached between the control pressure p_c and the outlet pressure p_{out}, the membrane deforms and obstructs the inlet channel, therefore separating the inlet from the outlet (closed condition). In this mode, the valve can be considered the fluidic equivalent of a PNP transistor, or, in the case of this study, of a resettable fuse. As such, if the valve in FOM is paired with a Soft Inflatable Element (SIE), like a pneumatic actuator or sensor, it can achieve passive, autonomous burst detection and isolation. The burst causes the pressure level underneath the membrane to drop, leading the membrane to deform downwards and obstruct the inlet channel. The valve, therefore, automatically switches from open to closed, isolating the faulty SIE and preserving the functionality of the rest of the system. Instrumental in achieving this result is the high impedance of the inlet channel, which decouples inlet and outlet pressures (Fig. 5.20 in the Supplementary Materials).

In ROM, Fig. 5.2C, the narrow channel serves as the outlet. The valve starts out closed and later opens when the pressure difference between the chambers either side of the membrane, $p_c - p_{in}$, drops below a threshold value Δp_{th} dependent on the geometry

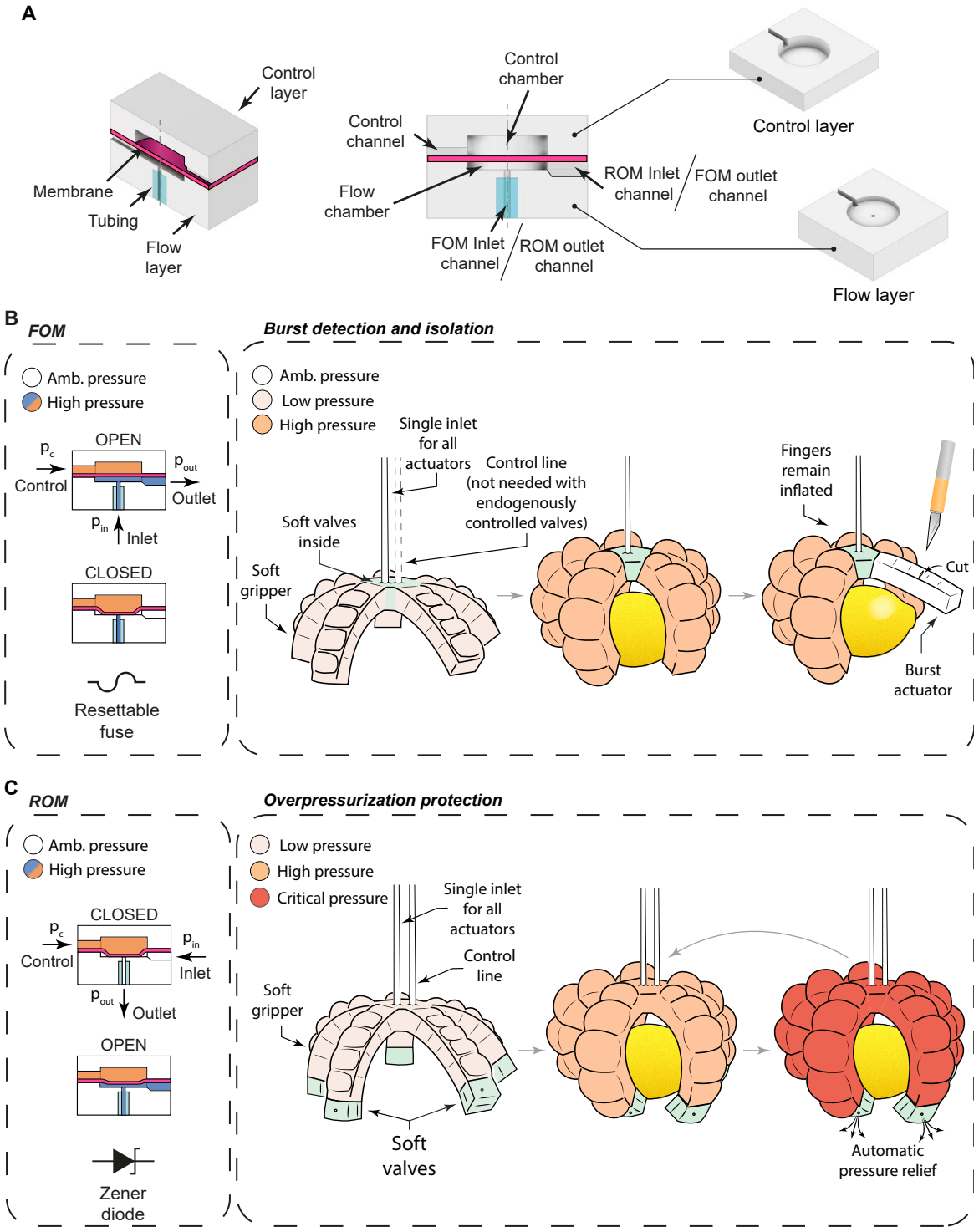

Fig. 5.2 **Details of the soft valve and possible applications.** (**A**) Internal structure of the valve and main components. (**B**) The soft valve, configured in Forward Operating Mode (FOM) can act either as a PNP transistor or a resettable fuse. When paired with soft actuators, the valve can therefore automatically detect and isolate bursts, preventing a single actuator fault from affecting the whole system. (**C**) The Reverse Operating Mode (ROM), which constitutes the second mode of operation of the valve, turns the valve into the equivalent of a Zener diode. In this configuration, the valve can protect actuators against damage from overpressurisation, caused either by controller error or by external disturbances.

and material properties of the valve. In this condition, the deformed membrane no longer obstructs the outlet channel and air can therefore discharge through the valve. In this mode the valve acts as the equivalent of a Zener diode and, as such, can be used to protect against overpressurisation of SIEs.

Multi-modality is achieved through the asymmetric geometry of the valve. The control pressure always acts on the same surface of the membrane, independent of the operating mode. The inlet pressure, conversely, acts on different areas depending on the mode. In FOM, with the valve closed, the area is equal to that of the inlet channel tubing, so the valve can stay closed, even when inlet and control pressure are equal in value. In ROM, the pressure acts on the side area of the deformed membrane that is not contacting the bottom of the flow layer chamber. This change in active area causes the valve to open, even when p_{in} is lower than p_c. In addition, thanks to this multi-modality, it is possible to create an Endogenously Controlled (EC) soft valve capable of self-tuning operation. This version of the soft valve is able to generate its own control signal, taking into account the behaviour of the SIE it is paired with. As a result, the passive burst detection and isolation functionality is achieved without an external control line being present.

5.3.2 Soft Valve Provides Resilience Against Bursts

Forward operation mode characterisation

In FOM, the valve is positioned between the main pressure source and an SIE and requires two external signals, inlet and control, at the same supply pressure level p_s to operate. Fig. 5.3A shows this configuration, together with the opening and closing conditions for the valve; while Fig. 5.3B presents an example of one of the burst detection and isolation experiments used to characterise the valve (see Material and Methods section and Fig. 5.12 for details). The flow layer is first pressurised, followed by the control layer. As the same pressure p_s is acting on the two sides of the membrane, the valve remains open for further inflation of the SIE. When a burst occurs ($t = 4\,\mathrm{s}$), the asymmetric distribution of internal fluidic resistances causes the pressure underneath the membrane to quickly drop, leading the membrane to deform and obstruct the inlet, isolating the outlet. The available pressure difference between the two sides of the membrane depends on the ratio of inlet to outlet resistance within the soft valve (Fig. 5.21). After the burst, the equilibrium equation for the membrane can be written as

$$\frac{\pi}{4}\left[p_c\left(D^2 - d_c^2\right) - d^2\left(p_c - p_{in}\right)\right] - fm = 0\,,$$

where D represents the membrane diameter (Fig. 5.3C), d the inlet channel diameter, d_c the diameter of the contact area between the membrane and the bottom of the flow layer chamber,

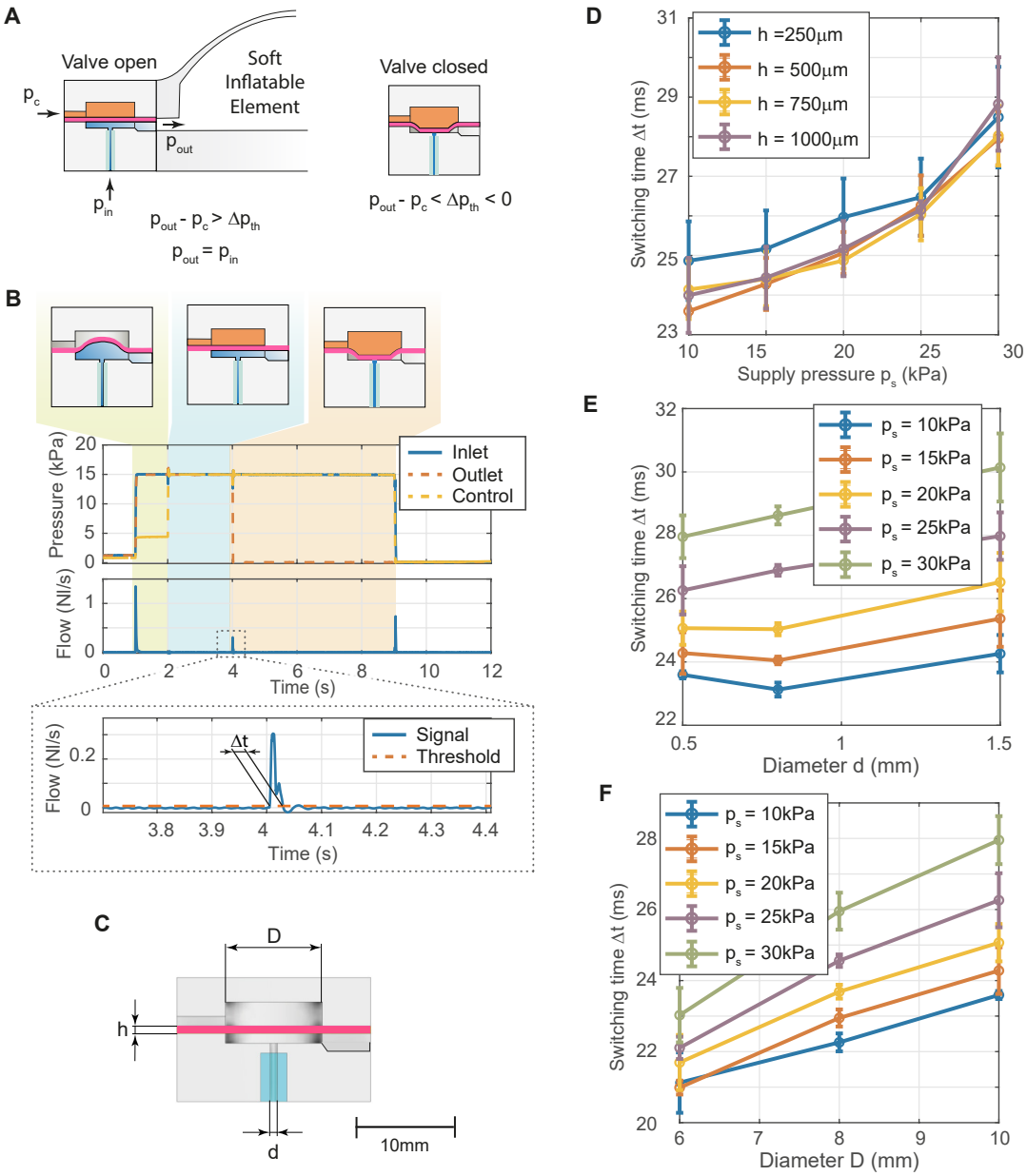

Fig. 5.3 **Experimental characterisation of the FOM behaviour.** (**A**) Working principle of the FOM behaviour and associated conditions for the two states of the valve, open and closed. (**B**) Example experiment used to demonstrate and evaluate the switching time of the valve upon a simulated burst. The beginning and end of the flow rate spike is used to compute the switching time Δt. (**C**) Internal structure of the valve and relevant geometrical parameters. (**D**) Comparison of the switching time of the soft valve with different membrane thicknesses, from 250 μm to 1 mm. Error bars in plots indicate the average standard deviation obtained in the trials. See Materials and Methods for additional details. (**E**) Switching times obtained by changing the diameter of the inlet channel d of the soft valve and the supply pressure. Narrower inlet channels provide reduced flow rate, leading to faster switching times ($\Delta t < 30$ ms). (**F**) Comparison of three different geometries of the valve with different chamber diameter D and same $d = 0.5$ mm. Narrower D and lower supply pressures translates into faster, more reactive valves.

and fm is the elastic force associated with the deformed membrane. The valve then remains closed until the control signal is removed.

For the valve to operate correctly for burst isolation, it needs quick response time and a sufficient input impedance. In order to understand the effects of the internal geometry of the valve, we investigated the effect of the membrane thickness h and both diameters d and D on the switching time Δt. As clearly visible in Fig. 5.3D, reaction times improve slightly at lower supply pressures. For the range being tested, the membrane thickness does not alter the performance in a significant manner (average p-value of one-way ANOVA was $p = 0.22$), with all the valves averaging a switching time of 25.11 ms ($SD = 1.99$ ms) and nearly identical patterns with respect to changes in the supply pressure: the switching time decreases from 29 ms to 23 ms on average, going from a supply pressure of 30 kPa to 10 kPa. A slight decrease in the standard deviation can be observed as the membrane thickness increases. This is likely due to slight differences caused by the manual fabrication steps, which have more impact on the thinner membranes. The use of thicker membranes is therefore to be preferred, as these are easier to fabricate, grant less dispersion in the results and are less prone to failure at high pressure values. When comparing different internal geometries, more pronounced changes can be observed. As to be expected, narrower inlet channels lead to faster switching times: in the event of a burst, a larger Δp is formed between the surfaces of the membrane, due to the increased input impedance. The largest channel ($d = 1.5$ mm) averaged 27.1 ms across the supply pressure levels, compared to 25.8 ms of the thinnest one (Fig. 5.3E). The largest change in performance, though, was observed by changing the diameter D of the chamber (Fig. 5.3F), with an average difference of 3.64 ms between the fastest ($D = 6$ mm) and slowest ($D = 10$ mm) geometries and an overall 17.6% improvement (at 30 kPa). A smaller diameter D leads to a smaller, more reactive membrane, but also to a smaller flow layer chamber and less air that has to escape when the burst occurs.

Burst detection and isolation in a five-finger soft gripper

In order to demonstrate the functionality of the valve in FOM, a five-finger elastomeric gripper was used. As shown in Fig. 5.4, A and B, each finger consists of a Pneu-Net-type actuator [134] which bends upon inflation. The fingers are connected to a palm that incorporates one soft valve for each finger, five in total. The valves have $D = 6$ mm, $d = 0.5$ mm, a membrane thickness h of 500 μm and fit inside a pentagon shaped palm whose edges measure 20 mm in length. All valves are configured in FOM and only two inlets to the system are required: one for the inflation of the gripper, the other for the pressurisation of the control channel, shared among all five valves.

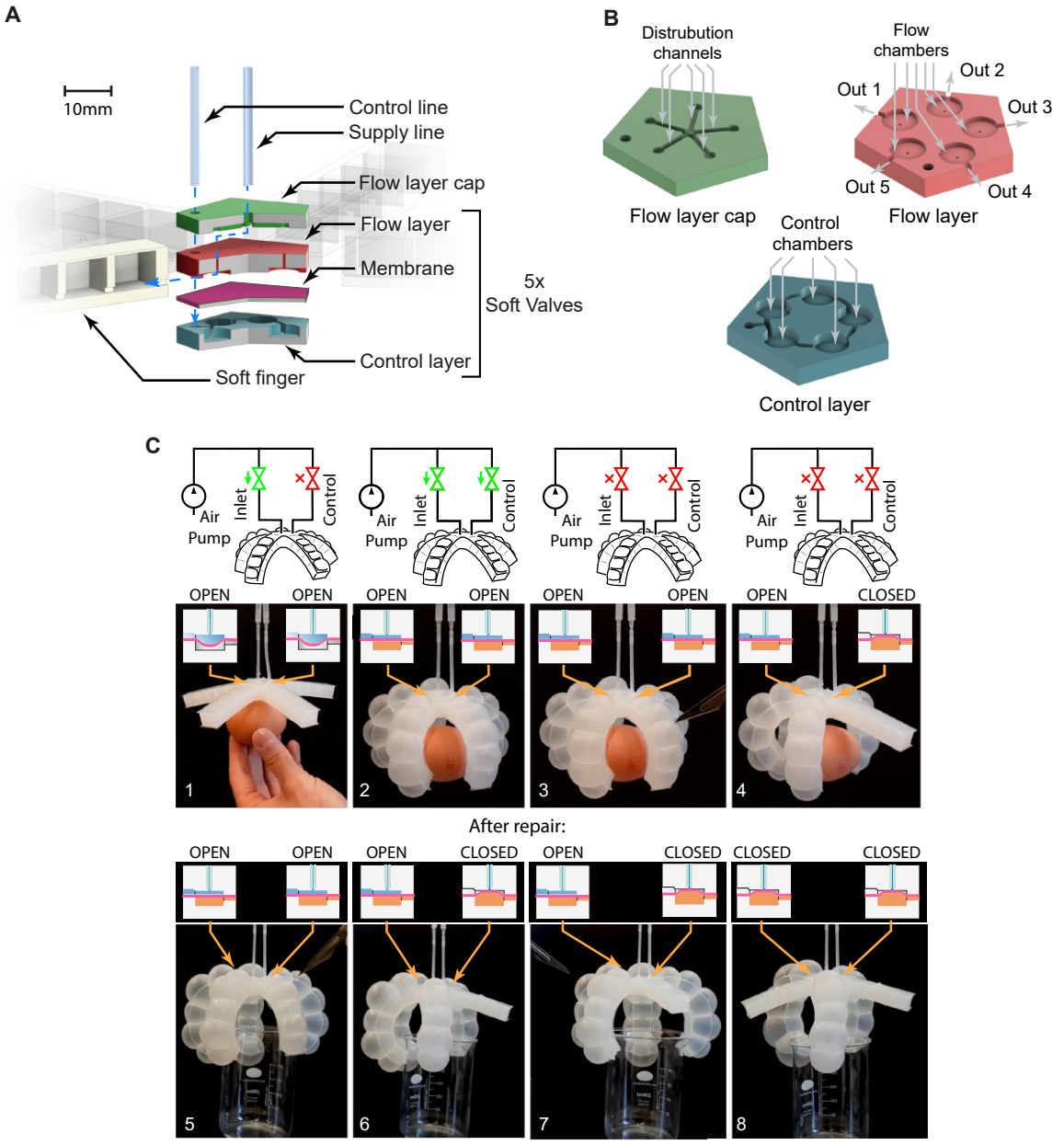

Fig. 5.4 **Automatic burst detection and isolation in a pneumatic soft gripper.** (**A**) Internal structure of the five-finger soft gripper with integrated soft valves. All the valves are embedded in the palm, which consists of four different layers, together with the channels to distribute the actuation fluid. Only one supply and one control channel are needed to control the gripper and achieve the burst isolation capability, therefore limiting hardware requirements and control logic complexity. (**B**) Detail view of the main layers forming the palm of the soft gripper and their relevant features. (**C**) Experimental trials demonstrating the burst detection and isolation capabilities in action. First, the gripper is inflated and isolated from the supply (1-2). One of the fingers is then burst, but the gripper maintains its grasp on the raw egg it is holding (3-4). The faulty finger is repaired using a thin layer of Sil-Poxy glue and then the gripper is reinflated (5-6). Two fingers are then burst, showing that more than one finger can fail and the fault detection and isolation still works, independently for each finger (7-8).

The gripper is inflated and grasps the object at hand, a raw egg in the first case. Meanwhile, the control channel is pressurised, activating the burst detection and isolation functionality (Fig. 5.4C, 1 and 2). When one of the fingers contacts a sharp object, it suddenly bursts, causing its corresponding soft valve to switch and isolate it from the rest of the fingers. As a result, the remaining four fingers keep their grasp on the object, preventing it from falling (Fig. 5.4C, 3 and 4). The hole in the faulty finger is then sealed using a thin layer of Sil-Poxy glue and the gripper is reused to grasp a different object (Fig. 5.4C step 5). This time, two fingers are punctured, further proving the independence between the fingers, while still maintaining a firm grasp on the object (Fig. 5.4C,steps 6 through 8).

5.4 Reversed Soft Valve Protects Against Overpressurisation

Reverse operation mode characterisation

In ROM, the control channel starts out pressurised at pressure p_s and the deformed membrane therefore obstructs the narrow outlet channel (valve closed). The second external input is represented by the inlet channel, supplied by the same p_s. Once $p_c - p_{in}$ reaches a threshold value Δp_{th}, the membrane cannot obstruct the outlet anymore and the soft valve opens (Fig. 5.5A). Contrary to what happens in FOM, in ROM the equilibrium equation for the membrane is:

$$\frac{\pi}{4}(p_c - p_{in})\left(D^2 - d_c^2\right) - fm = 0\,.$$

Fig. 5.5B experimentally captures the ROM behaviour of the soft valve. The control channel is pressurised, immediately reaching the supply pressure value p_s; the inlet channel is then activated. As the inlet pressure increases, the outlet pressure remains at ambient pressure level, proving that the outlet is isolated from the inlet. When the condition $p_c - p_{in} < \Delta p_{th}$ is reached, the valve opens and the outlet pressure p_{out} suddenly rises, matching p_{in} in value. The stability of the valve in proximity of the threshold pressure difference was also verified, checking for any autonomous unintended switching of the soft valve (Fig. 5.22 in Supplementary Materials).

Fig. 5.5C summarizes the experimental results obtained varying the membrane thickness. As visible, thicker membranes require lower values of p_{in}, larger Δp_{th}, for the valve to open, for the same control pressure. These results can be explained through the superposition of two effects. Thicker membranes deform less for the same control pressure, leaving more side area exposed to the effect of the inlet pressure p_{in}. The second effect is that of fm which increases with the membrane thickness and pressure p_c, lowering the threshold pressure

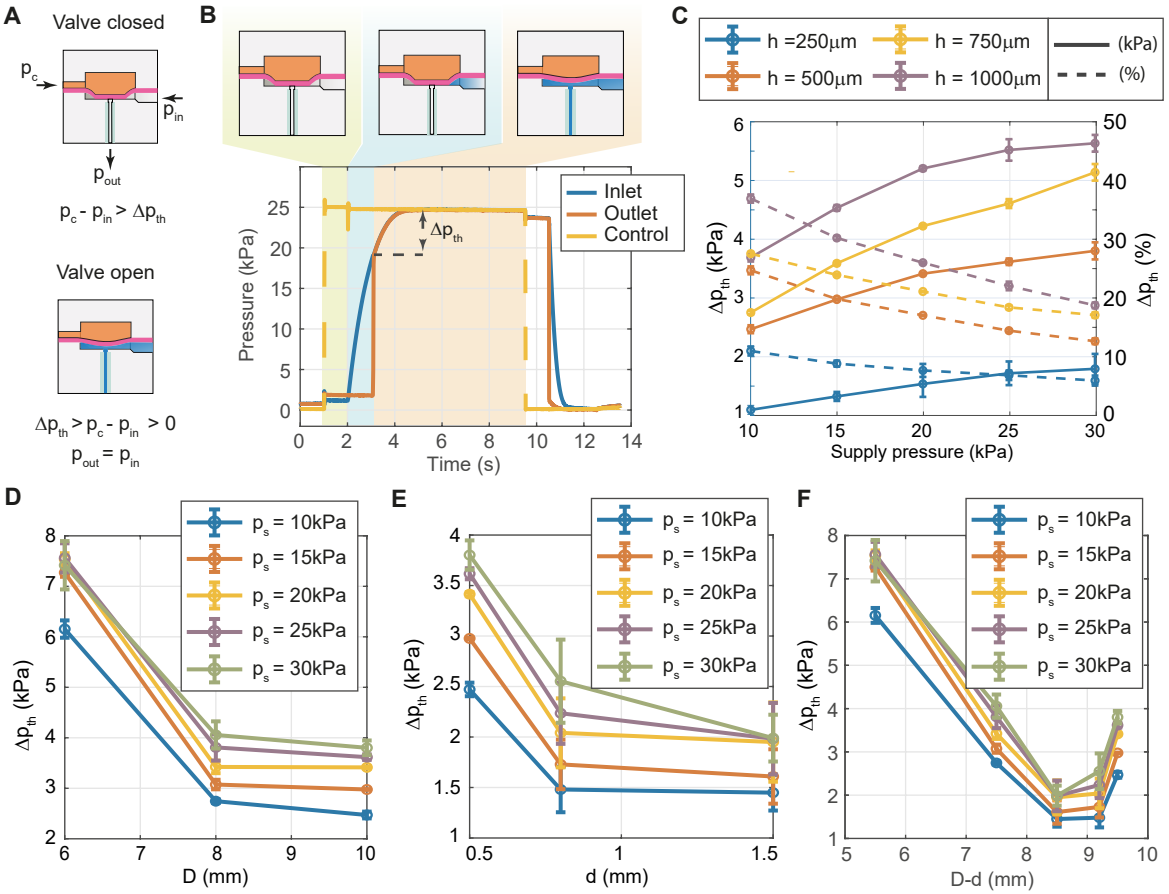

Fig. 5.5 **Experimental characterisation of the ROM behaviour.** (**A**) Working principle of the ROM behaviour and associated conditions for the two states of the valve, open and closed. (**B**) Example experiment used to characterise the behaviour of the valve. When the outlet pressure jumps to the inlet pressure value, the Δp between the control pressure and the inlet pressure is measured and used as the main comparison metric. (**C**) Comparison of different membrane thicknesses with $D = 10\,\text{mm}$ and $d = 0.5\,\text{mm}$. The solid lines refer to the results in kPa, while the dashed ones are in percentage terms. Error bars in plots indicate the average standard deviation obtained in the trials. See Materials and Methods for additional details. (**D**) Results obtained by changing the chamber diameter D from 6 mm to 10 mm. Larger chambers provide more uniform behaviour across the range of supply pressures tested, making for a better performing valve overall. (**E**) Comparison of geometries based on the outlet diameter d. (**F**) The parameter $D - d$, the difference between the diameter of the membrane and that of the outlet channel, is used as the metric to compare all geometries together. The best performing geometry, minimum of the curves, was obtained with a difference of 8.5 mm.

needed for the valve to open. A slight upward trend is present in the results, irrespective on the membrane thickness, but the change in Δp_{th} is always less than 2.5 kPa. The downward slope observed in the percentage results (obtained as $\frac{\Delta p_{th}}{p_s}$) demonstrates that this increase is more than compensated by the increase in the corresponding supply pressure. In addition, thinner membranes show a more uniform, flattened performance across the various supply pressures: an overall change of 0.7 kPa in Δp_{th} is observed for the 250 μm membrane, while this increases to 2.4 kPa with a 750 μm thick membrane.

When comparing different internal geometries, both D and d have an impact on performance (Fig. 5.5, D and E respectively), but a change in the chamber diameter D provides a larger variation, especially at lower pressure levels: more than 3.5 kPa change of Δp_{th} when increasing D from 6 mm to 10 mm, compared to a 1.7 kPa change when varying d from 0.5 m to 1.5 mm. Fig. 5.5F shows a comparison of all the different geometries through the metric $D-d$: the diameter of the chamber D is proportional to the contact diameter d_c of the membrane with the chamber, and the diameter of the tubing d represents the critical value for d_c below which the valve is open. As visible in the chart, there seems to be an optimal value for $D-d$ equal to 8.5 mm, with a 500 μm membrane, which minimises both the Δp_{th} for each supply pressure level, as well as its variation across supply levels, leading to an overall better performing ROM configured valve.

The results hint at how the soft valve configured in ROM can be used as a way to sequence actions based on the inlet pressure level, by setting the control pressure signal. In a more specialised setting, the valve can be used as a pressure relief solution, to limit the internal pressure of an SIE to safe levels, therefore providing resilience against overpressurisations due to control loop problems or external disturbances.

Reverse operation for overpressurisation protection in soft gripper

The ROM-configured soft valve was embedded in an elastomeric two-finger hand to demonstrate the overpressurisation protection (Fig. 5.6A). Upon actuation, the fingers inflate and bend, making it possible to simulate a hand shake for human-robot interaction scenarios. Only one of the fingers has a ROM configured soft valve at its tip ($D = 10$ mm, $d = 0.8$ mm and a membrane thickness of 500 μm), making it possible to better highlight the effect of the valve on the behaviour of the gripper. Before the gripper is inflated, the control chamber of the soft valve is pressurised. As visible in Fig. 5.6B, when a hand is placed close to the gripper, this is inflated to perform the hand shake. The soft digits are then squeezed, overpressurising them (Fig. 5.6, C and D). As visible, the finger with the soft valve at its tip lets the air out, deflating more, the tighter the squeeze. The other finger, conversely, suffers irreversible damage due to plastic deformation of two of the inflatable membranes at the tip

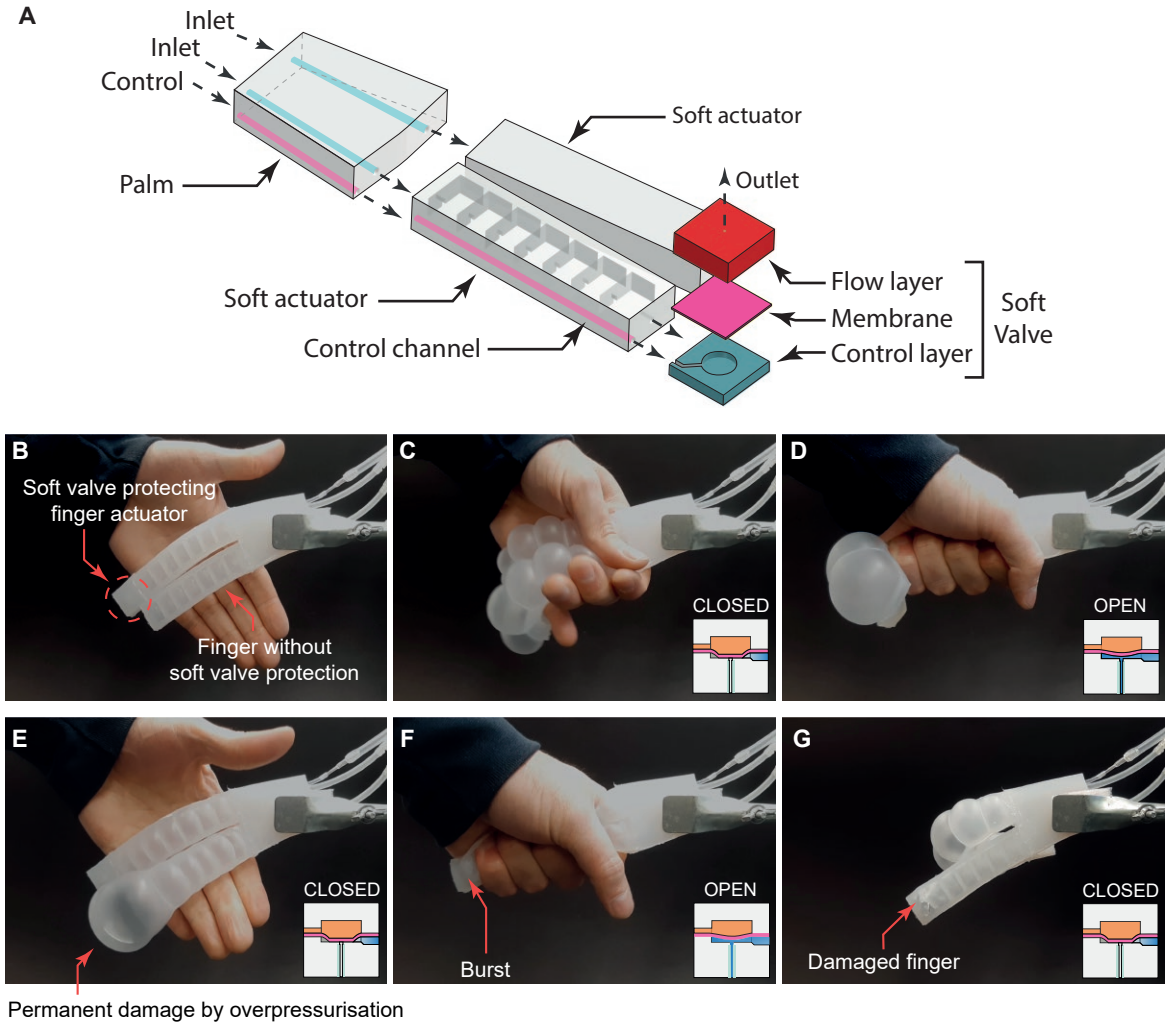

Fig. 5.6 **Automatic overpressurisation protection in a two-finger soft hand.** (**A**) Structure of the two-finger soft hand with all the relevant components and connections. (**B-G**) Experiment showing the overpressurisation protection capabilities of the ROM configured soft valve. Only one of the fingers, the top one in the figures, is being protected. Upon inflation, the fingers are squeezed, causing irreparable damage to the unprotected finger (B through E). The same finger then bursts after a second run of the experiment, while the finger protected by the valve still performs the same as upon the first inflation (F and G).

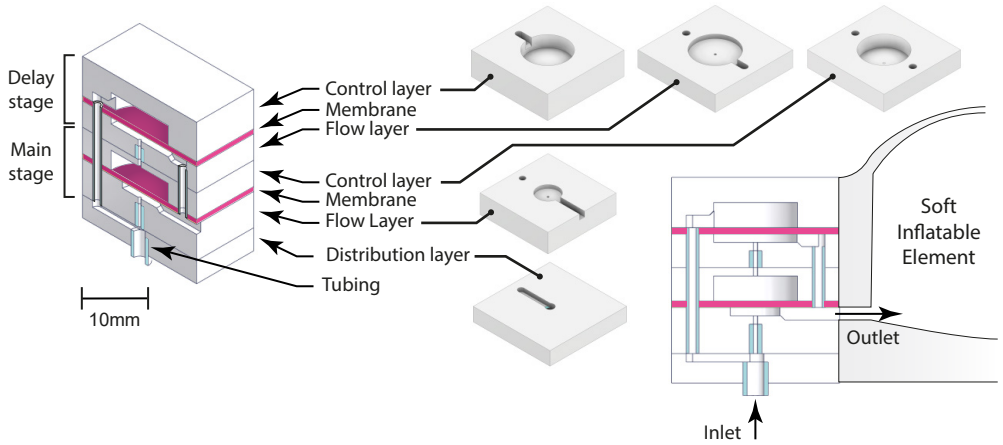

Fig. 5.7 **The Endogenously Controlled (EC) soft valve.** (**A**) Detailed view of the internal structure of the two-stage EC soft valve. The main stage at the bottom ($D = 6\,\text{mm}$, $d = 0.5\,\text{mm}$, $h = 0.5\,\text{mm}$) is internally connected to the delay stage at the top ($D = 10\,\text{mm}$, $d = 0.5\,\text{mm}$, $h = 0.5\,\text{mm}$). Thanks to its self-tuning capability, the valve can generate its own control signal. As a result, only two ports are open to the environment: the inlet, connected to the supply, and the outlet, going to the SIE.

(Fig. 5.6E).
Repeating the experiment shows that the behaviour of the damaged finger is compromised: the tip of the finger over inflates from the start and the bending angle of the digit is reduced. A second squeeze causes the actuator to burst at the site of the damage (Fig. 5.6F), making it unresponsive, in contrast to the performance of the finger that has the soft valve at its tip, which remains unaltered (Fig. 5.6G).

5.4.1 Two-Stage Soft Valve Achieves Endogenous Control and Fault Isolation

Endogenously controlled soft valve characterisation

When using the soft valves in FOM, one of the challenges that arises at the system level is knowing when to pressurise the control chamber, as its premature actuation might lead to the SIE being isolated from the supply. The delay that is required between the pressurisation of the two channels depends on multiple factors, such as the supply pressure level, the overall SIE volume, the material properties and the geometry of the SIE. Extensive system characterisation would be required, and even then, challenges would remain if different SIEs shared the same control line. To avoid such problems, two soft valves can be combined into a unit capable of endogenous control signal generation. This behaviour is automatic and does

not rely on external pressure sensors, valves or a controller, therefore removing the need for a control channel altogether.

Fig. 5.7 shows a section view of the newly designed Endogenously Controlled (EC) soft valve. This is created by stacking two of the soft valves in a main stage, at the bottom, and a delay stage, at the top, operating out of a single supply pressure level. Only two ports are open to the environment: the narrow bottom one serves as the inlet, while the larger side port is the outlet, to be connected to a SIE. All other connections are internally routed. The principle of operation is presented in Fig. 5.8A. The SIE is deflated and both membranes start out in their relaxed states (both soft valves are open). Upon activation of the inlet channel ($t = 1.0\,\mathrm{s}$), the control chamber of the delay stage is immediately pressurised. As a consequence, the top membrane deforms, closing that valve, initializing the delay stage in ROM. Meanwhile, the air-flow passes through the FOM configured main stage and reaches the SIE, whose pressure starts increasing. The increase in main stage control pressure during this initial phase is due to the slowly increasing outlet pressure, which deforms the main stage membrane upwards, compressing the air trapped in the control chamber. Once the outlet pressure reaches the correct threshold value, the delay stage opens, letting the air-flow through and pressurising the control chamber of the main stage ($t \approx 7.5\,\mathrm{s}$). From now on, if a burst were to occur, the delay stage would turn to FOM and the membrane would switch, trapping the air present in the control chamber of the main stage. The main stage would switch too, isolating the faulty SIE from the rest of the system. A main stage with a small chamber diameter ($D = 6\,\mathrm{mm}$) and inlet diameter ($d = 0.5\,\mathrm{mm}$) was selected to get the fastest FOM behaviour, while a larger chamber diameter ($D = 10\,\mathrm{mm}$) was used for the delay stage, to improve ROM behaviour performance.

The change in behaviour of the delay stage happens automatically, being dictated only by the change in pressure gradient between inflation transient and burst. The delay stage, which starts out in ROM, is the key to achieving endogenous control, as the control channel of the main stage gets pressurised only once the pressure in the SIE reaches a high enough level, independent of SIE volume, geometry or material. In case of voluntary deflation, the control channel of the delay stage would depressurise first, meaning that the soft valve would not interfere with the normal behaviour of the SIE.

To prove that the new EC soft valve can be paired with SIEs of any volume, self-tuning its own operation, valves were manufactured and tested by connecting them to a wide range of volumes, from 50 ml to 1.0 l, obtained by partially filling a rigid glass container with water. Fig. 5.8B shows the behaviour of one valve when supplied at 20 kPa. For clarity, only the outlet and main stage control signals are displayed for all the volumes tested. As the volume increases, the delay between the initial actuation ($t = 1.0\,\mathrm{s}$) and the control signal

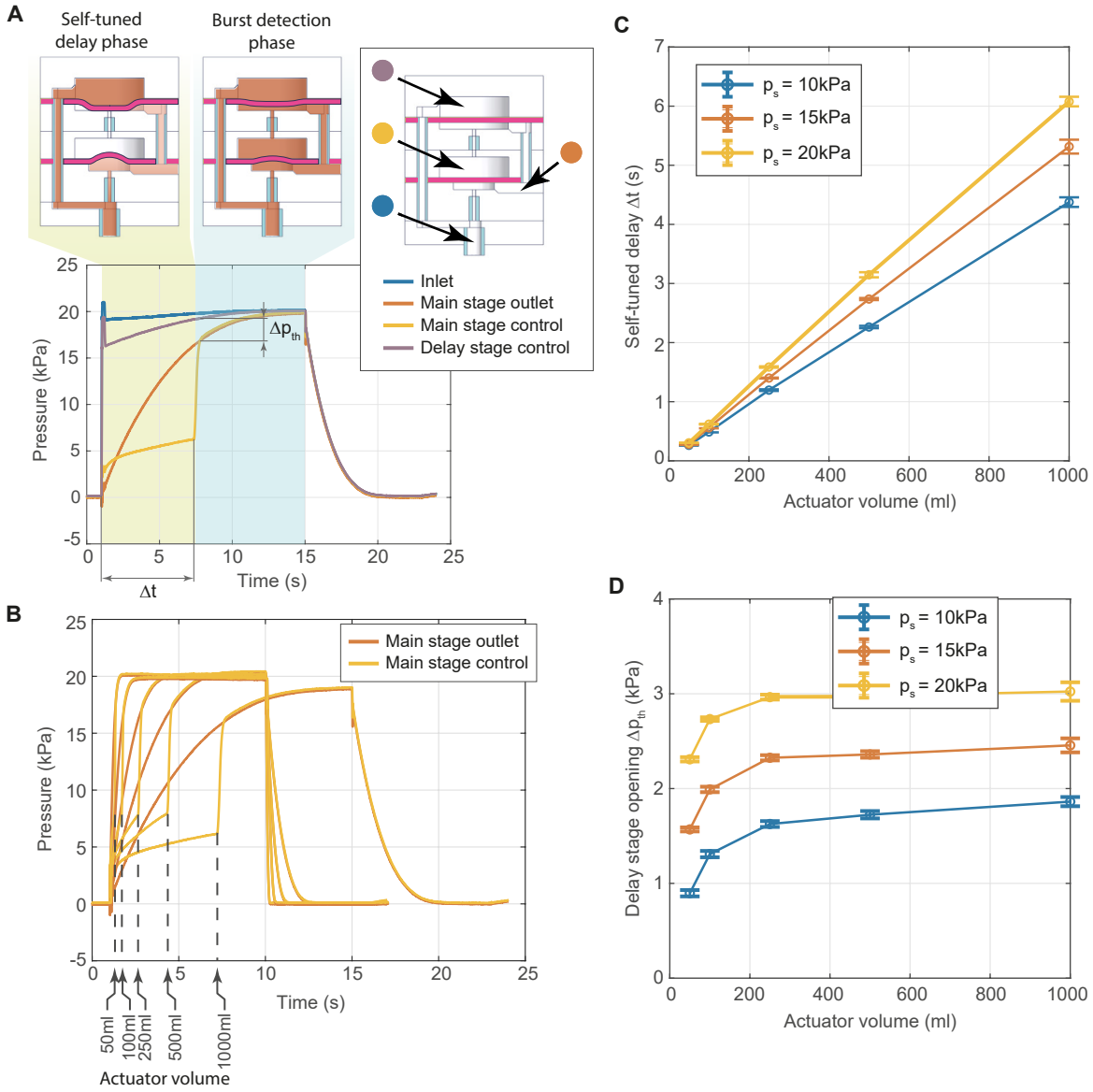

Fig. 5.8 **Experimental characterisation of the two-stage soft valve.** (**A**) Sample run of the experiment used to characterise the behaviour of the valve in terms of switching Δp_{th} and self-tuned delay time Δt. In the section views, a darker shade represents higher pressure values. The Δp_{th} is measured between the delay stage control pressure and the main stage outlet pressure when the delay stage opens, while the Δt is the amount of time elapsed between the first pressurisation of the inlet channel ($t = 1.0\,\text{s}$) and the opening of the delay stage. (**B**) Comparison of the Δt obtained with a constant supply pressure of 20 kPa, by changing the accumulator volume. Only the main stage outlet and control pressures are shown for clarity. Error bars represent the average standard deviation computed as detailed in the Materials and Methods. (**C**) Delay Δt obtained by varying the supply pressure and the accumulator volume between 50 ml and 1.0 l. The Δt increases linearly with the volume from 260 ms to 6.0 s, proving the self-tuning capabilities of the soft valve. (**D**) Comparison of the Δp_{th} obtained by varying supply pressure and accumulator volume. As expected from the ROM characterisation experiments, for the same volume, the Δp_{th} increases as the supply pressure increases. When keeping the supply pressure constant and changing the volume, the Δp_{th} remains almost constant, proving that the SIE volume only mainly affects Δt.

being fully present increases proportionally, from 200 ms to 6.8 s. At the same time, the Δp_{th} which causes the delay stage to open remains almost constant. Fig. 5.8C considers the effect that the SIE volume has on the Δt between the initial pressurisation of the inlet channel and the pressurisation of the main stage control chamber. This effect is evident, with the delay increasing almost linearly from around 260 ms to 6.0 s as the volume increases from 50 ml to 1.0 l. The figure also shows that an increase in the supply pressure has the effect of increasing the delay Δt too, and the effect becomes more pronounced at larger volumes: a 42 ms difference is observed for a 50 ml volume between 10 kPa and $20 kPa$, while at 1.0 l, the difference becomes 1.7 s. Fig. 5.8D, on the other hand, shows that the SIE pressure needed for the delay stage to open is almost constant and independent of the volume. The maximum measured difference was less than 1.0 kPa between the smallest and largest volumes, with a supply pressure of 10 kPa. Nevertheless, opening Δp_{th} measured across all volumes and supply pressure levels are consistent with the results previously obtained for the ROM configured simple valve ($D = 10$ mm, $d = 0.5$ mm and $h = 500\,\mu$m).

Fig. 5.9 shows the new EC soft valve achieving self-tuning and burst detection and isolation when paired with two ballooning soft actuators of different sizes. The self-tuning capability becomes apparent when comparing the green regions of subfigures A and B. The small actuator, with a membrane whose diameter measures 12 mm before inflation, only takes 0.4 s to fully inflate (Fig 5.9, A and C). As a result of this fast inflation transient, the delay stage soft valve opens after just 0.16 s. Around $t = 6.5$ s, the actuator is burst using a sharp blade. Following the sudden depressurisation of the outlet, the delay stage switches, isolating the main stage control chamber from the outlet (yellow line in Fig. 5.9A decoupled from the red one after the burst). The main stage also closes, separating the inlet pressure, which remains equal to the supply pressure, from the outlet, which drops to ambient pressure. As visible in the figure, following the burst, the main stage control pressure stabilizes to a pressure value intermediate between the supply one and ambient pressure. This value depends on two factors: the expansion of the control chamber when the main stage switches and the depressurisation due to the air that escapes from the chamber before the delay stage has closed. The second experiment, conducted with a larger actuator sporting a 24mm diameter membrane (Fig. 5.9D), shows a similar pattern, but the actuator has a much longer inflation transient. As a result of the self-tuning capability of the valve, the internal control signal is generated after 5.2 s. At $t = 8.0$ s, the actuator is burst and the EC soft valve again successfully detects and isolates the burst. Immediately after the bursts, the drops in pressure observed in the main stage control chamber between the two experiments are very similar: as the burst can be considered almost instantaneous, these only depend on the supply pressure and the specifics of the valve (internal geometry and material properties).

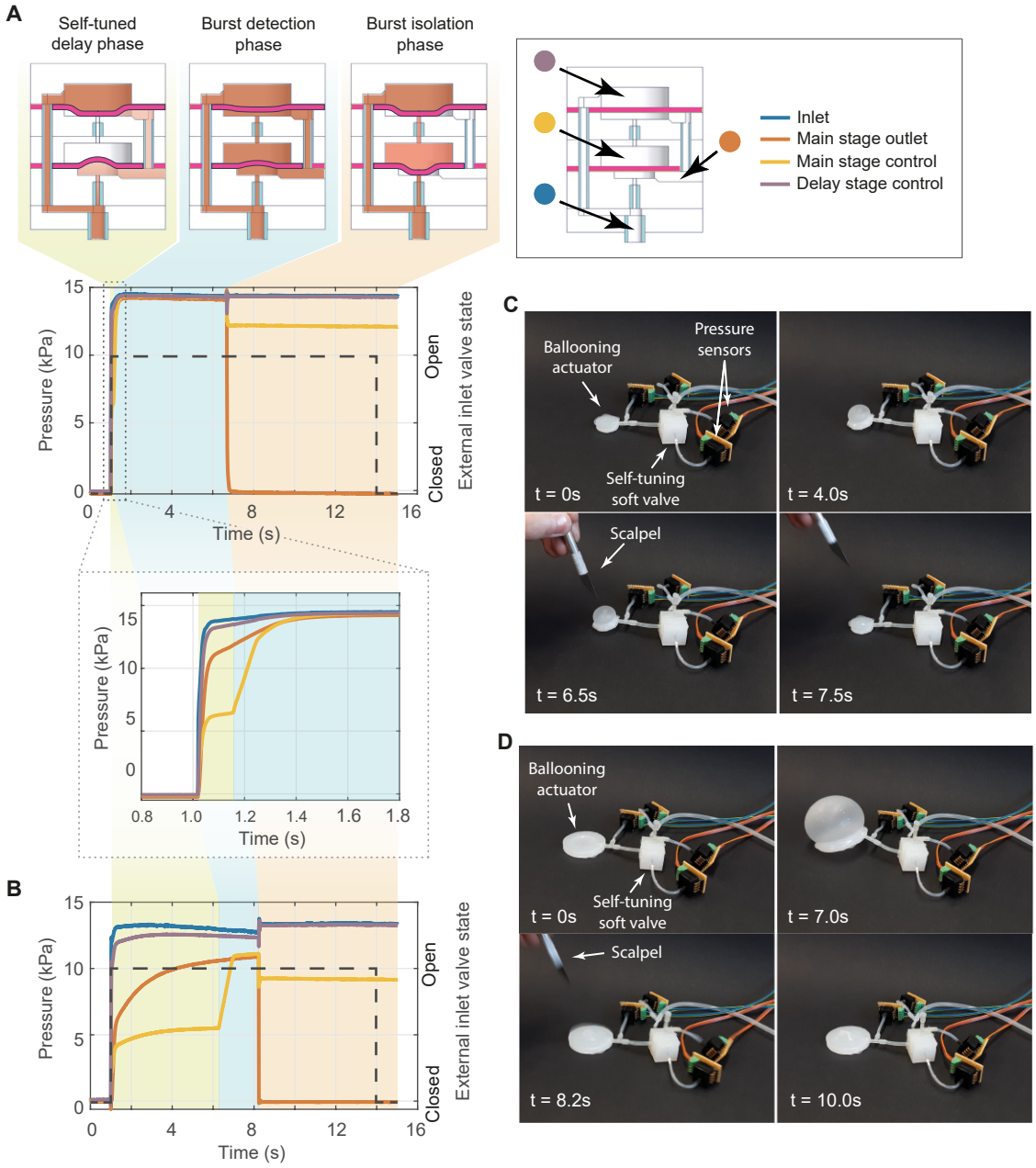

Fig. 5.9 **Automatic burst detection and isolation with the two-stage EC soft valve.** (**A-B**) Experiments showing the self-tuned delay and burst isolation capability of the EC soft valve. Two ballooning actuators of different sizes are used to compare the behaviours. (A) With the small actuator, the threshold pressure needed to open the delay stage is reached in less than 100 ms, while it takes around 5.0 s with the larger one (B), due to the different pressurisation transient of the actuator. (**C**) Experiment showing the inflation and burst isolation with the small ballooning actuator. The deflated membrane measures 12 mm in diameter. (**D**) Experiment showing the inflation and burst isolation with the large ballooning actuator (diameter of 24 mm).

Autonomous burst detection and isolation in a pneumatic soft crawler

The seamless integration of the EC valve in existing soft robots is demonstrated in a soft crawler, manufactured out of two bellows-type actuators. The actuators share the same supply line and are periodically inflated and deflated together (Fig. 5.10A), while the crawling motion is enabled by the asymmetric friction provided by the specific geometry of the feet. The valves are placed inside the empty volume of the actuators to achieve maximum compactness and simplify the routing of pneumatic channels. The crawler is supplied with a pressure of 12.5 kPa for 5.5 s and then partially deflated for 1.2 s, resulting in an actuation frequency of 0.15 Hz (Fig. 5.10B and Supplementary Video 4). The partial deflation of the actuators decreases the crawling speed, but keeps the internal channels of the EC valves pressurised. With the actuation sequence just described, the robot achieves an average crawling speed of 42 mm/min (Fig. 5.10C). When the front bellows is suddenly burst using a sharp blade, the front EC valve switches and isolates it from the supply (Fig. 5.10D). Because of the partial deflation technique, the pressure in the control chamber of the delay stage does not disappear, therefore maintaining the front actuator isolated, while the rear one is actuated. As a result, the robot can keep on crawling at a reduced speed of 21.4 mm/min (Fig. 5.10, E and F). No changes to the control sequence are needed and no sensors are present onboard, demonstrating the completely passive and autonomous nature of the approach. The robot is then submerged in water (Fig. 5.10G) to show the absence of air bubbles coming from the burst actuator, further proving its successful isolation.

5.5 Discussion

The development of soft valves have been instrumental in achieving control of soft robots without any onboard electronics [129, 104]. Soft valves offer the possibility of low-cost manufacturing and tailored performance, as well as the potential for monolithic integration, leading to fully soft robots. To this day, very few works have looked at the possibility of using these components for anything else other than as logic gates in control units. In this paper, we presented a multi-modal soft valve featuring endogenous control for resilience of soft robots through an embodied and passive approach. The valve can be easily integrated into existing pneumatic soft robotic designs, with small alterations required during the manufacturing process.

Inspired by innate mechanisms observed in biological systems, this paper explored the possibility of using soft valves as self-contained units to achieve in situ fault responsiveness, without controller intervention. The internal geometry of the valve enables multi-modality, leading to two distinct behaviours: FOM and ROM. In FOM, the soft valve can autonomously

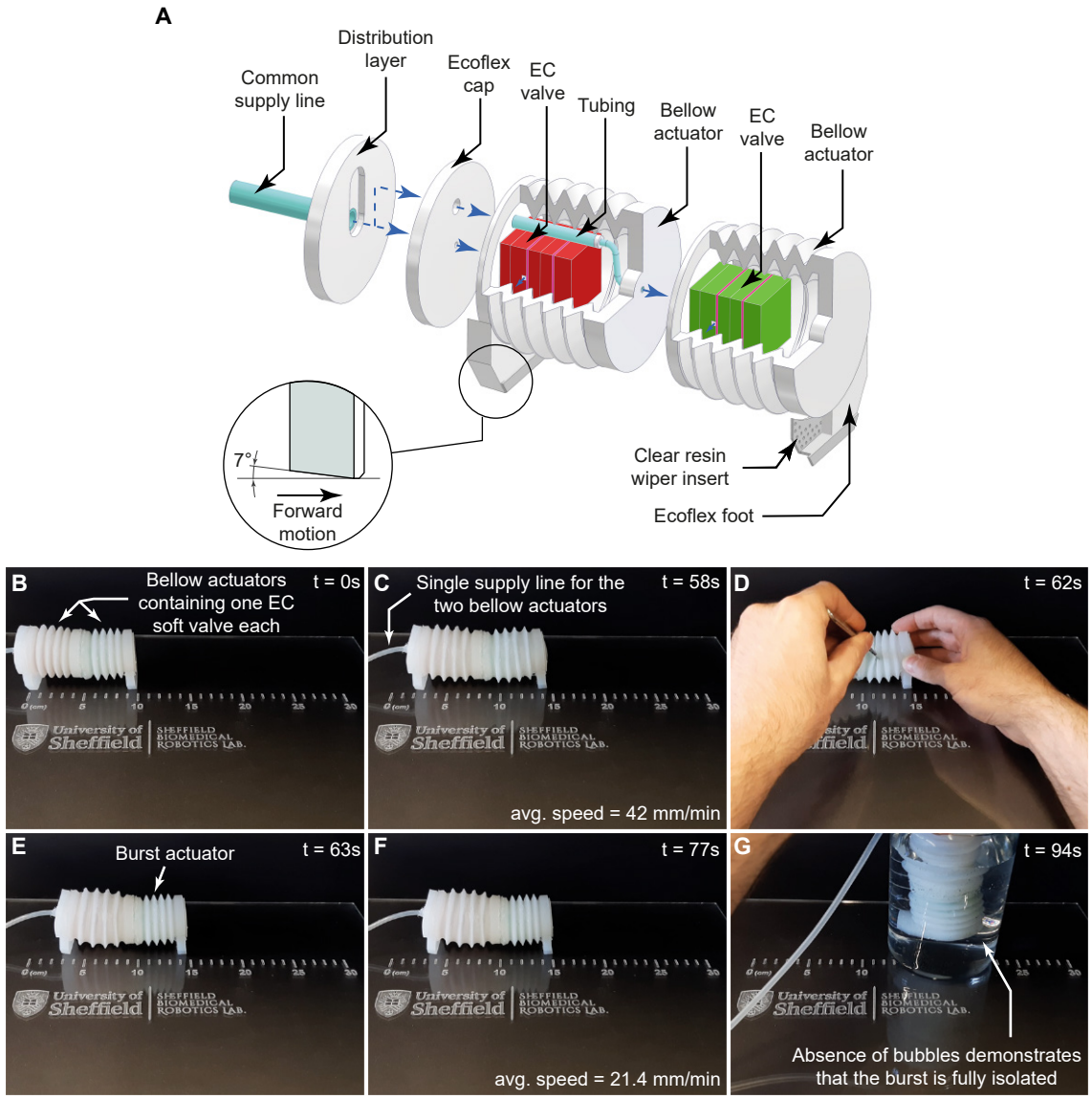

Fig. 5.10 **Automatic burst detection and isolation in a pneumatic soft crawler.** (**A**) Internal structure of the soft crawler integrating the EC soft valves. Two bellows actuators form the body of the robot and share the common supply line. The valves were placed inside of the empty cavities in the bellows to achieve maximum compactness of the design. The connection between the supply and the front bellows is also internally routed. The periodic inflation and deflation of the actuators, together with the asymmetric friction provided by the feet, enable the crawling motion. (**B-C**) The soft crawler achieves an average moving speed of 42 mm/min with a supply pressure of 12.5 kPa. A 5.5 s inflation transient is followed by a 1.2 s deflation one, giving an actuation frequency of 0.15 Hz. The actuators are never fully deflated; this reduces the crawling speed, but makes it possible to isolate a faulty actuator, while the other one keeps working. (**D**) A sharp blade is used to cut into the side of the front actuator, bursting it. (**E-F**) Thanks to the partial deflation technique, the burst front actuator is kept isolated, while the back one operates normally. As a result of the partial loss of actuation, the crawling speed is decreased to 21.4 mm/min. (**G**) To prove the successful isolation of the burst, the robot is submerged in water while still being actuated and no air bubbles are observed.

detect and isolate bursts in pneumatic SIEs, reacting to the sudden drop in pressure created by the burst itself. Experimental characterisation highlighted the effect of critical design parameters, such as geometry of the inlet channel, on the switching time of the valve, leading to a design that can consistently isolate burst SIEs in less than 25 ms, 8 ms faster than the average duration of a human blink [135]. This capability makes it possible to fabricate grippers that can maintain their grasp in case one or more fingers burst, with just one common inlet channel, therefore drastically reducing the need for external hardware (such as tubing, external valves and sensors) as well as reducing the complexity of the control logic. In addition, a partial deflation technique similar to that used for the soft crawler can be used to operate the gripper while maintaining the faulty fingers fully isolated. Swapping the inlet and outlet channels activates the ROM behaviour, which can be used to protect against accidental overpressurisation. The importance of such capability is demonstrated in a human robot interaction experiment. During the experiment, prior to bursting, one of the soft actuators plastically deforms, leading to irreparable damage. This type of damage irrecoverably alters the performance of the actuator, with overinflation of the damaged section, but it would not be detected by material self-healing approaches, as the continuity of the material matrix is not compromised. The ROM configured valve therefore enables a pre-emptive type of resilience, as opposed to the more common ex-post one. The threshold value which toggles the valve can be tuned by varying the control pressure, as well as geometrical design parameters as demonstrated in the paper. According to the experiments, a difference of 8.5 mm between the diameter of the membrane and that of the inlet channel yields optimum performance for all supply pressure levels, with a membrane thickness of 500 μm.

One of the common challenges in soft robot control stems from the hyperelasticity of soft materials which leads to their accentuated nonlinear behaviour upon repetitive inflation. Successful control usually requires pre-emptive knowledge about the SIEs, achieved either through numerical modelling or extensive experimental training. This limits the usability of the valve in FOM, whereas the ROM behaviour is not affected, as the control signal is always present. By pairing the FOM and ROM valve configurations, we demonstrated the possibility of creating an endogenously controlled soft valve. This valve can generate its own control signal, using direct feedback from the SIE it is paired with, without the need for pre-existing knowledge of the SIE or intervention from an external controller. As a result, despite only having one inlet and one outlet port, the valve can achieve autonomous burst detection and isolation, irrespective of the non-linear behaviour or size of the SIE. For this to happen, the delay stage valve automatically swaps from ROM to FOM when a burst occurs, further highlighting the importance of the valve's multi-modality. The absence of an external

control line makes this pneumatic component a truly self-contained solution for soft robotic resilience, increasing its usability as a drop-in solution for many soft robotic applications.

Despite the capabilities and advantages, some limitations remain to be addressed. Even though full integration in the body of soft robots is possible, fabrication currently requires a number of manual steps which slow down manufacturing and limit accuracy and repeatability. Additive manufacturing techniques could provide a solution, leading to semi-autonomous or fully autonomous, monolithic fabrication [129, 104, 130]. A second advantage of additive manufacturing techniques entails miniaturisation of the design. Currently, the smallest samples manufactured have $D = 6\,\text{mm}$, with five such valves tightly packed in the 34 mm-diameter of the soft gripper's palm. Minimum sizes achieved in this study were constrained by technological limitations and manufacturing techniques, but further miniaturization efforts might be needed in order to might be needed in order to exploit the full potential of this distributed approach to resilience at larger scales. For this, advancements in microfluidic component design and manufacturing could provide valuable insights [136, 128]. One drawback of miniaturization might be the reduction of maximum flow rates through fluidic components, leading to increased delays and consequent negative effect on system dynamics. Nevertheless, with thoughtful design, we believe that the local distributed control approach presented in this paper would still be beneficial in reducing reaction times associated with long and narrow supply lines, characteristic of complex microfluidic systems. In such systems, minimising the physical distance between logic and actuation is critical in achieving the fast reaction times needed for critical applications such as burst detection and isolation.

In addition, the soft valve presented in this work can form a unifying platform for resilient soft robots, by integrating passive pre-emptive fault isolation with material healing techniques. As discussed, some of the current limitations of approaches based on self-healing materials entail time to recovery and inactivity during healing. The FOM configured soft valve responds to these limitations by providing selective deflation and isolation of the faulty actuator. Pairing the two technologies would result in the creation of soft robots that can carry on working while their bodies are healing from previous faults. The further inclusion of fault signalling [137, 55] could lead to the possibility of performing system-level behaviour change to compensate for the faulty section of the robot, either temporarily, while the system is healing, or permanently, further improving the overall resilience.

The proposed approach represents an evolution in fluid control of soft robots; a first step towards taking what so far has been a centralised architecture, with one fluidic controller managing the whole robot, and transforming it into a distributed architecture, where local control units autonomously manage the resilience of each SIE. In a way, the valves give hard-coded primitive responses to the system, independent of the higher-level control logic, meant

to protect and preserve the welfare of the system as a whole, similar to the instinctive reactions humans experience when responding to a threat. Building on responsive mechanisms, more complex systems can be built where robot units can exchange signals and transfer information, possibly using fluidics as a medium. The breath and importance of behaviour adaptation to resilience has been clearly demonstrated by software-based fault-tolerant approaches. Information sharing will therefore be a crucial step in the development of fluidically controlled resilient soft robots. In the long term, the inclusion of research on biodegradable self-healing materials [138, 40, 17] would enable the creation of robots that can maximise their life expectancy, recovering from multiple faults while carrying out various tasks and, in the end, degrade and provide resources for other organisms/robots to use. Capitalising on key intrinsic capabilities of soft robots, such as better adaptation to unstructured environments, and improving upon them by adding self-preservation mechanisms, a new generation of life-like bio-inspired machines can be developed, for a more sustainable future.

5.6 Materials and Methods

5.6.1 Fabrication of valves

Single valve fabrication

The soft valve consists of three layers, moulded out of Ecoflex 00-50 (1:1 ratio of parts A and B, mixed for 3 minutes in an orbital mixer). All moulds are printed in clear resin (Formlabs) using 50 μm resolution on a Form2 printer. Tubing is cut to length and inserted in the inlet channel area of the flow-layer mould. The tubing is cut slightly short, and stops about 1 mm before entering the flow layer chamber. This is so that the membrane, when deformed, interfaces with an uninterrupted, smooth, soft surface, therefore maximising sealing potential. The moulds are prepared by spraying them with Ease Release 200 and the silicon is then cast and cured at room temperature for 4 hours. Once solid, the flow and control layers are unmoulded, while the membrane is left untouched, to avoid wrinkling. A small amount of Sil-Poxy glue is uniformly applied to the surface of the flow layer, which is then pressed onto the membrane. The pair is then joined to the control layer with in the same way. Again, the glue is applied to the control layer, not the membrane directly, in order to avoid applying the adhesive to areas that do not need it, with the risk of locally altering the mechanical properties of the membrane.

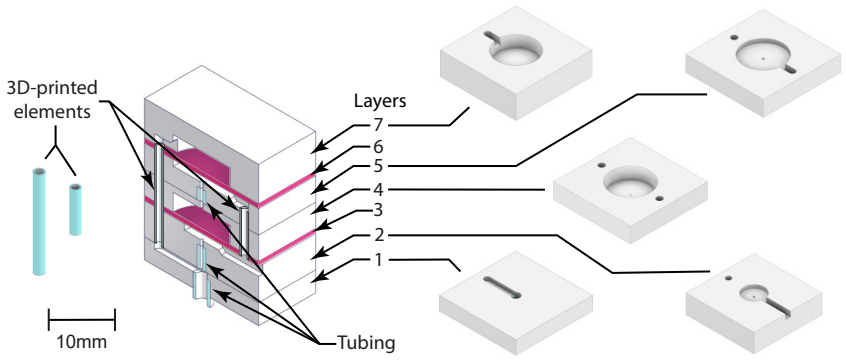

Fig. 5.11 **Structure of the two-stage EC soft valve.** The valve consists of seven separate layers glued together using Sil-Poxy adhesive and two 3D-printed inserts.

Two-stage EC valve

With reference to Fig. 5.11, after moulding, layers 2 and 3 are glued together, as well as layers 4 and 5. Once the glue is set, a syringe needle (external diameter of 1 mm) is passed through the central hole of components 4 and 5, to make sure the channel is free of glue. The pairs are then joined, gluing together layers 3 and 4. A wide needle is run through the side channels, cutting the membrane that is obstructing them, and 3D-printed elements, components 8 and 9 (printed using Formlabs' clear resin on a Form3 printer), are inserted into these. Finally, one at a time, layers 1 and 7 are added to the stack, completing the fabrication process. As visible in the figure, the main stage has the following geometric parameters: $D = 6\,\text{mm}$, $d = 0.5\,\text{mm}$, $h = 500\,\mu\text{m}$. For the delay stage, a valve with $D = 6\,\text{mm}$, $d = 0.5\,\text{mm}$ and $h = 500\,\mu\text{m}$ is used.

5.6.2 Characterisation of the valves

During the characterisation of the soft valves and the demo applications, an Arduino Nano paired with a custom designed PCB was used to control the setups. In addition, all sensors were sampled at 10 kHz using a custom designed data acquisition system capable of simultaneous sampling on eight channels at 16-bit resolution. The remaining hardware included five 12 Vdc solenoid valves (0520D-DC12V), five pressure sensors (Honeywell ASDXAVX005PGAA5), a volumetric flow sensor (Renesas FS1012-1100-NG), a peristaltic pump, two 5.0 l accumulators, a flow regulator, a 50 ml syringe, tubing (4 mm ID) and Tee tubes. Refer to the next subsections for a detailed guide of the hardware needed for each experiment.

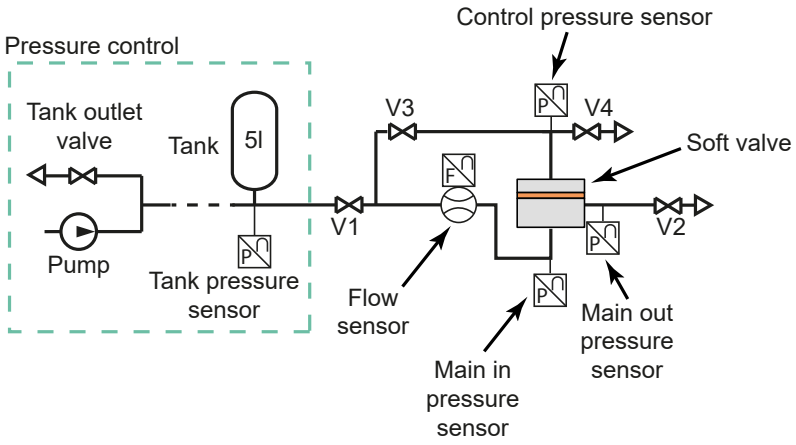

Fig. 5.12 **Pneumatic test circuit used for the FOM characterisation.**

FOM characterisation experiments

The pressure in the accumulator is stabilized to the target pressure and then the pump is switched off to enable accurate pressure measurements. Valve V1 controls the inlet to the flow layer of the valve, V2 the outlet, while V3 and V4 manage the inlet and outlet of the control channel respectively (Fig. 5.12). There are four phases to the experiment: the inlet channel is pressurised first, followed by the control channel. After two seconds, V2 is opened to simulate the burst, connecting the main supply with the atmosphere. After a brief initial discharge of air, the membrane inside the soft valve blocks the flow and isolates the main supply. This discharge is picked up by the flow sensor present in the circuit and makes it possible to evaluate the response time of the valve, as detailed in Fig. 5.3B. The time Δt required for the valve to isolate the burst is defined by the intersections between the flow-rate and a threshold line. The threshold value was set to be 10% higher of the output noise of the flow-sensor at rest. The fourth and last step is to reset the pneumatic circuit by depressurising the control line. The spikes visible in the flow rate data refer respectively to the initial pressurisation of the circuit, to the simulated burst, and to the reset of the pneumatic circuit before the next experiment.

Seven designs were manufactured (three samples for each design) and tested. Four different membrane thickness have been produced: 250 μm, 500 μm, 750 μm and 1000 μm. The inlet channel diameter d was varied from 0.5 mm to 0.8 mm to 1.5 mm (constant membrane thickness of 500 mum), while the chamber diameter D was changed from 6 mm to 8 mm to 10 mm (constant membrane thickness of 500 μm). In addition, the supply pressure level p_s was varied from 10 kPa to 30 kPa. Each data point in the charts represents the average of 15

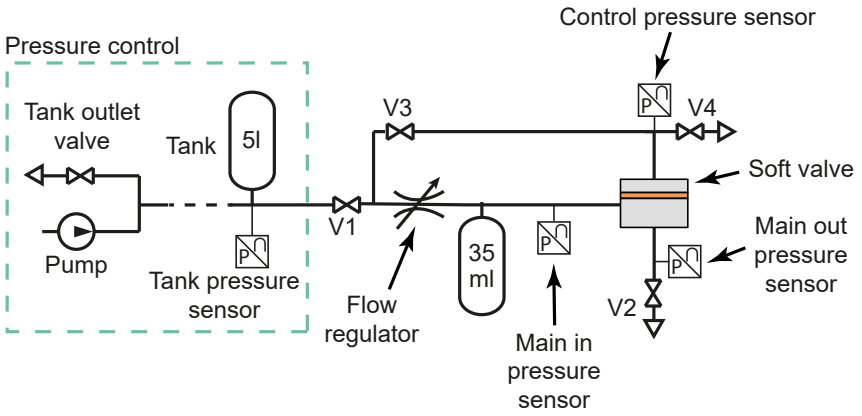

Fig. 5.13 **Pneumatic test circuit used for the ROM characterisation.**

trials (5 trials for each of the 3 samples per each design). Average standard deviations are computed using the formula: $SD = \sqrt{1/3 * \left(SD_1^2 + SD_2^2 + SD_3^2\right)}$.

When evaluating whether the membrane thickness had a statistically significant impact on the switching time, separate one-way ANOVA tests were conducted and the five resulting p-values were then averaged to get the final one. For each supply pressure value, four groups were compared, one for each membrane thickness, and each group contained data from all three samples and all five repetitions (15 data-points in total in each group).

ROM characterisation experiments

Similar to the FOM experiments, the pressure is stabilised in the tank and then the pump is switched off. Valve V1 manages the inlet to the soft valve, V2 the outlet, V3 allows the pressurisation of the control channel and V4 its deflation (Fig. 5.13). A 35 ml volume, together with a flow regulator are used to slow down the pressurisation of the inlet channel and allow for more precise measurements. One could think of these as the SIE connected to the soft valve. The same membrane thicknesses and internal geometries as before are used. Each experimental trial consists of 3 phases. Valve V3 is first opened, pressurizing the control channel. V1 is opened one second later, letting air into the main channel of the soft valve. When the pressure at the inlet of the soft valve reaches a threshold value dependent on the value of p_c, the valve opens and the outlet channel is pressurised. At that instant, the difference between the control pressure and the inlet pressure determines the opening $\Delta p = p_c - p_{in}$ for the valve in those conditions. The last phase consists in the reset of the circuit for the next trial. The main inlet valve is closed, the control channel is depressurised and the outlet valve is opened. Finally, after 3,s, the outlet valve is closed.

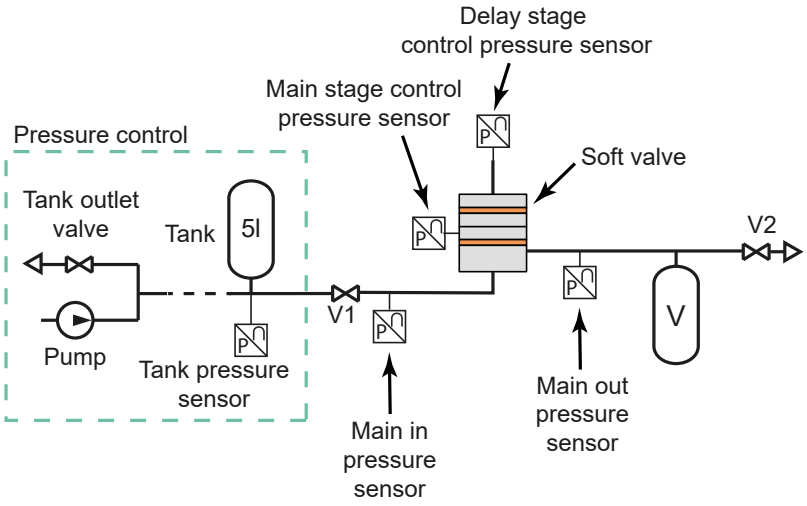

Fig. 5.14 **Pneumatic test circuit used for the EC soft valve characterisation.**

Two-stage valve characterisation

For the characterisation of the EC soft valve, only two external valves are needed: V1 controls the main inlet, while V2 the outlet (Fig. 5.14). A 5 l glass container, partially filled with water, is used as the varying SIE volume. Three samples of the soft valve were manufactured and tested at three different supply pressure levels: 10 kPa, 15 kPa, 20 kPa. Five trials were carried out for each supply pressure level and actuator volume and the results were then averaged. The actuator volume was varied from 50 ml to 1.0 l to cover a wide range of soft robotics applications and better highlight the self-tuning capability of the soft valve.
During each experiment, valve V1 is opened and kept open for a duration of time that is long enough for the actuator volume to reach the supply pressure level. V1 is then closed and V2 is opened to depressurise the actuator and the soft valve, resetting the circuit for the next run.

5.6.3 Fabrication of the robots

Fabrication of the 5-finger gripper

All elements are cast out of Ecoflex 00-50 (for preparation, refer to the valve manufacturing process) and bonded together using Sil-Poxy glue. Each finger is a Pneu-Net-type actuator composed of two layers, while the palm of the gripper, which contains five soft valves, is made out of four different layers (Fig. 5.15A). The moulds for the Pneu-Net fingers were printed in PLA on a Prusa Mk3S printer, while those for the palm were manufactured out of clear resin on a Form2 printer.

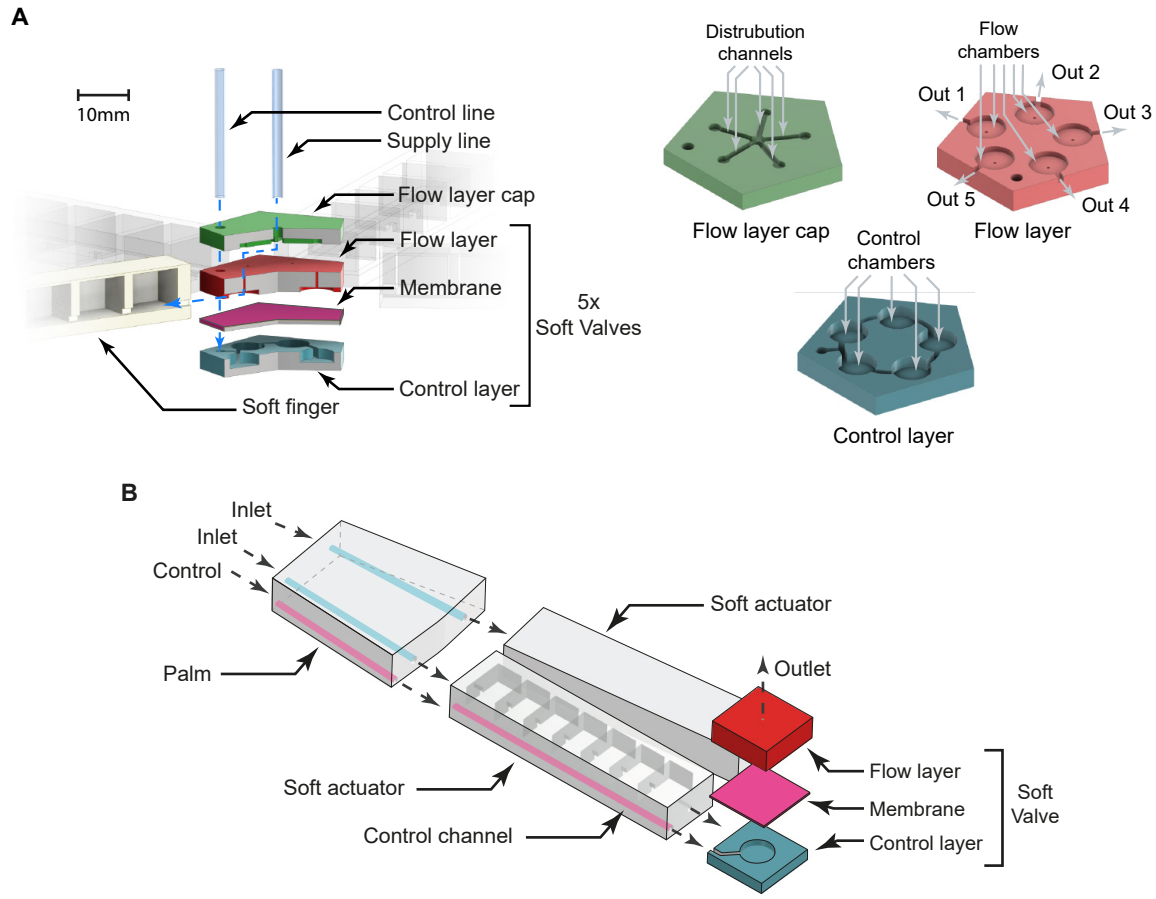

Fig. 5.15 **Manufacturing of the soft grippers**. (**A**) Structure of the five-finger soft gripper and detailed view of the layers constituting the palm embedding the soft valves. (**B**) Detailed view of the assembled two-finger hand.

Tubing is placed in the relevant areas of the moulds before casting the silicon and then the layers are glued together one by one. The palm is then tested to make sure that all the channels are unobstructed, before gluing the pre-assembled soft fingers in place, one at a time.

Fabrication of the 2-finger hand

The procedure is similar to the one followed for the 5-finger gripper. The moulds for the palm and the finger are printed out of PLA on a Prusa Mk3S, while for the valve clear resin was used on a Form2 printer. The moulds are prepared by placing the tubing to create the internal channels and then spraying with a releasing agent. There are four main elements to the design: the palm, the two fingers and the ROM configured valve (Fig. 5.15B). The fingers and the valve are assembled first and then the fingers are bonded to the palm. The

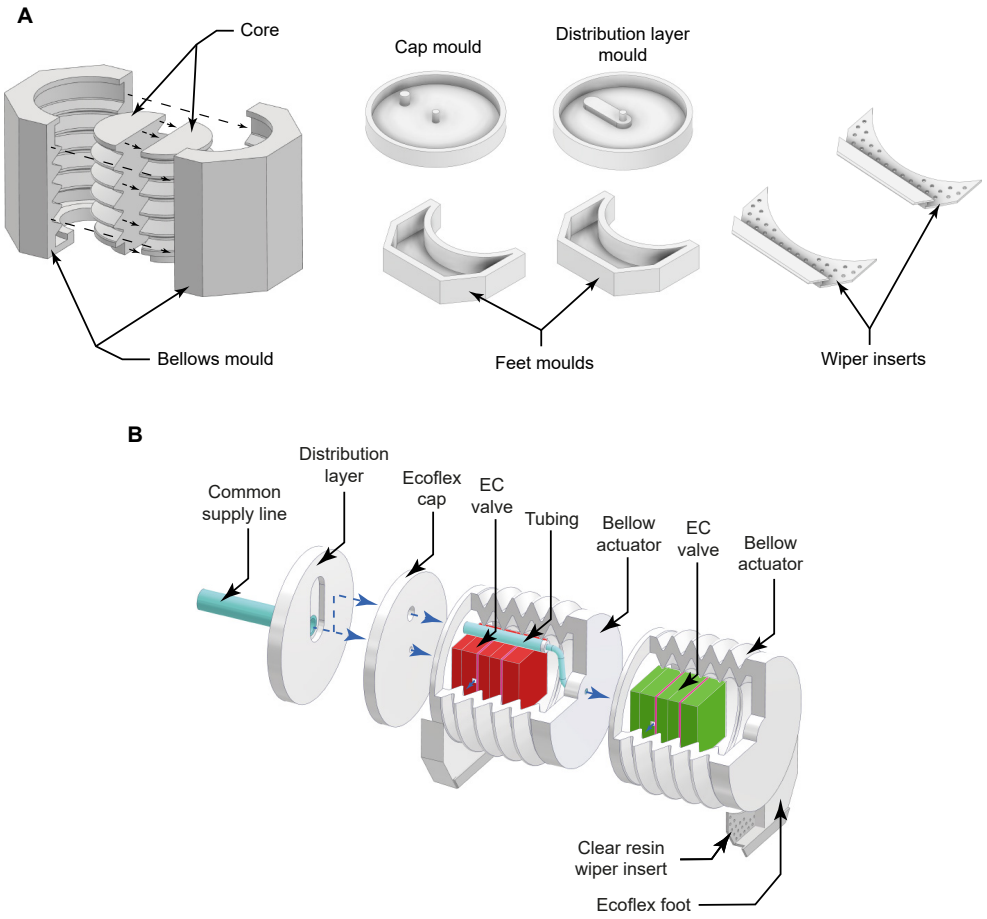

Fig. 5.16 **Manufacturing of the soft crawler**. (**A**) Moulds necessary for the manufacturing of the robot. The bellows actuator moulds are printed in four separate pieces for ease of printing and demoulding. (**B**) Detailed view of the assembled robot.

gripper and the valve are tested to make sure that all channels are working correctly, finally, the valve is added at the tip of the soft finger which has the control channel.

Fabrication of the soft crawler robot

To create the soft crawler, two EC soft valves are manufactured following the technique previously described. With reference to Fig. 5.16, the moulds for the bellows actuators, the feet, the distribution layer and the cap are 3D-printed out of PLA on a Prusa Mk3S. All moulds are sprayed with release agent before casting the Ecoflex 00-50 silicone. The moulds for the feet are partially filled, the wiper inserts, printed in clear resin on a Form2 printer, are then laid in place before resuming the casting of the silicone.

After the Ecoflex is set, the front EC valve is bonded to the rear bellows actuator using Sil-Poxy glue. The front bellows is then glued to the rear one, while the rear EC valve is

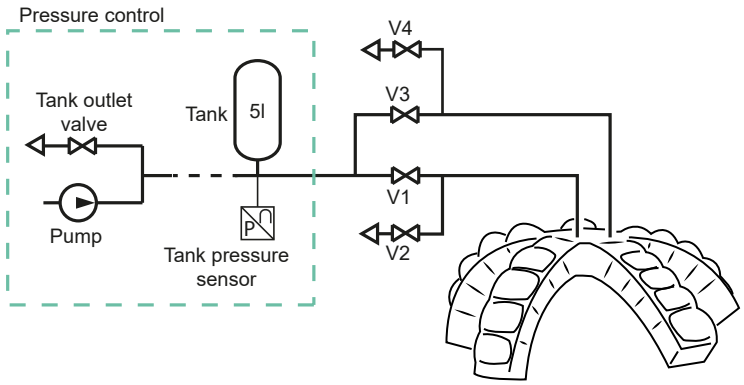

Fig. 5.17 **Pneumatic circuit for the control of the 5-finger soft gripper.**

bonded to the cap. The connection between the front EC valve and the distribution layer is then routed, before the cap, bearing the rear EC valve, is connected to the rear bellows using Sil-Poxy. After testing each actuator individually, the distribution layer is glued in place, followed by the feet.

5.6.4 Control and characterisation of robots

Burst isolation in a five-finger soft-gripper

For the fault isolation in a five-finger soft gripper, the circuit of Fig. 5.17 was used. Four valves are needed to control the pressurisation and depressurisation of the fingers and the control channel respectively. The inlet valve V1 is opened for 10 s, to inflate the gripper ($p_s = 15$ kPa). Valve V3 is then opened to pressurise the control channel. This staggered actuation of the channels is needed to avoid prematurely isolating the actuators from the supply. After 2 s both V1 and V3 are closed, fully isolating the gripper from the supply. One or more fingers are then repeatedly burst using a knife to showcase the burst detection and isolation capability.

Overpressurisation protection in soft hand

For the overpressurisation protection experiment, the circuit of Fig. 5.18 is needed. Valve V2 and V3 control the inflation of the two soft fingers. Valve V1 manages the control channel of the soft valve connected to one of the soft fingers, while V4 acts as the common deflation channel. The two soft fingers are managed independently for demonstration purposes. In real world applications, both fingers would have a soft valve at the tip and only one supply and one control lines would be required. During the experiment, V1 is opened and closed after 2 s ($p_s = 20$ kPa). The fingers are then inflated. Pressure sensor P1 is used to isolate the

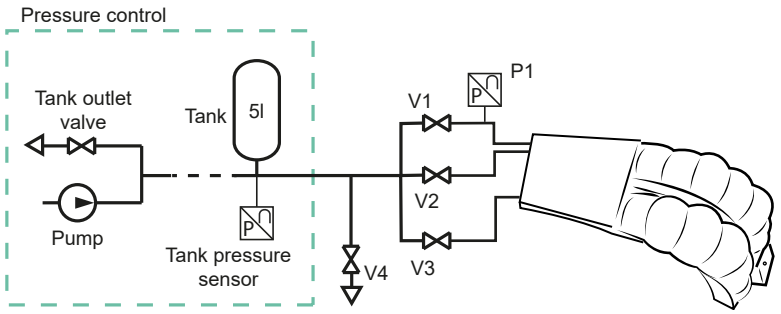

Fig. 5.18 **Pneumatic circuit for the control of the 2-finger soft hand.**

gripper from the supply when the pressure in the fingers reaches a value which, according to the ROM characterisation experiments, is not enough to trigger the opening of the soft valve for the control pressure used. This setup makes it possible to only use one supply pressure level, instead of separate ones for control pressure and inflation pressure. When the pressure in the fingers drops below the a threshold value of 12 kPa, valves V2 and V3 are opened again, triggering the reinflation of the gripper.

Burst isolation in soft crawler

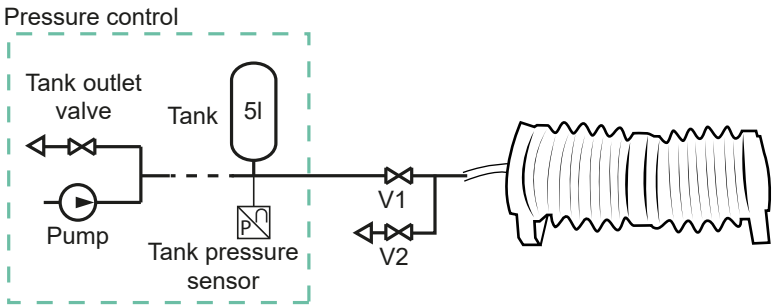

Fig. 5.19 **Pneumatic circuit for the control of the soft crawler robot.**

The inflation and deflation of the robot are managed through valves V1 and V2 (Fig. 5.19). The repeating actuation sequence has a period of 6.7 s. The robot is connected to a supply pressure of 12.5 kPa for 5.5 s and then deflated for 1.2 s. The partial deflation maintains the delay stage control chambers of the EC soft valves pressurised, making it possible to maintain the burst actuator isolated, while still controlling the other one. The geometry of the feet is fundamental to achieve asymmetric friction during the inflation/deflation transient, enabling the crawling motion. Various angles, from 5 deg to 30 deg were tested, with the optimal performing one being 7 deg. The clear resin wiper inserts further reduce friction during the dragging forward of the foot, increasing the overall efficiency of the movement.

5.7 Supplementary Materials

This section contains additional results referenced in the previous sections of the chapter and meant to provide further insights on the behaviour and modelling of the soft valve in its two modes of operation.

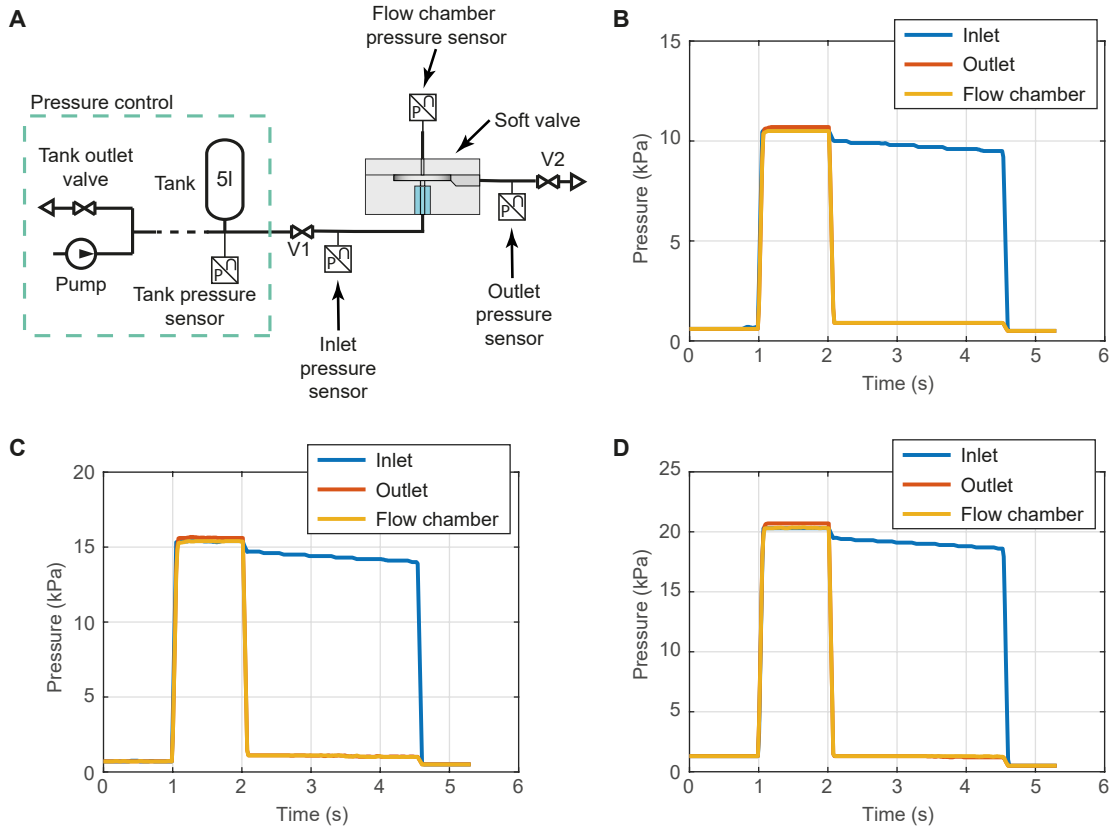

Fig. 5.20 **Decoupling action of the valve.** (**A**) Pneumatic circuit used for the experiment. The test sample is a version of the soft valve with $d = 0.5\,\text{mm}$ and $D = 10\,\text{mm}$, without the membrane and the control layer. A pressure measurement port is used to measure the pressure in the flow chamber, at the exit of the inlet channel. (**B-D**) Experiments that show the decoupling effect that, upon a burst, the inlet channel resistance has. The inlet valve V1 is opened at $t = 1.0\,\text{s}$. The outlet valve V2 is opened at $t = 2.0\,\text{s}$ to simulate a sudden burst; the outlet pressure immediately drops to almost ambient pressure levels, whereas the inlet pressure remains close to the supply pressure value. The decrease in inlet pressure from 2.0s onwards is due to the 5.0l tank discharging through the soft valve and V2.

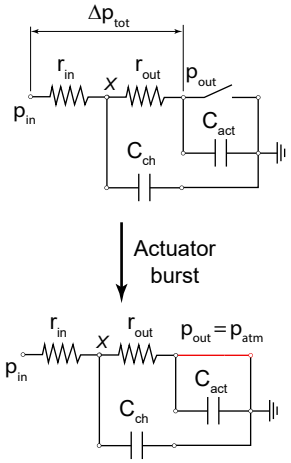

Hagen-Poiseuille:

$r = 128\mu L / (\pi d^4)$

$\Delta p_{tot} = (r_{in} + r_{out})Q$

After burst:

$p_x = r_{out} / (r_{in} + r_{out})p_s = kp_{in}$

L_{in}	L_{out}	d_{in}	d_{out}	k
6.5 mm	7.0 mm	0.5mm	1.5 mm	0.013
		0.8mm		0.080
		1.5mm		0.519

Fig. 5.21 **Zero-order model of the FOM valve connected to a soft actuator.** This simplified model neglects the effect of the supply line. A burst in the actuator can be assimilated to a sudden short circuit which forces the outlet pressure p_{out} to ambient pressure level. Point X in the circuit represents the inside of the flow layer chamber, while r_{in} and r_{out} are respectively the inlet and outlet resistances of the soft valve. C_{act} is the capacitive effect associated with the soft actuator, while C_{ch} is that of the flow layer chamber, negligible compared to C_{act}. The Hagen-Poiseuille law can be applied as the air-flow in the system is fully laminar: the maximum estimated Reynolds number is $Re = 61$, with a flow rate of 2 Nl/s. As a result, assuming a constant chamber diameter $D = 10$ mm, it is possible to estimate the pressure underneath the membrane for the various designs that were tested in the study. After a burst, the pressure p_X varies from 51% of the inlet pressure, with the widest inlet channel, to just 1.3% of the inlet pressure, when $d = 0.5$ mm.

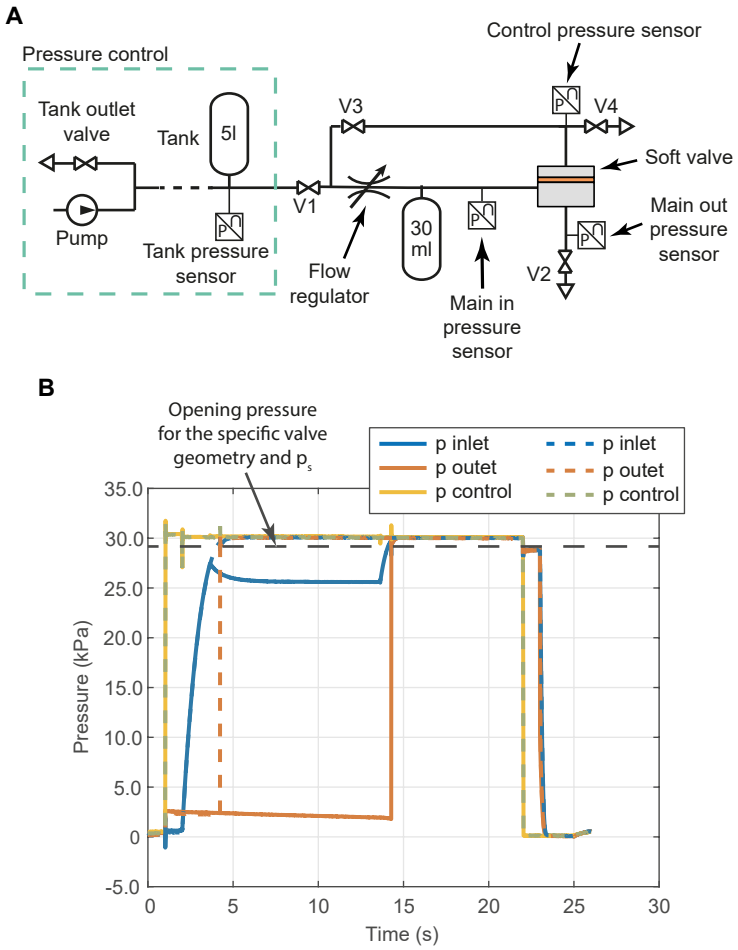

Fig. 5.22 **Stability of the ROM behaviour.** (**A**) Pneumatic test circuit used for the experiment. (**B**) The dashed lines refer to an experiment where a soft valve ($D = 10\,\text{mm}$, $d = 0.5\,\text{mm}$, $h = 500\,\mu\text{m}$) is tested using the ROM procedure as detailed in the Materials and methods section and $p_s = 30\,\text{kPa}$. As visible, when the inlet pressure reaches the threshold pressure for the valve to open (back dashed line), the outlet pressure instantly jumps to the inlet pressure value (valve open). The solid lines refer to an experiment where the external inlet valve is closed right before the soft valve inlet pressure reaches the ROM switching threshold for the valve. The external valve is then kept closed for 10 s during which the soft valve remains closed (no relevant changes were observed in the outlet pressure). The external inlet valve is then reopened and, once the soft valve inlet pressure reaches the threshold value, the outlet pressure jumps to the inlet pressure value (soft valve open), highlighting how the ROM switching is a pressure-based phenomenon and not a time based one.

Chapter 6

Discussion

6.1 Conclusions

Hybrid rigid-soft and fully soft robots have been largely investigated in the past two decades as possible replacement for traditional rigid robots. Their inherent compliance and low-cost fabrication makes them ideal candidates for a number of applications such as human robot interaction, medical and implantable robots, marine and space robots. In addition, the introduction of smart and composite materials has enabled the development of robots whose physical body represents both sensors and actuators, without neat distinction between the two, as typically seen in traditional machines. Despite their interesting capabilities, for soft robots to see widespread adoption and replace their traditional, rigid counterparts in everyday applications, some critical challenges have to be overcome. Among these, resilience remains a crucial, yet understudied problem.

The ability to cope with faults has been a core subject of research in autonomous systems since the dawn of digital technologies and control theory. Hardware redundancy, which constitutes the basis for fail-safe systems, has been widely adopted in critical subsystems for high-risk applications such as aviation and space exploration. Pushed to its limits, this concept led researchers to the development of reconfigurable systems, where robots are made out of a finite number of types of modules, so that, when one becomes faulty, another one can take its place to preserve operation. With the advent of more powerful, low-cost micro-controllers and microprocessors and the goal of reducing system cost and complexity, novel approaches have been developed, that do not require hardware redundancy. These, classified as fault-tolerant techniques, use adaptation at the controller level, and sometimes partial hardware reconfiguration, to maintain the system in operation after the fault. As no redundancy is present, the system's performance will be impacted by a fault, but the impact can be limited, through masterful changes in the control algorithm. One of the limitations

of these approaches, the need for a detailed model of the system, has been overcome in the past two decades by data-driven and machine learning approaches, at the expenses of longer training time and computational cost.

When trying to adapt some of these techniques to soft robots, a number of challenges emerge; most importantly, the high non-linearities inherent to the mechanical behaviour hyperelastic materials and the large number of degrees of freedom. In addition, with the goal of achieving fully soft, electronics free robots, new paradigms have to be introduced, that do not rely on traditional rigid sensors and other hardware. Self-healing materials have shown great potential in this respect, by exploiting reversible chemical bonds to achieve reconstitution of the material matrix, without the need for models of the system, sensors or controllers. Nevertheless, human intervention is often needed for the process to be successful, as well as external stimuli to trigger or speed up the healing cycle. In the case of fluidically actuated robots, that require pressurised enclosed volumes to operate, healing can only occur if the internal pressure is removed, so that no actuation fluid is leaking out of the faulty section of the robot. As healing takes time, from minutes to days, this translates into long down times for the robots.

This thesis explores the field of soft robotic resilience first through a more traditional software-based technique and then by taking an embodied approach. In Chapter 3 a flexible extendable robotic implant, the FERI, is used to test a data-driven fault detection and identification framework. As the robot is meant to be coupled to soft tissue and promote tissue regeneration through mechanostimulation, a soft tissue simulator was also developed, to try to closely replicate the interaction between the implant and the tissue it operates on. The growth of the tissue over a long period of time introduces challenges linked to the absence of a steady state condition for the robot and consequent relative drift in the sensors' signals. The compliance of the robot, granted by the flexible rack that connects the two mirror units together, is exploited to gain understanding about the state of the system for fault detection purposes. In addition, to make up for the partial lack of redundancy in information, an active identification strategy is presented, where the robot monitors its sensors during a partial retraction and re-elongation using only its force sensors. At the end of the transient, the Pearson Correlation Coefficient between pairs of sensors is used to establish which sensor, between the encoders and the flex sensor, is the faulty one. Overall, the approach exploits the understanding of the mechanics of the FERI, to devise a straightforward, data-driven fault detection and identification process. The data-driven nature of the framework means that similar techniques can be expanded to other, potentially more complex systems, without the necessity for their precise mathematical modelling. In addition, the work in the chapter highlights the possibility of using custom designed and tuneable physical tissue simulators

as a way of reducing pre-clinical animal trials, meanwhile providing physiologically relevant solutions for the training and testing phases of the robotic implants. Some limitations that emerged during the study closely follow those highlighted for machine learning based approaches in traditional rigid robots. In particular, the need for extensive training, either in simulation or in the real world. This requirement is particularly taxing for applications where very limited information is available on the operating environment of the robot, which is the case of medium and long-term robotic implants. Physical simulators, like the one presented in the chapter, represent a viable solution, but a complete replication of the interaction between the robot and its surrounding environment is yet to be achieved. The need for sensors in order to perform the fault detection and identification, leads to concerns regarding feasibility for high degrees of freedom systems, both in terms of hardware requirement and placement as well as computational effort. In addition, being the technique software based, it requires a transduction from the fluidic realm typical of many soft robots, to the digital one, making it less relevant for the development fully soft resilient machines.

The development of the fully soft valve for burst detection and isolation presented in Chapter 4 represents a first of its kind attempt at replicating embodied consistency based fault detection in pneumatic soft robots. In doing so, it exploits the fundamental principle of the framework developed for the FERI to create a physical self-sufficient computational unit. Designed to be used in systems where multiple actuators share the same supply line, the valve internally senses the difference between the pressure in the soft actuator it is connected to and the supply pressure and, when this difference surpasses a threshold level, the valve shuts itself off, isolating the faulty actuator. As the entire process is passive, no additional sensors or controller intervention is needed. In addition to providing an equivalent counterpart for a software-based approach, and providing a way of avoiding fault propagation, the soft valve represents an attempt to overcome one of the main limitations of self-healing materials applied to pneumatic soft robots, that is the need for selective deflation of the faulty actuator. As a result, the valve can be used to maintain the rest of the soft robot inflated and functioning while isolating the burst actuator, either temporarily, while this is healing, or permanently, if healing fails.

Chapter 5, further elaborates the concept of embodied resilience through the use of soft valves by developing a multi-modal design as a stepping stone towards the creation of an endogenously controlled soft valve. The two distinct behaviours, FOM and ROM, exhibited by the valve are enabled by swapping inlet and outlet, without changes to the internal structure. The same valve can be used either to detect and isolate bursts, in a resettable fuse-like behaviour, or to protect soft robots against overpressurisation, as a Zener diode would protect electronic circuits against overvoltage. In addition, both behaviours are

demonstrated by fully embedding the valves in soft robots, at the manufacturing stage. The combination of two valves together creates a unit capable of generating its own control signal for passive burst detection and isolation. Thanks to this evolution, the valve works without an external control line being present, leading to a simplification of the system. In addition, the self-tuning capability, which enables the endogenous control, means that the same valve can be used with actuators independent on their size or behaviour during inflation. Despite only a limited range of supply pressures and one material have been used during the study, the working principle should scale to higher pressure values together with stiffer materials. As a result, the EC soft valve represents a fully self-contained drop-in solution for burst detection and isolation in pneumatic soft actuators. As no externally actuated control line is present, no modifications to the control algorithm of the soft robot are needed, further simplifying its integration into existing soft robotic designs.

Fig. 6.1, presents a qualitative comparison of the three main types of robotic resilience techniques and compares them with the embodied one based on the use of soft valves. The criteria used for the analysis try to highlight strengths and weaknesses of each approach, while making the comparison as complete as possible. A qualitative representation was chosen due to the very limited availability of common quantitative metrics across studies and research fields. The scores in each criterion were assigned based on the perceived average performance of the most representative studies for each approach to robotic resilience.
Redundancy-based resilience faster response times, compared to other methods, and perfect recovery after a fault are achieved at the expenses of hardware requirements (and therefore system costs), which limits the scalability of the approach. This is why, in most cases, only particularly critical sub-systems are made redundant into larger assemblies. In contrast, software-based fault tolerance tries to overcome this problem by exploiting functional adjustment at the expense of more complex control software and computational effort. The recovery after a fault is usually only partial and the response time is made longer by the need to find an alternative control law to adjust for the faulty component/s. The gains in terms of reduced hardware costs are non-negligible though. In addition, this type of resilience makes it possible to create robots that have the potential to cope with a wider spectrum of faults, that might not have been accounted for through sheer hardware redundancy, making them more adaptable in unknown environments. Challenges still remain with respect to scalability to high degrees of freedom systems, mainly in terms of computational complexity, limiting its applicability in the realm of soft robotics. On the opposite end of the spectrum, self-healing materials do away with hardware redundancy and software and purely rely on material properties for resilience. This change in perspective, from the system overall, down to the individual molecules, leads, in theory, to the most scalable approach. At the time of

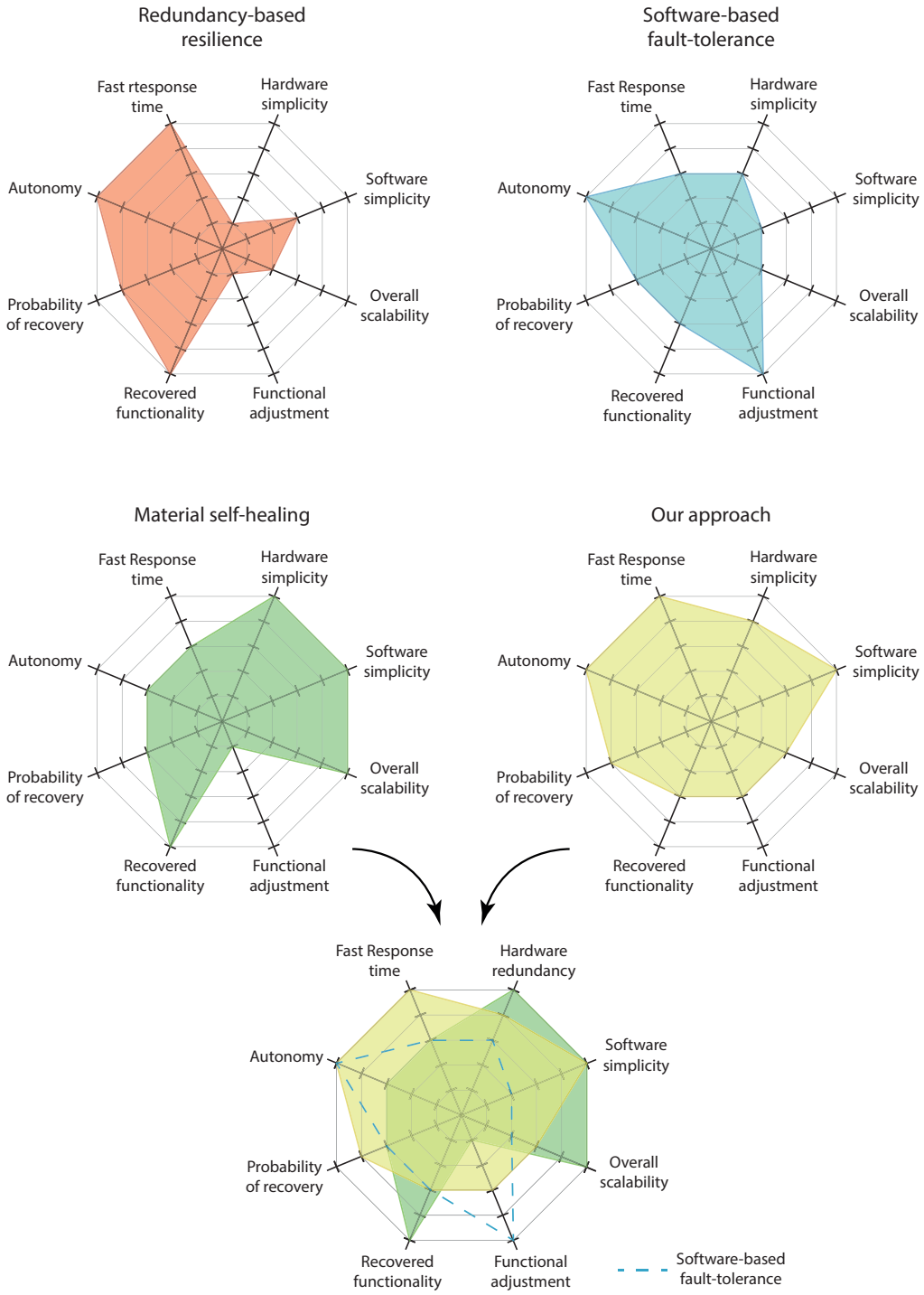

Fig. 6.1 The spider charts highlight strengths and weaknesses of the three state-of-the-art forms of resilience and the embodied approach based on soft valves. The scores in each criterion were assigned based on the perceived average performance of the most representative studies for each approach to robotic resilience. The bottom image combines the latter with self-healing techniques and visually suggests how these together could provide a valuable alternative to software-based fault-tolerance.

this study, the main limitations revolve around the overall response time and probability of recovery, as explained earlier. with respect to the future, concerns remain when multiple functional materials are needed in a design: the state-of-the-art self-healing approaches seem to target monolithic robotic designs. A recent exception presents a Pneu-Net finger assembly consisting of two sub-assemblies with different electrical properties, but the bulk material is still the same [137]. Finally, the embodied approach presented in this thesis capitalises on fast response time and a high degree of autonomy. The scalability is not as good as self-healing materials, but through miniaturization and additive manufacturing, it has greater potential than the traditional paradigms developed for rigid robots. In addition, compared to self-healing materials soft valves enable the possibility of preventative reactions to avoid faults altogether, as demonstrated by the multi-modal design of Chapter 5.

6.2 Future works

The main limitation of the reactive approaches presented in the thesis is the lack of inherent regeneration capabilities: the valves can be used to try and prevent fault, or isolate one when this occurs, but no long-term regeneration is present that can take the robot back to its fully-functioning state. This limitation can be overcome, though, through the addition of self-healing capabilities, as shown in the bottom chart of Fig. 6.1. This development should represent a natural and straightforward evolution of the two technologies, leading to immediate increased impact and applicability of both. The valves only require one material, therefore aligning with the monolithic fabrication techniques common for self-healing robots. In addition, as demonstrated in Chapter 5, it is possible to embed the valves at the manufacturing stage, with minimal changes to the structure of existing soft robotic designs, providing the foundation for a unifying approach to pre-emptive and material healing-based resilience of soft robots.

A second avenue of research consists in the possibility of feedback/signalling of the faults to the controller or adjacent parts of the system. This would enable the possibility for the system to adopt large scale changes in behaviour to try and maximise performance after a fault, while protecting the area that would be in the process of healing, behaviour similar to that adopted by living creatures when dealing with minor injuries. This feedback could be achieved through the use of conductive polymers to sense the deformation of the internal membranes of the valves. This information could then be used by the controller to decide which behaviour to adopt. In the long-term, with the goal of creating resilient electronic-free soft robots, chemical signalling could be used to achieve analogous results, taking inspiration from hormonal responses seen in humans.

The combination of approaches, on top of expanding the resilience with novel, unique capabilities, also provide a form of redundancy that, unlike the traditional one, is not rooted in hardware, but in available strategies to deal with the same problem. As such, these two further developments, self-healing and system-level signalling and adaptation, could finally lead to the creation of truly bio-inspired soft robots capable of mimicking the resilient behaviours of living creatures together with their regenerative capabilities. Thanks to these developments, important advancements could be made in safety-critical fields such as space exploration, robotic implants and search and rescue, all of which require robots to be resilient and possess good adaptation capabilities. Furthermore, they would fast-track the widespread adoption of soft robots for everyday human robot interaction, without the need for controlled and safe environments to maximise the life expectancy of the robots.

References

[1] George M. Whitesides. Soft robotics. *Angewandte Chemie (International ed.)*, 57(16):4258–4273, 2018.

[2] Daniela Rus and Michael T. Tolley. Design, fabrication and control of soft robots. *Nature*, 521(7553):467–475, 2015.

[3] Yongchang Zhang, Pengchun Li, Jiale Quan, Longqiu Li, Guangyu Zhang, and Dekai Zhou. Progress, challenges, and prospects of soft robotics for space applications. *Advanced Intelligent Systems*, 5(3):2200071, 2023.

[4] Rolf Pfeifer, Fumiya Iida, and Max Lungarella. Cognition from the bottom up: on biological inspiration, body morphology, and soft materials. *Trends in cognitive sciences*, 18(8):404–413, 2014.

[5] Michael T. Tolley, Robert F. Shepherd, Bobak Mosadegh, Kevin C. Galloway, Michael Wehner, Michael Karpelson, Robert J. Wood, and George M. Whitesides. A resilient, untethered soft robot. *Soft robotics*, 1(3):213–223, 2014.

[6] Chelsea Shan Xian Ng and Guo Zhan Lum. Untethered soft robots for future planetary explorations? *Advanced Intelligent Systems*, 5(3):2100106, 2023.

[7] Ellen T. Roche, Markus A. Horvath, Isaac Wamala, Ali Alazmani, Sang Eun Song, William Whyte, Zurab Machaidze, Christopher J. Payne, James C. Weaver, Gregory Fishbein, Joseph Kuebler, Nikolay V. Vasilyev, David J. Mooney, Frank A. Pigula, and Conor J. Walsh. Soft robotic sleeve supports heart function. *Science Translational Medicine*, 9(373), 2017.

[8] Eduardo Perez-Guagnelli, Joanna Jones, Ahmet H. Tokel, Nicolas Herzig, Bryn Jones, Shuhei Miyashita, and Dana D. Damian. Characterization, simulation and control of a soft helical pneumatic implantable robot for tissue regeneration. *IEEE Transactions on Medical Robotics and Bionics*, 2(1):94–103, 2020.

[9] Hongbo Wang, Massimo Totaro, and Lucia Beccai. Toward perceptive soft robots: Progress and challenges. *Advanced Science*, 5(9):1800541, 2018.

[10] Taekyoung Kim, Sudong Lee, Taehwa Hong, Gyowook Shin, Taehwan Kim, and Yong-Lae Park. Heterogeneous sensing in a multifunctional soft sensor for human-robot interfaces. *Science robotics*, 5(49):eabc6878, 2020.

[11] Pierre Schegg and Christian Duriez. Review on generic methods for mechanical modeling, simulation and control of soft robots. *PloS one*, 17(1):e0251059–e0251059, 2022.

[12] Malte Grube, Jan Christian Wieck, and Robert Seifried. Comparison of modern control methods for soft robots. *Sensors (Basel, Switzerland)*, 22(23):9464, 2022.

[13] Seppe Terryn, Joost Brancart, Dirk Lefeber, Guy Van Assche, and Bram Vanderborght. Self-healing soft pneumatic robots. *Science Robotics*, 2(9), 2017.

[14] R Adam Bilodeau and Rebecca K Kramer. Self-healing and damage resilience for soft robotics: A review. *Frontiers in Robotics and AI*, 4:48, 2017.

[15] Olga Speck and Thomas Speck. An overview of bioinspired and biomimetic self-repairing materials. *Biomimetics (Basel)*, 4(1):26, 2019.

[16] Michael D. Bartlett, Michael D. Dickey, and Carmel Majidi. Self-healing materials for soft-matter machines and electronics. *NPG Asia Materials*, 11(1):19–22, 2019.

[17] Melanie Baumgartner, Florian Hartmann, Michael Drack, David Preninger, Daniela Wirthl, Robert Gerstmayr, Lukas Lehner, Guoyong Mao, Roland Pruckner, Stepan Demchyshyn, et al. Resilient yet entirely degradable gelatin-based biogels for soft robots and electronics. *Nature Materials*, 19(10):1102–1109, 2020.

[18] A. Avizienis, G. C. Gilley, F. P. Mathur, D. A. Rennels, J. A. Rohr, and D. K. Rubin. The star (self-testing and repairing) computer: An investigation of the theory and practice of fault-tolerant computer design. *IEEE Transactions on Computers*, C-20(11):1312–1321, 1971.

[19] D. A. Rennels. Fault-tolerant computing—concepts and examples. *IEEE Transactions on Computers*, C-33(12):1116–1129, 1984.

[20] H. Durnova. Sovietization of czechoslovakian computing: The rise and fall of the sapo project. *IEEE Annals of the History of Computing*, 32(2):21–31, 2010.

[21] M. Blanke, R. Izadi-Zamanabadi, S. A. Bøgh, and C. P. Lunau. Fault-tolerant control systems — a holistic view. *Control Engineering Practice*, 5(5):693–702, 1997.

[22] Tan Zhang, Wenjun Zhang, and Madan M. Gupta. Resilient robots: Concept, review, and future directions. *Robotics*, 6(4), 2017.

[23] Josh Bongard, Victor Zykov, and Hod Lipson. Resilient machines through continuous self-modeling. *Science*, 314(5802):1118–1121, 2006.

[24] Sylvain Koos, Antoine Cully, and Jean Baptiste Mouret. Fast damage recovery in robotics with the t-resilience algorithm. *The International Journal of Robotics Research*, 32(14):1700–1723, 2013.

[25] Antoine Cully, Jeff Clune, Danesh Tarapore, and Jean Baptiste Mouret. Robots that can adapt like animals. *Nature*, 512(7553):503—-507, 2015.

[26] Robert Kwiatkowski and Hod Lipson. Task-agnostic self-modeling machines. *Science Robotics*, 4(26), 2019.

[27] Josh Bongard. Morphological change in machines accelerates the evolution of robust behavior. *Proceedings of the National Academy of Sciences of the United States of America*, 108(4):1234–1239, 2011.

[28] Josh Bongard. Evolutionary robotics. *Commun. ACM*, 56(8):74—83, 2013.

[29] K. Gilpin and D. Rus. Modular robot systems. *IEEE Robotics Automation Magazine*, 17(3):38–55, 2010.

[30] Daniela Rus, Zack Butler, Keith Kotay, and Marsette Vona. Self-reconfiguring robots. *Commun. ACM*, 45(3):39–45, 2002.

[31] T. Fukuda and S. Nakagawa. Dynamically reconfigurable robotic system. In *Proceedings. 1988 IEEE International Conference on Robotics and Automation*, volume 3, pages 1581–1586, 1988.

[32] T. Fukuda, S. Nakagawa, Y. Kawauchi, and M. Buss. Structure decision method for self organising robots based on cell structures-cebot. In *Proceedings, 1989 International Conference on Robotics and Automation*, volume 2, pages 695–700, 1989.

[33] S. Murata, E. Yoshida, A. Kamimura, H. Kurokawa, K. Tomita, and S. Kokaji. M-tran: self-reconfigurable modular robotic system. *IEEE/ASME Transactions on Mechatronics*, 7(4):431–441, 2002.

[34] H. Kurokawa, A. Kamimura, E. Yoshida, K. Tomita, S. Kokaji, and S. Murata. M-tran ii: metamorphosis from a four-legged walker to a caterpillar. In *Proceedings 2003 IEEE/RSJ International Conference on Intelligent Robots and Systems (IROS 2003) (Cat. No.03CH37453)*, volume 3, pages 2454–2459, 2003.

[35] Haruhisa Kurokawa, Kohji Tomita, Akiya Kamimura, Shigeru Kokaji, Takashi Hasuo, and Satoshi Murata. Distributed self-reconfiguration of m-tran iii modular robotic system. *The International Journal of Robotics Research*, 27(3-4):373–386, 2008.

[36] Andreas Lyder, Ricardo Franco Mendoza Garcia, and Kasper Stoy. Mechanical design of odin, an extendable heterogeneous deformable modular robot. In *2008 IEEE/RSJ International Conference on Intelligent Robots and Systems*, pages 883–888, 2008.

[37] Jonas Neubert and Hod Lipson. Soldercubes: a self-soldering self-reconfiguring modular robot system. *Autonomous Robots*, 40(1):139–158, 2016.

[38] Feili Hou. *Self-reconfiguration planning for modular robots*. PhD thesis, Department of Computer Science, University of Southern California, Los Angeles, CA, USA, 2011.

[39] Charles E. Diesendruck, Nancy R. Sottos, Jeffrey S. Moore, and Scott R. White. Biomimetic self-healing. *Angewandte Chemie International Edition*, 54(36):10428–10447, 2015.

[40] Zhao Wei, Jian Hai Yang, Zhen Qi Liu, Feng Xu, Jin Xiong Zhou, Miklós Zrínyi, Yoshihito Osada, and Yong Mei Chen. Novel biocompatible polysaccharide-based self-healing hydrogel. *Advanced Functional Materials*, 25(9):1352–1359, 2015.

[41] Martin D. Hager, Peter Greil, Christoph Leyens, Sybrand Van Der Zwaag, and Ulrich S. Schubert. Self-healing materials. *Advanced Materials*, 22(47):5424–5430, 2010.

[42] M. M. Diaz, J. Brancart, G. Van Assche, and B. Van Mele. Room-temperature versus heating-mediated healing of a diels-alder crosslinked polymer network. *Polymer*, 153:453–463, 2018.

[43] Seppe Terryn, Joost Brancart, Dirk Lefeber, Guy Van Assche, and Bram Vanderborght. A pneumatic artificial muscle manufactured out of self-healing polymers that can repair macroscopic damages. *IEEE Robotics and Automation Letters*, 3(1):16–21, 2018.

[44] P. H. Geubelle, J. S. Moore, M. R. Kessler, S. R. Sriram, E. N. Brown, and S. Viswanathan. Autonomic healing of polymer composites. *Nature*, 409(6822):794–797, 2001.

[45] E. N. Brown, S. R. White, and N. R. Sottos. Microcapsule induced toughening in a self-healing polymer composite. *Journal of Materials Science*, 39(5):1703–1710, 2004.

[46] Kathleen S. Toohey, Nancy R. Sottos, Jennifer A. Lewis, Jeffrey S. Moore, and Scott R. White. Self-healing materials with microvascular networks. *Nature Materials*, 6(8):581–585, 2007.

[47] Christopher J. Hansen, Willie Wu, Kathleen S. Toohey, Nancy R. Sottos, Scott R. White, and Jennifer A. Lewis. Self-healing materials with interpenetrating microvascular networks. *Advanced Materials*, 21(41):4143–4147, 2009.

[48] Philippe Cordier, François Tournilhac, Corinne Soulié-Ziakovic, and Ludwik Leibler. Self-healing and thermoreversible rubber from supramolecular assembly. *Nature*, 451(7181):977–980, 2008.

[49] Guangyong Li, Xuan Wu, and Dong Weon Lee. A galinstan-based inkjet printing system for highly stretchable electronics with self-healing capability. *Lab on a Chip*, 16(8):1366–1373, 2016.

[50] Eric J. Markvicka, Michael D. Bartlett, Xiaonan Huang, and Carmel Majidi. An autonomously electrically self-healing liquid metal-elastomer composite for robust soft-matter robotics and electronics. *Nature Materials*, 17(7):618–624, 2018.

[51] Shunli Liu, Kewen Li, Imtiaz Hussain, Olayinka Oderinde, Fang Yao, Jiuyang Zhang, and Guodong Fu. A conductive self-healing double network hydrogel with toughness and force sensitivity. *Chemistry - A European Journal*, 24(25):6632–6638, 2018.

[52] Ellen Roels, Seppe Terryn, Joost Brancart, Robrecht Verhelle, Guy Van Assche, and Bram Vanderborght. Additive manufacturing for self-healing soft robots. *Soft Robotics*, 0(0):1–13, 2020.

[53] Tan Phat Huynh, Prashant Sonar, and Hossam Haick. Advanced materials for use in soft self-healing devices. *Advanced Materials*, 29(19), 2017.

[54] Michael J. Ford, Cedric P. Ambulo, Teresa A. Kent, Eric J. Markvicka, Chengfeng Pan, Jonathan Malen, Taylor H. Ware, and Carmel Majidi. A multifunctional shape-morphing elastomer with liquid metal inclusions. *Proceedings of the National Academy of Sciences of the United States of America*, 116(43):21438–21444, 2019.

[55] Huijiang Wang, Seppe Terryn, Zhanwei Wang, Guy Van Assche, Fumiya Lida, and Bram Vanderborght. Self-regulated self-healing robotic gripper for resilient and adaptive grasping. *Advanced Intelligent Systems*, 2023.

[56] Rolf Pfeifer, Fumiya Iida, and Max Lungarella. Cognition from the bottom up: On biological inspiration, body morphology, and soft materials. *Trends in Cognitive Sciences*, 18(8):404–413, 2014.

[57] Rolf Pfeifer and Josh Bongard. *How the Body Shapes the Way We Think: A new view of intelligence*. MIT Press, Cambridge, MA, 2007.

[58] Marcin Miłkowski. Morphological computation: Nothing but physical computation. *Entropy*, 20(12), 2018.

[59] Vincent C. Müller and Matej Hoffmann. What is morphological computation? on how the body contributes to cognition and control. *Artificial Life*, 23(1):1–24, 2017.

[60] J. A.E. Hughes, P. Maiolino, and F. Iida. An anthropomorphic soft skeleton hand exploiting conditional models for piano playing. *Science Robotics*, 3(25):1–12, 2018.

[61] Helmut Hauser, Auke J. Ijspeert, Rudolf M. Füchslin, Rolf Pfeifer, and Wolfgang Maass. Towards a theoretical foundation for morphological computation with compliant bodies. *Biological Cybernetics*, 105(5):355–370, 2011.

[62] Kohei Nakajima, Helmut Hauser, Rongjie Kang, Emanuele Guglielmino, Darwin G. Caldwell, and Rolf Pfeifer. A soft body as a reservoir: Case studies in a dynamic model of octopus-inspired soft robotic arm. *Frontiers in Computational Neuroscience*, 7, 2013.

[63] Kohei Nakajima, Helmut Hauser, Tao Li, and Rolf Pfeifer. Information processing via physical soft body. *Nature Scientific Reports*, 5, 2015.

[64] Gouhei Tanaka, Toshiyuki Yamane, Jean Benoit Héroux, Ryosho Nakane, Naoki Kanazawa, Seiji Takeda, Hidetoshi Numata, Daiju Nakano, and Akira Hirose. Recent advances in physical reservoir computing: A review. *Neural Networks*, 115:100–123, 2019.

[65] Christos Bergeles and Guang Zhong Yang. From passive tool holders to microsurgeons: Safer, smaller, smarter surgical robots. *IEEE Transactions on Biomedical Engineering*, 61(5):1565–1576, 2014.

[66] Huu Minh Le, Thanh Nho Do, and Soo Jay Phee. A survey on actuators-driven surgical robots. *Sensors and Actuators, A: Physical*, 247:323–354, 2016.

[67] Dana D Damian, Karl Price, Slava Arabagi, Ignacio Berra, Zurab Machaidze, Sunil Manjila, Shogo Shimada, Assunta Fabozzo, Gustavo Arnal, David Van Story, Jeffrey D Goldsmith, Agoston T Agoston, Chunwoo Kim, Russell W Jennings, Peter D Ngo, Michael Manfredi, and Pierre E Dupont. In vivo tissue regeneration with robotic implants. *Science Robotics*, 3(14), 2018.

[68] Ellen T. Roche, Robert Wohlfarth, Johannes T.B. Overvelde, Nikolay V. Vasilyev, Frank A. Pigula, David J. Mooney, Katia Bertoldi, and Conor J. Walsh. A bioinspired soft actuated material. *Advanced Materials*, 26(8):1200–1206, 2014.

[69] Christopher J. Payne, Isaac Wamala, Colette Abah, Thomas Thalhofer, Mossab Saeed, Daniel Bautista-Salinas, Markus A. Horvath, Nikolay V. Vasilyev, Ellen T. Roche, Frank A. Pigula, and Conor J. Walsh. An implantable extracardiac soft robotic device for the failing heart: Mechanical coupling and synchronization. *Soft robotics*, 4(3):241–250, 2017.

[70] Gregory Mone. Robotic implants. *Communications of the ACM*, 61(9):17–18, 2018.

[71] Ivan R. Minev, Daniel J. Chew, Evangelos Delivopoulos, James W. Fawcett, and Stéphanie P. Lacour. High sensitivity recording of afferent nerve activity using ultra-compliant microchannel electrodes: An acute in vivo validation. *Journal of Neural Engineering*, 9(2), 2012.

[72] Ivan R. Minev, Pavel Musienko, Arthur Hirsch, Quentin Barraud, Nikolaus Wenger, Eduardo Martin Moraud, Jérôme Gandar, Marco Capogrosso, Tomislav Milekovic, Léonie Asboth, Rafael Fajardo Torres, Nicolas Vachicouras, Qihan Liu, Natalia Pavlova, Simone Duis, Alexandre Larmagnac, Janos Vörös, Silvestro Micera, Zhigang Suo, Grégoire Courtine, and Stéphanie P. Lacour. Electronic dura mater for long-term multimodal neural interfaces. *Science*, 347(6218):159–163, 2015.

[73] Seung Ho Lee, Young Bin Lee, Byung Hwi Kim, Cheol Lee, Young Min Cho, Se Na Kim, Chun Gwon Park, Yong Chan Cho, and Young Bin Choy. Implantable batteryless device for on-demand and pulsatile insulin administration. *Nature Communications*, 8, 2017.

[74] Michael D. Bartlett, Michael D. Dickey, and Carmel Majidi. Self-healing materials for soft-matter machines and electronics. *NPG Asia Materials*, 11(1):19–22, 2019.

[75] Panagiotis Polygerinos, Nikolaus Correll, Stephen A. Morin, Bobak Mosadegh, Cagdas D. Onal, Kirstin Petersen, Matteo Cianchetti, Michael T. Tolley, and Robert F. Shepherd. Soft robotics: Review of fluid-driven intrinsically soft devices; manufacturing, sensing, control, and applications in human-robot interaction. *Advanced Engineering Materials*, 19(12), 2017.

[76] Jean Baptiste Chossat, Yong Lae Park, Robert J. Wood, and Vincent Duchaine. A soft strain sensor based on ionic and metal liquids. *IEEE Sensors Journal*, 13(9):3405–3414, 2013.

[77] Hadrien O. Michaud, Joan Teixidor, and Stéphanie P. Lacour. Soft metal constructs for large strain sensor membrane. *Smart Materials and Structures*, 24(3), 2015.

[78] Chwee Lin Choong, Mun Bo Shim, Byoung Sun Lee, Sanghun Jeon, Dong Su Ko, Tae Hyung Kang, Jihyun Bae, Sung Hoon Lee, Kyung Eun Byun, Jungkyun Im, Yong Jin Jeong, Chan Eon Park, Jong Jin Park, and U. In Chung. Highly stretchable resistive pressure sensors using a conductive elastomeric composite on a micropyramid array. *Advanced Materials*, 26(21):3451–3458, 2014.

[79] GiannacciniMaria Elena et al. Novel design of a soft lightweight pneumatic continuum robot arm with decoupled variable stiffness and positioning. *Soft robotics*, 2018.

[80] Loai AT Al Abeach, Samia Nefti-Meziani, and Steve Davis. Design of a variable stiffness soft dexterous gripper. *Soft robotics*, 4(3):274–284, 2017.

[81] Seyed M. Mirvakili and Ian W. Hunter. Artificial muscles: Mechanisms, applications, and challenges. *Advanced Materials*, 30(6):1–28, 2018.

[82] Carter S. Haines, Márcio D. Lima, Na Li, Geoffrey M. Spinks, Javad Foroughi, John D.W. Madden, Shi Hyeong Kim, Shaoli Fang, Mônica Jung De Andrade, Fatma Göktepe, Özer Göktepe, Seyed M. Mirvakili, Sina Naficy, Xavier Lepró, Jiyoung Oh, Mikhail E. Kozlov, Seon Jeong Kim, Xiuru Xu, Benjamin J. Swedlove, Gordon G. Wallace, and Ray H. Baughman. Artificial muscles from fishing line and sewing thread. *Science*, 343(6173):868–872, 2014.

[83] Michael C. Yip and Günter Niemeyer. High-performance robotic muscles from conductive nylon sewing thread. In *Proceedings - IEEE International Conference on Robotics and Automation*, pages 2313–2318, 2015.

[84] Xiangyu Gong, Ke Yang, Jingjin Xie, Yanjun Wang, Parth Kulkarni, Alexander S. Hobbs, and Aaron D. Mazzeo. Rotary actuators based on pneumatically driven elastomeric structures. *Advanced Materials*, 28(34):7533–7538, 2016.

[85] Elliot W. Hawkes, Laura H. Blumenschein, Joseph D. Greer, and Allison M. Okamura. A soft robot that navigates its environment through growth. *Science Robotics*, 2(8):1–8, 2017.

[86] Joseph D. Greer, Tania K. Morimoto, Allison M. Okamura, and Elliot W. Hawkes. A soft, steerable continuum robot that grows via tip extension. *Soft Robotics*, 6(1):95–108, 2019.

[87] Laura H. Blumenschein, Lucia T. Gan, Jonathan A. Fan, Allison M. Okamura, and Elliot W. Hawkes. A tip-extending soft robot enables reconfigurable and deployable antennas. *IEEE Robotics and Automation Letters*, 3(2):949–956, 2018.

[88] Margaret M. Coad, Rachel P. Thomasson, Laura H. Blumenschein, Nathan S. Usevitch, Elliot W. Hawkes, and Allison M. Okamura. Retraction of soft growing robots without buckling. *IEEE robotics and automation letters*, 5(2):2114–2121, 2020.

[89] Sehyuk Yim and Metin Sitti. Softcubes: Stretchable and self-assembling three-dimensional soft modular matter. *International Journal of Robotics Research*, 33(8):1083–1097, 2014.

[90] Stephen A Morin, Robert F Shepherd, Sen Wai Kwok, Adam A Stokes, Alex Nemiroski, and George M Whitesides. Camouflage and display for soft machines. *Science*, 337:828–832, 2012.

[91] Whitney Crooks, Gabrielle Vukasin, Maeve O'Sullivan, William Messner, and Chris Rogers. Fin ray® effect inspired soft robotic gripper: From the robosoft grand challenge toward optimization. *Frontiers Robotics AI*, 3, 2016.

[92] Ramses V. Martinez, Jamie L. Branch, Carina R. Fish, Lihua Jin, Robert F. Shepherd, Rui M.D. Nunes, Zhigang Suo, and George M. Whitesides. Robotic tentacles with three-dimensional mobility based on flexible elastomers. *Advanced Materials*, 25(2):205–212, 2013.

[93] E. Acome, S. K. Mitchell, T. G. Morrissey, M. B. Emmett, C. Benjamin, M. King, M. Radakovitz, and C. Keplinger. Hydraulically amplified self-healing electrostatic actuators with muscle-like performance. *Science*, 359(6371):61–65, 2018.

[94] Lishuai Jin, Antonio Elia Forte, Bolei Deng, Ahmad Rafsanjani, and Katia Bertoldi. Kirigami-inspired inflatables with programmable shapes. *Advanced materials (Weinheim)*, 32(33):e2001863–n/a, 2020.

[95] Seungki Hong, Jongsu Lee, Kyungsik Do, Minbaek Lee, Ji Hoon Kim, Sangkyu Lee, and Dae-Hyeong Kim. Stretchable electronics: Stretchable electrode based on laterally combed carbon nanotubes for wearable energy harvesting and storage devices (adv. funct. mater. 48/2017). *Advanced functional materials*, 27(48):1770285–n/a, 2017.

[96] Daeil Kim, Doyeon Kim, Hyunkyu Lee, Yu Ra Jeong, Seung-Jung Lee, Gwangseok Yang, Hyoungjun Kim, Geumbee Lee, Sanggeun Jeon, Goangseup Zi, Jihyun Kim, and Jeong Sook Ha. Body-attachable and stretchable multisensors integrated with wirelessly rechargeable energy storage devices. *Advanced materials (Weinheim)*, 28(4):748–756, 2016.

[97] Ryan L. Truby and Jennifer A. Lewis. Printing soft matter in three dimensions. *Nature*, 540(7633):371–378, 2016.

[98] Rolf Pfeifer, Max Lungarella, and Fumiya Iida. The challenges ahead for bio-inspired 'soft' robotics. *Communications of the ACM*, 55(11):76–87, 2012.

[99] Hod Lipson. Challenges and opportunities for design, simulation, and fabrication of soft robots. *Soft Robotics*, 1(1):21–27, 2014.

[100] Keene Chin, Tess Hellebrekers, and Carmel Majidi. Machine learning for soft robotic sensing and control. *Advanced Intelligent Systems*, 2(6), 2020.

[101] Thomas George Thuruthel, Egidio Falotico, Mariangela Manti, Andrea Pratesi, Matteo Cianchetti, and Cecilia Laschi. Learning closed loop kinematic controllers for continuum manipulators in unstructured environments. *Soft Robotics*, 4(3):285–296, 2017.

[102] Y. Ansari, M. Manti, E. Falotico, M. Cianchetti, and C. Laschi. Multiobjective optimization for stiffness and position control in a soft robot arm module. *IEEE Robotics and Automation Letters*, 3(1):108–115, 2018.

[103] Eric Brown, Nicholas Rodenberg, John Amend, Annan Mozeika, Erik Steltz, Mitchell R. Zakin, Hod Lipson, and Heinrich M. Jaeger. Universal robotic gripper based on the jamming of granular material. *Proceedings of the National Academy of Sciences of the United States of America*, 107(44):18809–18814, 2010.

[104] Michael Wehner, Ryan L. Truby, Daniel J. Fitzgerald, Bobak Mosadegh, George M. Whitesides, Jennifer A. Lewis, and Robert J. Wood. An integrated design and fabrication strategy for entirely soft, autonomous robots. *Nature*, 536(7617):451–455, 2016.

[105] Stephen T Mahon, Anthony Buchoux, Mohammed E Sayed, Lijun Teng, and A Stokes. Soft robots for extreme environments : Removing electronic control. In *RoboSoft 2019 - 2019 IEEE International Conference on Soft Robotics*, pages 782–787, 2019.

[106] Robert F. Shepherd, Adam A. Stokes, Rui M.D. Nunes, and George M. Whitesides. Soft machines that are resistant to puncture and that self seal. *Advanced Materials*, 25(46):6709–6713, 2013.

[107] Marco Pontin and Dana D Damian. Data-driven and compliance-based fault-tolerance for a flexible and extendable robotic implant coupled to a growing tissue. *IEEE Robotics and Automation Letters*, 8(4):1943–1950, 2023.

[108] Mogens Blanke, Michel Kinnaert, Jan Lunze, and Marcel Staroswiecki. *Diagnosis and Fault-Tolerant Control*, pages 13–17. Springer-Verlag Berlin, Heidelberg, Heidelberg, DE, 2006.

[109] Carmel Majidi. Soft-matter engineering for soft robotics. *Advanced Materials Technologies*, 4(2):1800477, 2019.

[110] Kingson Man and Antonio Damasio. Homeostasis and soft robotics in the design of feeling machines. *Nature Machine Intelligence*, 1(10):446–452, 2019.

[111] Alberto Brunete, Avinash Ranganath, Sergio Segovia, Javier Perez De Frutos, Miguel Hernando, and Ernesto Gambao. Current trends in reconfigurable modular robots design. *International Journal of Advanced Robotic Systems*, 14(3):1729881417710457, 2017.

[112] Kyle Gilpin and Daniela Rus. Modular robot systems. *IEEE robotics & automation magazine*, 17(3):38–55, 2010.

[113] Timothy J Koh and Luisa Ann DiPietro. Inflammation and wound healing: the role of the macrophage. *Expert reviews in molecular medicine*, 13:e23, 2011.

[114] Sabine A Eming, Paul Martin, and Marjana Tomic-Canic. Wound repair and regeneration: mechanisms, signaling, and translation. *Science translational medicine*, 6(265):265sr6–265sr6, 2014.

[115] Kristen L Dorsey. Electronics-free soft robot has a nice ring to it. *Science Robotics*, 7(63):eabn6551, 2022.

[116] Vito Cacucciolo, Jun Shintake, Yu Kuwajima, Shingo Maeda, Dario Floreano, and Herbert Shea. Stretchable pumps for soft machines. *Nature*, 572(7770):516–519, 2019.

[117] Siyi Xu, Cara M Nunez, Mohammad Souri, and Robert J Wood. A compact dea-based soft peristaltic pump for power and control of fluidic robots. *Science Robotics*, 8(79):eadd4649, 2023.

[118] Wei Tang, Chao Zhang, Yiding Zhong, Pingan Zhu, Yu Hu, Zhongdong Jiao, Xiaofeng Wei, Gang Lu, Jinrong Wang, Yuwen Liang, et al. Customizing a self-healing soft pump for robot. *Nature communications*, 12(1):2247, 2021.

[119] Sukho Song, Sagar Joshi, and Jamie Paik. Cmos-inspired complementary fluidic circuits for soft robots. *Advanced Science*, 8(20):2100924, 2021.

[120] Francisco Antonio Perdigones, Antonio Luque, and Jose M Quero. Correspondence between electronics and fluids in mems: Designing microfluidic systems using electronics. *IEEE Industrial Electronics Magazine*, 8(4):6–17, 2014.

[121] Philipp Rothemund, Alar Ainla, Lee Belding, Daniel J Preston, Sarah Kurihara, Zhigang Suo, and George M Whitesides. A soft, bistable valve for autonomous control of soft actuators. *Science Robotics*, 3(16):eaar7986, 2018.

[122] Dylan Drotman, Saurabh Jadhav, David Sharp, Christian Chan, and Michael T Tolley. Electronics-free pneumatic circuits for controlling soft-legged robots. *Science Robotics*, 6(51):eaay2627, 2021.

[123] Daniel J Preston, Haihui Joy Jiang, Vanessa Sanchez, Philipp Rothemund, Jeff Rawson, Markus P Nemitz, Won-Kyu Lee, Zhigang Suo, Conor J Walsh, and George M Whitesides. A soft ring oscillator. *Science Robotics*, 4(31):eaaw5496, 2019.

[124] Won-Kyu Lee, Daniel J Preston, Markus P Nemitz, Amit Nagarkar, Arthur K MacKeith, Benjamin Gorissen, Nikolaos Vasios, Vanessa Sanchez, Katia Bertoldi, L Mahadevan, et al. A buckling-sheet ring oscillator for electronics-free, multimodal locomotion. *Science Robotics*, 7(63):eabg5812, 2022.

[125] Minsoung Rhee and Mark A. Burns. Microfluidic pneumatic logic circuits and digital pneumatic microprocessors for integrated microfluidic systems. *Lab on a Chip*, 9(21):3131–3143, 2009.

[126] Erik C. Jensen, William H. Grover, and Richard A. Mathies. Micropneumatic digital logic structures for integrated microdevice computation and control. *Journal of Microelectromechanical Systems*, 16(6):1378–1385, 2007.

[127] Bobak Mosadegh, Tommaso Bersano-Begey, Joong Yull Park, Mark A Burns, and Shuichi Takayama. Next-generation integrated microfluidic circuits. *Lab on a Chip*, 11(17):2813–2818, 2011.

[128] Philip N Duncan, Siavash Ahrar, and Elliot E Hui. Scaling of pneumatic digital logic circuits. *Lab on a Chip*, 15(5):1360–1365, 2015.

[129] Yichen Zhai, Albert De Boer, Jiayao Yan, Benjamin Shih, Martin Faber, Joshua Speros, Rohini Gupta, and Michael T Tolley. Desktop fabrication of monolithic soft robotic devices with embedded fluidic control circuits. *Science Robotics*, 8(79):eadg3792, 2023.

[130] Sihan Wang, Liang He, and Perla Maiolino. A modular approach to design multichannel bistable valves for integrated pneumatically-driven soft robots via 3d-printing. *IEEE Robotics and Automation Letters*, 7(2):3412–3418, 2022.

[131] Michael Wehner, Michael T Tolley, Yiğit Mengüç, Yong-Lae Park, Annan Mozeika, Ye Ding, Cagdas Onal, Robert F Shepherd, George M Whitesides, and Robert J Wood. Pneumatic energy sources for autonomous and wearable soft robotics. *Soft robotics*, 1(4):263–274, 2014.

[132] Marco Pontin, Shuhei Miyashita, and Dana D Damian. Development and characterization of a soft valve for automatic fault isolation in inflatable soft robots. In *2022 IEEE 5th International Conference on Soft Robotics (RoboSoft)*, pages 62–67. IEEE, 2022.

[133] Carlo Bosio, Debora Zrinscak, Cecilia Laschi, and Matteo Cianchetti. Soft mini fuse valve for resilient fluidically-actuated robots. *IEEE Robotics and Automation Letters*, 8(5):2716–2723, 2023.

[134] Robert F Shepherd, Filip Ilievski, Wonjae Choi, Stephen A Morin, Adam A Stokes, Aaron D Mazzeo, Xin Chen, Michael Wang, and George M Whitesides. Multigait soft robot. *Proceedings of the national academy of sciences*, 108(51):20400–20403, 2011.

[135] Kyung-Ah Kwon, Rebecca J Shipley, Mohan Edirisinghe, Daniel G Ezra, Geoff Rose, Serena M Best, and Ruth E Cameron. High-speed camera characterization of voluntary eye blinking kinematics. *Journal of the Royal Society Interface*, 10(85):20130227, 2013.

[136] Yuan-Sheng Lee, Nirveek Bhattacharjee, and Albert Folch. 3d-printed quake-style microvalves and micropumps. *Lab on a Chip*, 18(8):1207–1214, 2018.

[137] Seyedreza Kashef Tabrizian, Fatemeh Sahraeeazartamar, Joost Brancart, Ellen Roels, Pasquale Ferrentino, Julie Legrand, Guy Van Assche, Bram Vanderborght, and Seppe Terryn. A healable resistive heater as a stimuli-providing system in self-healing soft robots. *IEEE Robotics and Automation Letters*, 7(2):4574–4581, 2022.

[138] Aleix Costa Cornella, Seyedreza Kashef Tabrizian, Pasquale Ferrentino, Ellen Roels, Seppe Terryn, Bram Vanderborght, Guy Van Assche, and Joost Brancart. Self-healing, recyclable, and degradable castor oil-based elastomers for sustainable soft robotics. *ACS Sustainable Chemistry & Engineering*, 11(8):3437–3450, 2023.